The Dissertation Committee for Damion Vanton Demeter Certifies that this is the approved version of the following Dissertation:

Quantifying Individual Differences in Patterns of Functional Brain Network Organization in Youths

Committee:

Jessica Church-Lang, Supervisor

Jarrod A. Lewis-Peacock

Alison R. Preston

Evan M. Gordon

Quantifying Individual Differences in Patterns of Functional Brain Network Organization in Youths

by

Damion Vanton Demeter

Dissertation

Presented to the Faculty of the Graduate School of

The University of Texas at Austin

in Partial Fulfillment

of the Requirements

for the Degree of

Doctor of Philosophy

The University of Texas at Austin

August 2021

Dedication

This dissertation is dedicated to my mom, who has always enthusiastically supported every endeavor I have pursued, and who sacrificed so much for herself to provide me with the opportunities to make it to where I am today.

Acknowledgements

This dissertation would not exist if not for the people who have supported me in a multitude of ways and believed in my potential throughout the years. First, I would like to acknowledge Jess for all the support and mentorship throughout this process. From reeling back my wild ideas to trusting me to take on projects even I wasn't completely sure I could accomplish, I wouldn't have made it to this point without the level of true mentorship you provide your trainees. My committee members, Jarrod, Ali, and Evan, who have not only provided guidance during this dissertation process but who have each invested a considerable amount of their time to my academic and personal growth prior to joining my dissertation committee. I must also thank and acknowledge Damien Fair, who gave me my first opportunity to gain experience and train in a new field. At a time when all doors appeared closed, he welcomed me and gave me the opportunity to show I was capable. To my first research family, Eric, Sam, Michaela, Marguerite, Kamari, Kate, Bene (and so many more) who not only initially trained me, but quickly turned into an invaluable support system and showed me that research should also be fun. My lab and officemate Tehila for listening to me rant about research ideas (or just rant in general). Dr. Jagpat for the support and guidance over many bumps in the road. All my family and friends for supporting me through this entire process in so many ways; even "allegedly" sneaking into my very first (and solo) scientific conference, just so I wouldn't have to give my first talk to a room full of strangers. The Brainhack community for welcoming me and allowing me to make an impact on scientific inclusion, while also becoming part of my support network that goes far beyond events. Lastly, I absolutely want to acknowledge all the members of the lab, past and present for all they've done to keep the science flowing, and of course all the families and participants that spent hours of their time providing the data that makes our research possible.

"This [was] an adventure."

Abstract

Quantifying Individual Differences in Patterns of Functional Brain Network Organization in Youths

Damion V. Demeter, Ph.D.

The University of Texas at Austin, 2021

Supervisor: Jessica A. Church-Lang

During childhood, the brain undergoes rapid periods of development that are vital for the cognitive processes supporting goal directed behavior. Some of these processes are termed 'executive functions', and the development of these skills not only impacts academic achievement, but also lifelong success. Successful navigation of executive function relies on the specialized integration of brain regions, thus requiring a network-level view of brain organization to better understand associations with behavioral outcomes. This dissertation examines multiple methods of quantifying patterns of brain activity at rest and tests the association of these measures with individual differences in youth executive function task performance. Study 1 identified patterns of brain activity unique to an individual (termed resting state neural fingerprints) in both youths and adults, using support vector machine classifiers. We found that the classifiers successfully identified an individual's scan from their own previous scan and one twin's scan from their co-twin's scan. Our results suggest that resting state functional fingerprints are stable over time and vary by genetic relatedness. Study 2 quantified patterns of resting state functional network organization in youths, using graph metrics chosen from previous work in the

literature. We then tested methodological factors that impact the ability of these graph metrics to predict measures of executive function task performance. Sample size had the largest impact on our models and even successful models accounted for very little sample variance. These results suggest that graph metrics do capture functional network organization associated with executive functions, but that graph metrics alone are too reductionist to capture complex patterns of brain activation associated with executive function behaviors. Study 3 identified and categorized cortical hubs in youths – regions supporting communication between brain networks – and tested their ability to predict executive function task outcomes. We found that cortical hub parcels in youths qualitatively resemble those found in adults, but form unique, youth-specific categories. Additionally, hubs integrating sensorimotor information and executive function networks related to behavioral outcomes. These studies demonstrate how measures of brain network organization and integration can improve our understanding of the developing brain, and their role in supporting goal directed behavior and individual differences.

Table of Contents

List of Tables

List of Figures

General Introduction

Childhood and adolescence are the periods of life most filled with the accelerated development of novel skills and behaviors. As youth begin to explore the world, their experiences are supported by periods of rapid brain development and growth (Barnea-Goraly et al., 2005; Giedd et al., 1999; Houston, Herting, & Sowell, 2014; Mills et al., 2016; Stiles & Jernigan, 2010). Critically, navigating these ages and the associated development of higher-order cognitive function is not a homogenous process across individuals. Many successes and delays may, at least partially, be associated with individual variations of the normative trajectory of growth and refinement of neural systems throughout the brain. A better understanding of how these systems are organized during development can provide a resource to help mitigate delays and support successes across different youths.

Functional neuroimaging studies have revealed much about how topographically distant cortical regions of the brain coordinate patterns of activation to accomplish biological and behavioral goals. Even while the brain is a rest – not actively engaged in the completion of a specific task – areas across the cortex show synchronization of neural activity over time, in regions responsible for similar biological functions. Evidence for this temporally synchronized coactivation while the brain is in a "resting state" was first identified in functional MRI (fMRI) data within the bilateral motor cortex (Biswal, Zerrin Yetkin, Haughton, & Hyde, 1995). Similar results of resting state coactivation, which resembled activation patterns of these systems during task, were later reported for the other primary sensory systems: the auditory and visual cortex (Cordes et al., 2001; Lowe, Mock, & Sorenson, 1998). However, the same methods used to identify pairwise coactivation between cortical regions of interest in the early sensory systems, has since revealed that coactivation of the "resting" brain is organized into a large network that is further sub-divided into in integrated set of smaller, more specialized networks.

Remarkably, a similar set of these resting state functional networks have been identified in adults, across multiple studies, using different methods, and appear stable across individuals (Gordon et al., 2016; Power et al., 2011; Thomas Yeo et al., 2011). Region of interest (ROI) sets created from these identified networks provide researchers with a method of generalizable comparison of functional coactivation across the cortex, between individuals. One benefit of these generalizable ROI sets, is that they provide a stable, whole-brain representation of the network of coactivation that occurs across the cortex. By analyzing the organizational properties of functional networks that span the entire cortex, resting state fMRI research can identify individual differences in organizational patterns of cortical co-activation that are directly associated with a task, mental health diagnosis, or specific behavioral outcome. Indeed, an increasing body of research has focused on multivariate analyses of fMRI data to identify individual differences associated with human cognition and behavior.

One potential aspect of individual differences that are of specific interest, especially in regard to human development, regards the brain processes supporting executive function. Executive function (EF) is linked to goal achievement, and is related to academic and life success (Best, Miller, & Naglieri, 2011; Jacob & Parkinson, 2015). Identifying how the brain develops and organizes functional networks to complete tasks that rely on the successful use of EFs, can offer valuable insight to how individual differences in functional brain organization may support or hinder the successful navigation of academic and societal situations in childhood.

EF engages higher-level cognitive processes, such as updating of working memory, inhibition, and cognitive flexibility, that are not found to be isolated to any single brain region. Instead, EFs appear to recruit and integrate multiple brain regions (Nowrangi, Lyketsos, Rao, & Munro, 2014). Across three EF task domains of working memory, inhibitory control, and cognitive flexibility, cortical regions in the cingulo-opercular, dorsal attention, fronto-parietal, and ventral attention networks, such as the dorsolateral prefrontal cortex (DL-PFC) and the superior parietal

cortex, have been identified as key neural substrates of task performance (Fiske & Holmboe, 2019; Gao et al., 2013; Nowrangi et al., 2014). The developing brain refines and specializes connections between fronto-parietal cortical regions; this refinement may be a key element to increasing "adult-like" performance on EF tasks (Buss & Spencer, 2018; Mehnert et al., 2013). Previous work has also shown that EF task performance is highly heritable (Engelhardt, Briley, Mann, Harden, & Tucker-Drob, 2015) and that the core neural architecture engaged during those EF tasks is established by mid-childhood (Engelhardt, Harden, Tucker-Drob, & Church, 2019). However, specific individual differences in childhood brain network organization that can explain variations in EF performance are not fully understood. Thus, the examination of brain function associated with EF task performance would benefit from an approach that examines the brain as a large, spatially integrated network of localized activation that is further clustered into highly specialized sub-networks.

The integrated network view of brain activation has provided a richer understanding of how the brain organizes during development (Grayson & Fair, 2017). Even during infancy, functional networks beyond those only associated with sensory stimuli begin to emerge, and representations of higher-order networks found in adults can be identified (Eggebrecht et al., 2017). Further, this network view brain coactivation has also improved our understanding of how the infant brain begins to integrate cortically distributed sub-networks as it begins to establish cortical hub regions (De Asis-Cruz, Bouyssi-Kobar, Evangelou, Vezina, & Limperopoulos, 2016; Fransson, Åden, Blennow, & Lagercrantz, 2011; Gao et al., 2011).

Current research leveraging the integrated network view of brain activity has also begun to identify specific patterns of functional brain network organization that are stable across development (Gordon et al., 2016; Gratton et al., 2018a; Power, Fair, Schlaggar, & Petersen, 2010), unique to an individual (Demeter et al., 2020; Finn et al., 2015; Miranda-Dominguez et al., 2014), or indicative of a mental state or psychological diagnosis (Cordova et al., 2020; Craddock,

Holtzheimer, Hu, & Mayberg, 2009). Much of this network-based fMRI work leverages resting state functional connectivity (RSFC) - resting state brain activation occurring in the absence of a specific externally directed task and fluctuates over time - due to its independence from a specific task state. Although RSFC can be used to reliably map stable patterns of brain activation that are common across different groups and multiple stages of the lifespan, individual differences in functional network organization must also be examined (Gordon, Laumann, Adeyemo, & Petersen, 2017a). By quantifying specific patterns of RSFC organization at the individual level, researchers can identify underlying patterns that may facilitate or impair performance during complex cognitive processes.

This dissertation quantified individual differences in patterns of RSFC network organization, with the aim of improving our understanding of the underlying functional network organization that is associated with successful EF task performance in youths. Specifically, this work 1) tested one method for identifying patterns of RSFC that were unique to an individual in childhood and adulthood, 2) tested whether patterns of information flow in RSFC networks were associated with EF task performance in youths, and 3) measured the association of RSFC brain network integration (using hub development as a measure) with individual differences in EF task performance.

The first study in this dissertation identified a resting state neural fingerprint (a unique characterization of brain function that can distinguish one individual from another) in both youth and adult samples (Demeter et al., 2020). Subjects in this study were included from three locally collected youth neuroimaging datasets and two publicly available adult datasets to create a large cross-sectional sample. The dataset included repeat-scan individuals, monozygotic (MZ) twin pairs, and dizygotic (DZ) twin pairs. This project predicted individuals and co-twin pairs from independent data by applying support vector machine classifiers to RSFC data. In doing so, we were able to identify functional connections that are most vital to a resting state neural fingerprint.

The classifiers successfully identified individuals with 100% accuracy in both age groups, even when repeat-scan collection was separated by months. This result suggests that the neural fingerprint identified with this method is stable over time. Classifier accuracy also decreased as genetic similarity of individuals decreased, suggesting a genetic influence on the organization of RSFC brain networks. Finally, we isolated critical functional connections within each age group to create one common fingerprint for the youth group and one common fingerprint for the adult group. We then retrained the classifiers using the connections identified in the opposite age group (i.e., group-common pediatric connections to identify adults) to assess the similarity of neural fingerprints across age. All classifier accuracies using the opposite-age connections decreased by an average of 31% but remained significantly above chance in all groups except the adult DZ twins. These results suggest that resting state functional fingerprints are stable within individuals and families, are similar over a few decades of life, and vary by genetic relatedness.

The second study applied a literature-informed approach to quantify specific patterns of network organization in RSFC data that are associated with EF task performance in youths. This study also probed common methodological factors that can impact our ability to test for relations between patterns of RSFC network organization and EF task performance. Previous work has theorized that graph metrics (GMs) - measurements that quantify specific organizational patterns within a network - can help identify how brain connectivity at rest is related to behavioral outcomes. Thus, identifying GMs that are associated with EF task performance is of great interest to the neuroimaging community. However, previous results are mixed, primarily focus on adults, and may not replicate after accounting for key RSFC methodological considerations such as sample size and scan length (Farahani, Karwowski, & Lighthall, 2019; Kruschwitz, Waller, Daedelow, Walter, & Veer, 2018). This current work leveraged a combined fMRI dataset of 567 youths, ages 8-17 years old collected either locally at UT Austin (n=67) or for the publicly available Adolescent Brain Cognitive Development (ABCD) Study (n=500). We used resting state

data to calculate four GMs of interest (characteristic path length, efficiency, rich-club coefficient, centrality) previously associated with EF task performance or general intelligence in adults (Farahani et al., 2019; Sinclair et al., 2015). We assessed the impact of 1) length of resting state fMRI scan, 2) sample size, and 3) fMRI processing decisions on the ability of GMs to predict EF task performance scores. We found that sample size, more so than resting state scan length, functional network makeup, or fMRI preprocessing decisions, impacted our models' ability to predict task performance using GMs. Additionally, the chosen GMs accounted for very little of the variance in our models. Our results suggest that GMs are a valid and moderately useful tool for explaining a portion of the variance in EF performance in youths. However, these results also indicate that GMs alone may be too reductionist for the rich and complex nature of neuroimaging data. This reduction of neuroimaging data to a single metric may be the source of differences in extant results and replication difficulty in studies using GMs with RSFC data, as well as the low explanatory power of our results. Our results suggest the need for future work to combine GMs with other measures of neuroimaging data for improved generalization and replication of findings.

The third study expanded upon previous work on adult brain organization and aimed to 1) identify specific categories of hub regions in the brain that integrate RSFC networks in youths, and 2) quantify the association between cortical hub types found in our youth sample and individual differences of EF task performance. Functional networks in the brain are integrated by hub regions that provide strong links between functional networks during task performance and at rest (Cohen & D'Esposito, 2016; Gratton, Sun, & Petersen, 2018b; Wig, 2017). Recently, three specific connector hub categories ("control-default", "cross-control", and "control-processing" hubs) were identified in adults (Gordon et al., 2018) and provide a greater level of specificity in understanding functional network integration across the brain. Further, this work in adults provides evidence that cross-control hubs may play a vital role during EF task performance. However, the extent to which RSFC network hubs can be classified into distinct categories in youths is currently

unknown. Study Three adapted the hub identification methods developed for adult data by Gordon et al. (2018) to our youth data (using the same neuroimaging sample as Study Two, n=567). We identified cortical hubs using the participation coefficient graph metric, categorized youth-specific clusters of hubs based on their RSFC profile, and tested whether greater connectivity in each hub type could predict EF task performance in youths. We found that resting state cortical hubs identified in youths resemble those found in adults. However, youths display stable and developmentally-unique variations of these adult-derived hub categories. Most interestingly, only the two hub categories integrating sensorimotor and classic cognitive control network parcels related to EF task performance. This suggests that, in youths, greater resting state coactivation of hubs that support the coordination of sensorimotor information to and from primary cognitive control networks may facilitate better cognitive performance when engaged in working memory and cognitive flexibility tasks. This study provides a greater understanding of the development of resting state connector hubs during childhood, and how these hubs are categorized into stable, youth-specific groups that qualitatively resemble those found in adults.

As a whole, this dissertation quantifies individual differences in patterns of RSFC network organization and tested the relationship of specific patterns of brain organization to EF task performance. With an improved understanding of how different methods of quantifying functional brain network organization can highlight individual differences in brain activation at rest, this work contributes to a better understanding of unique organizational aspects of the developing brain, and the relationship between brain organization and behaviors that relate to life and academic success.

Study 1: Functional Connectivity Fingerprints at Rest Are Similar Across Youths and Adults and Vary with Genetic Similarity[1]

INTRODUCTION

One anticipated use of functional magnetic resonance imaging (fMRI) data is to identify reliable and clinically viable biomarkers for disease states. However, a more precise understanding of healthy functional brain network organization is necessary to achieve this goal. Resting state functional connectivity (rs-fcMRI) holds promise as a noninvasive method of reaching this goal, due to its low behavioral demand, consistency within individuals, and stability over time (Poldrack et al., 2015). Further, rs-fcMRI reveals inherent functional brain networks absent of a specific task state. These averaged networks are reliably observed across adult samples (Cohen et al., 2008; Power et al., 2011), and early functional network organization is readily identified early in life. By six months of age, early organizational patterns of common adult resting state networks such as the default mode (DMN), somatosensory motor (SSM), and visual (VIS) networks are identified (Mitra et al., 2017) and appear to become more adult-like in their organization and interaction during development (Gao et al., 2013; Lin et al., 2008).

Given the goal of identifying distinct biomarkers of disease, combined with the stability of rs-fcMRI brain networks, it is not surprising that a growing body of neuroimaging research has focused on defining functional "connectomes" or "fingerprints" of individuals based on their fMRI data (Byrge & Kennedy, 2019; Finn et al., 2015; Horien, Shen, Scheinost, & Constable, 2019; Miranda-Dominguez et al., 2018, 2014; Xu et al., 2016). A greater understanding of how functional connections become organized into reliable, functional fingerprints of an individual could give researchers and clinicians alike a quantifiable measure of individual change over time. Additionally, a more precise understanding of the genetic influence on normative network

[1]Adapted from: Demeter, D. V., Engelhardt, L. E., Mallett, R., Gordon, E. M., Nugiel, T., Harden, K. P., … Church, J. A. (2020). Functional Connectivity Fingerprints at Rest Are Similar across Youths and Adults and Vary with Genetic Similarity. *IScience*, *23*(1), 100801. https://doi.org/10.1016/j.isci.2019.100801

organization throughout development may help pave the way for a more precise measure of the impact of environmental and disease variables on brain network organization. While extant research consistently reveals the presence of a functional fingerprint in rs-fcMRI data across multiple methodologies (Balsters, Mantini, & Wenderoth, 2018; Finn et al., 2015; Haak, Marquand, & Beckmann, 2018; Kaufmann et al., 2017; Miranda-Dominguez et al., 2014), far less is known about the specific pattern of discrete functional connections that distinguish individuals from one another; specifically, whether these patterns differ at different ages or stages of development.

Studies using rs-fcMRI to identify individuals via functional fingerprint implicate the DMN and its connectivity to putative control networks -- such as the cingulo-opercular (CO), dorsal attention (DA), fronto-parietal (FP), and ventral attention (VA) networks -- as the most highly distinctive between individuals (Finn et al., 2015; Horien et al., 2019; Miranda-Dominguez et al., 2018). Given previous evidence that the FP network coordinates other networks for task performance (Cole et al., 2013; Dixon et al., 2018; Marek & Dosenbach, 2018; Marek, Hwang, Foran, Hallquist, & Luna, 2015; Power, Schlaggar, Lessov-Schlaggar, & Petersen, 2013; Zanto & Gazzaley, 2013), specific patterns of connectivity between the FP and other networks could be highly individualized during rest (Gordon et al., 2018), and that degree of network integration may be reflected in functional fingerprints. The network integrating role of the FP network and the DMN's role in internal, self-focused mentation and mind-wandering (Buckner, Andrews-Hanna, & Schacter, 2008; Mason et al., 2007; Raichle, 2015) are presumably highly individualized and may explain their importance in the functional fingerprint, but this connection has not yet been explored directly. Despite the growing understanding of the functional networks involved in the make-up of a functional fingerprint, a consensus of specific functional connections that yield the most accurate identification of individuals has not yet been established.

Crucial to establishing a functional fingerprint, is a better examination of the impact of individual variance in relation to expected functional network organization, and the influence of heritable factors on rs-fcMRI. Gratton and colleagues (2018) recently revealed that averaged group differences in functional network organization are driven more by individual variability and common participant features, with only a modest influence of cognitive or task demands. This suggests that group-level results that do not explicitly account for individual differences in functional network organization may misattribute person-specific effects to group-level task performance. Similarly, evidence of distinct organizational variations from the expected group-level resting state functional network topography was found in a subset of the adult population (Gordon et al., 2017a). Given that individual differences in functional network organization can be buried in group-averaged analyses, an individual variance framework is vital for accurately characterizing functional network organization across multiple samples.

Another factor to consider in characterizing a functional fingerprint is the genetic impact on rs-fcMRI network organization. Fu and colleagues (2015) observed a significant genetic influence on resting state organization across sensory – but not cognition-related -- networks in a pediatric sample of twins (ages 12-19 years). The authors posited that the age of their sample and the protracted development of cognitive functions that require coordination across many networks might be why cognition-related networks showed a weaker genetic influence. Indeed, in genetic studies of adult twins, within-network connectivity of the DMN is found to be the most heritable (Glahn et al., 2010; Xu et al., 2017). Recent work has found evidence that an individual's functional fingerprint, calculated via a model-based approach to identifying a functional fingerprint called "connectotyping", also shows a pattern of genetic influence in adults (Miranda-Dominguez et al., 2018). In this study, identification accuracy was highest in identical (monozygotic, or MZ) twins, followed by fraternal (dizygotic, or DZ) twins, with non-twin siblings showing the lowest accuracy. However, analyses that include larger and more age-diverse twin

samples are necessary to identify specific patterns and developmental trajectories of highly heritable and individually unique functional connections within resting state data. The inclusion of genetically informative, age-varying neuroimaging datasets is important to gain a complete understanding of the genetic influence on individually unique rs-fcMRI connections.

Based on mounting evidence from functional fingerprint research, we hypothesized that adapting resting state timecourses to use ANOVA feature selection would benefit our analyses. Current resting state approaches often use all available features from a chosen ROI set -- thus providing too many features that can overpower the signal with noise -- or apply feature reduction methods that may be more appropriate for group membership classification (Dosenbach et al., 2010; Greene et al., 2016). This shift in resting state feature selection could provide a clean and straightforward method of isolating a core-set of unique functional connections for each individual, which then contributes to the group feature set. Additionally, tracking these specific sets of connections across developmentally diverse samples and testing the degree of similarity within MZ and DZ twin pairs, may advance our understanding of the influence of genetic similarity on the functional fingerprint and its stability into adulthood. The current work uses three in-house pediatric datasets and two publicly available adult datasets (see Study 1, Table 1 for detailed subgroup demographics) to identify individuals and twin pairs via support vector machine (SVM) classifiers (De Martino et al., 2008; LaConte, Strother, Cherkassky, Anderson, & Hu, 2005) applied to rs-fcMRI data.

Study 1, Table 1: Participant Demographics

Group Characteristics							
	UT Repeat	**MSC Repeat**	**UT MZ**	**HCP MZ**	**UT DZ**	**HCP DZ**	**UT SS**
Scan Count	30	20	30	50	38	50	34
"Pairs" (# Female)	15 (9)	10 (5)	15 (24)	25 (26)	19 (16)	25 (26)	17 (12)
Age Range	9.8 - 18.3	24 - 34	8.9 - 13.2	26 - 34	9.1 - 13.9	22 - 35	8.8 - 18.6
Age (M ± SD)	12.9 ± 2.6	29.1 ± 3.3	10.8 ± 1.3	29.8 ± 2.2	11.3 ± 1.3	29.2 ± 3.5	12.2 ± 2.7
IQ/PMAT (M ± SD)	102.3 ± 14.1	128.8 ± 6.6	106.3 ± 17.2	17.2 ± 4.3	105.2 ± 11.7	18.3 ± 4.0	108.3 ± 13.0
Mean FD (M ± SD)	0.10 ± 0.02	0.13 ± 0.02	0.10 ± 0.03	0.12 ± 0.02	0.10 ± 0.02	0.12 ± 0.02	0.10 ± 0.02

Note: We included two scans for each participant in the repeat scan groups. All other groups consist of one scan per individual. HCP participants' intelligence score was calculated from the Raven's Progressive Matrices; all other groups are IQ scores. Framewise displacement (FD) means and standard deviations are post-motion scrubbing.

UT = Developmental participants collected at The University of Texas at Austin
MSC = Midnight Scan Club adult participants
MZ = Monozygotic Twin Pairs, DZ = Dizygotic Twin Pairs

HCP = Human Connectome Project adult participants
SS = Developmental same-sex pairs (Includes DZ twins and non-twin sibling pairs of the same sex)

Starting from a common pre-defined region of interest (ROI) set (Power et al., 2011), we isolated subsets of functional connections via ANOVA feature selection that best discriminated between individuals within each group. Next, we identified individuals and twin pairs by training and testing fMRI pattern classifiers using those connections identified during feature selection. Groups of repeat scan individuals had one scan from that individual in the training set and a different scan of the same individual in the testing set. For twin groups, one twin's scan was in the training set and their co-twin's scan was in the testing set (see Transparent Methods in the supplemental information for detailed information on feature selection and classification). We then mapped those functional connections consistently chosen as features to identify a functional fingerprint for each group. Finally, we tested the generalizability of commonly selected connections across our two age groups, by first defining an age-specific feature set for each age group, then applying pediatric features on adult groups during classification and vice versa. The

aim of this work was to extend the current body of emerging research by providing a better understanding of the impact of development and genetic similarity on the resting state functional fingerprint. Our research suggests: (1) Individually unique patterns of functional connectivity are similar among family members and vary with genetic similarity; (2) The general pattern of resting state functional connections that are highly predictive of an individual translates across different ages and groups, and appears stable within individuals during development and into adulthood.

RESULTS

SVM classifiers predict individuals and co-twin pairs:

We applied ANOVA feature selection on segmented resting state timecourses to identify features that best discriminated between individuals (see methods for detailed description). We then applied the resulting feature mask on all full 5-minute resting state timecourses used for SVM classification (Study 1, Figure 1). For all groups, the SVM classifier accurately predicted matched scans (individual repeat scans, co-twins, or same-sex siblings) at levels significantly above chance (Study 1, Figure 2a). This set of accurate classifications was observed when the classifier was run with a single leave-one-group-out cross-validation (2-fold) scheme, as well as with our permutation average accuracy, but only the permutation accuracies are reported (Study 1, Table 2). The classifier accuracies for all groups: (1), UT Repeats: accuracy=1.0, chance= 0.06, $p<.001$; (2), MSC Repeats: accuracy=1.0, chance= 0.1, $p<.001$; (3), UT MZ Twins: accuracy=0.52, chance=0.06, $p<.001$; (4), HCP MZ Twins: accuracy=0.56, chance=0.04, $p<.001$; (5), UT DZ Twins: accuracy=0.24, chance=0.05, $p<.001$; (6), HCP DZ Twins: accuracy=0.22, chance=0.04, $p<.001$; (7), UT Same-sex Sibling Pairs: accuracy=0.35, chance=0.06, $p<.001$.

Study 1, Figure 1: ANOVA feature selection and SVM classification

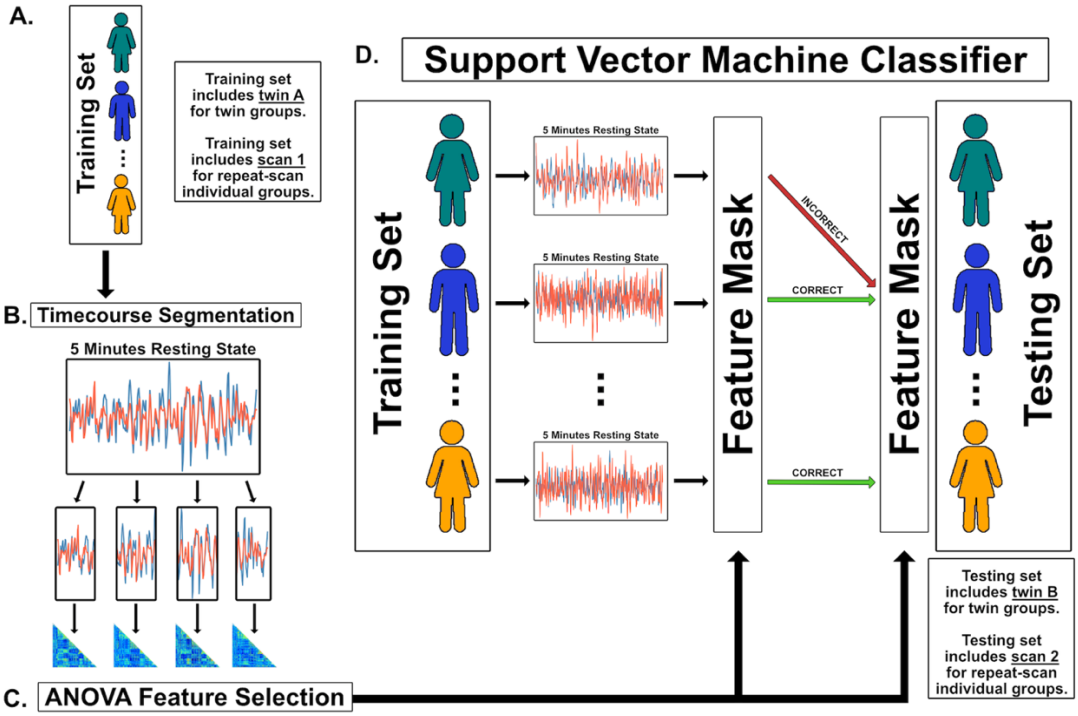

Note: (A.) Individuals within the training set (twin A for twin groups or scan 1 for repeat-scan individuals) provided 5-minutes of resting state timecourses, extracted from each of the 255 ROIs. (B.) Timecourses were then split into 20-second segments and a correlation matrix was created for each segment. All correlation matrices were then converted into vectors of unique, off-diagonal correlation values. (C.) These vectors were then used for ANOVA feature selection to create the feature mask used by the classifier. (D.) The resulting feature mask is then applied to each full 5-minute resting state timecourse and the SVM classifier is trained on the same training set used for feature selection, and tested on the held-out testing set (either the individual's second scan or co-twin data).

Functional fingerprints are similar across age groups:

The summed fold-rank matrices for the pediatric (Study 1, Figure S2) and adult (Study 1, Figure S3) groups were examined to explore which functional connections were repeatedly chosen as features across subgroups. The data indicated that connections carrying the most consistently useful identifiers of an individual belonged to the fronto-parietal network (FP) and the default-mode network (DMN) (Study 1, Figure 3a). Out of the total 32,385 possible unique functional connections, our fold-rank matrix thresholding revealed 87 connections in the pediatric group and 110 in the adult group that were the most consistently representative of an individual in the SVM classifier. Both the pediatric and adult groups revealed a functional fingerprint mask dominated by

longer, ipsilateral connections in the front-parietal (FP) and default-mode network (DMN) and short-range contralateral connections in the posterior DMN and visual (VIS) networks. Of the total 197 post-threshold features within both age groups, 13 features (6.59%) were identical across the pediatric and adult groups.

Study 1, Figure 2: SVM classifiers predict individuals and co-twin pairs

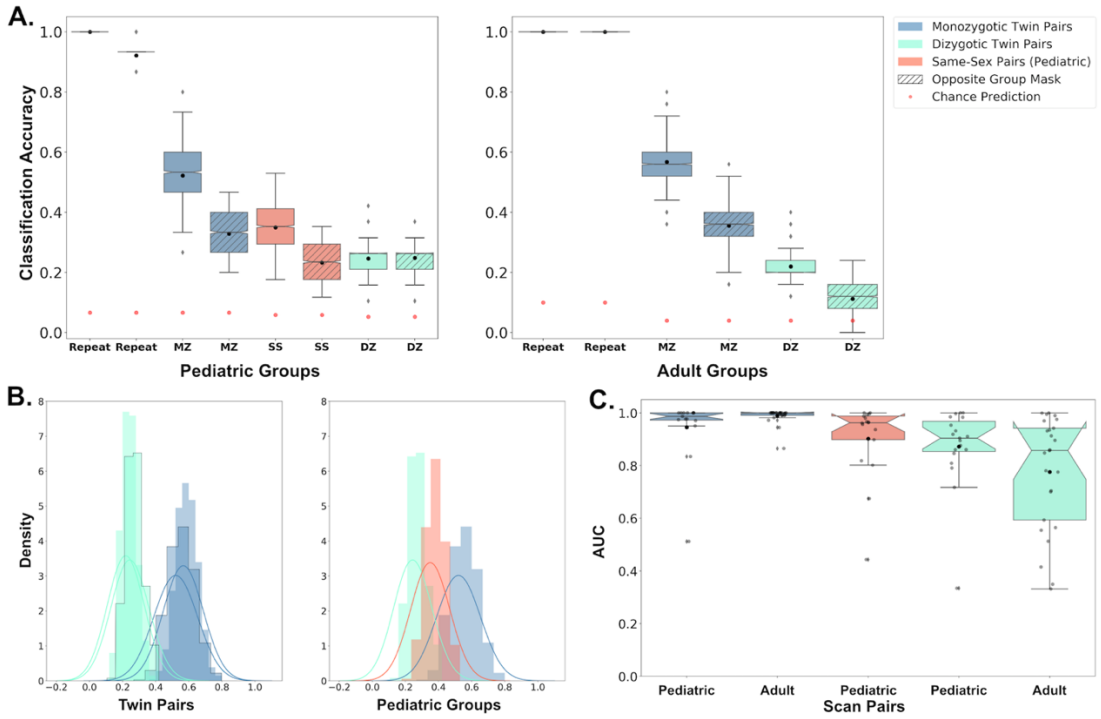

Note: (A.) Mean SVM classifier accuracies, per group. Error bars are 95% confidence intervals. Both repeat visit subgroup accuracy scores were 1.0. Monozygotic (MZ) twins in both subgroups outperformed dizygotic (DZ) twins. Hatched box plots indicate when the opposite age-group's feature mask was used for classification. All group accuracies are reduced when using the opposite mask, except for the Adult MZ twins, but all groups prediction scores were significantly better than chance, except the Adult DZ group.
(B.) Distributions of accuracy scores in the twin groups, across age sets, show a similar distribution and mean accuracy score. The spread of distributions reinforces the decision to shuffle twin labels to ensure accidental group assignment bias does not influence group accuracy. The pediatric same-sex sibling pair group outperformed pediatric DZ twins, suggesting an influence of sex on functional network organization.
(C.) AUC values, which represent classifier sensitivity for each related scan pair. Repeat visit individuals are not plotted, as AUC values were 1.0 for all. A lower group average and larger distribution of AUC values in both DZ groups suggests differences in DZ twin pairs' functional fingerprint resulted in more false positives when classifying DZ twins than MZ twins. This is amplified in the adult DZ twins, compared to their pediatric counterparts.

We then examined the functional network affiliation of the ROIs chosen as features in the pediatric and adult group. Post-threshold features were labeled by their functional network

affiliation and ordered by frequency. This revealed a similar pattern of network representation between the two age groups (Study 1, Figure 3b): The largest percentage of network representation was 1) within the DMN network (DMN to DMN) (Adults = 29 (26.3%); Pediatric = 21 (24.1%)), followed by 2) between the DMN and FP network (Adults = 18 (16.3%); Pediatric = 12 (13.7%)), and 3) within the FP network (FP to FP; Adults = 16 (14.5%); Pediatric = 12 (13.7%)). After the top ~50% of connections, chosen features did not show any discernable pattern between the two groups and involved networks that often consisted of only a few connections.

To test the impact of the number of ROIs within each network on the observed patterns of network representation for each group, we simulated 10,000 feature sets for each group. Each simulated feature set consisted of the same number of features as our group fold-rank matrices (Adult = 110; Pediatric = 87), with all connections chosen at random (without replacement) from the list of all possible connection types. We then averaged how often the main connection types found in our group matrices were included in the 10,000 simulations and calculated the proportion of the feature set each accounted for. The average network representation in our simulated feature sets were 1) within DMN network (Adults = 5.4 (4.95%); Pediatric = 4.3 (4.92%)), 2) between the DMN and FP network (Adults = 4.8 (4.40%); Pediatric = 3.8 (4.38%)), and 3) within FP network (Adults = 1.0 (0.90 %); Pediatric = 0.8 (0.91%)).

Study 1, Figure 3: Chosen Features of the Functional Fingerprint

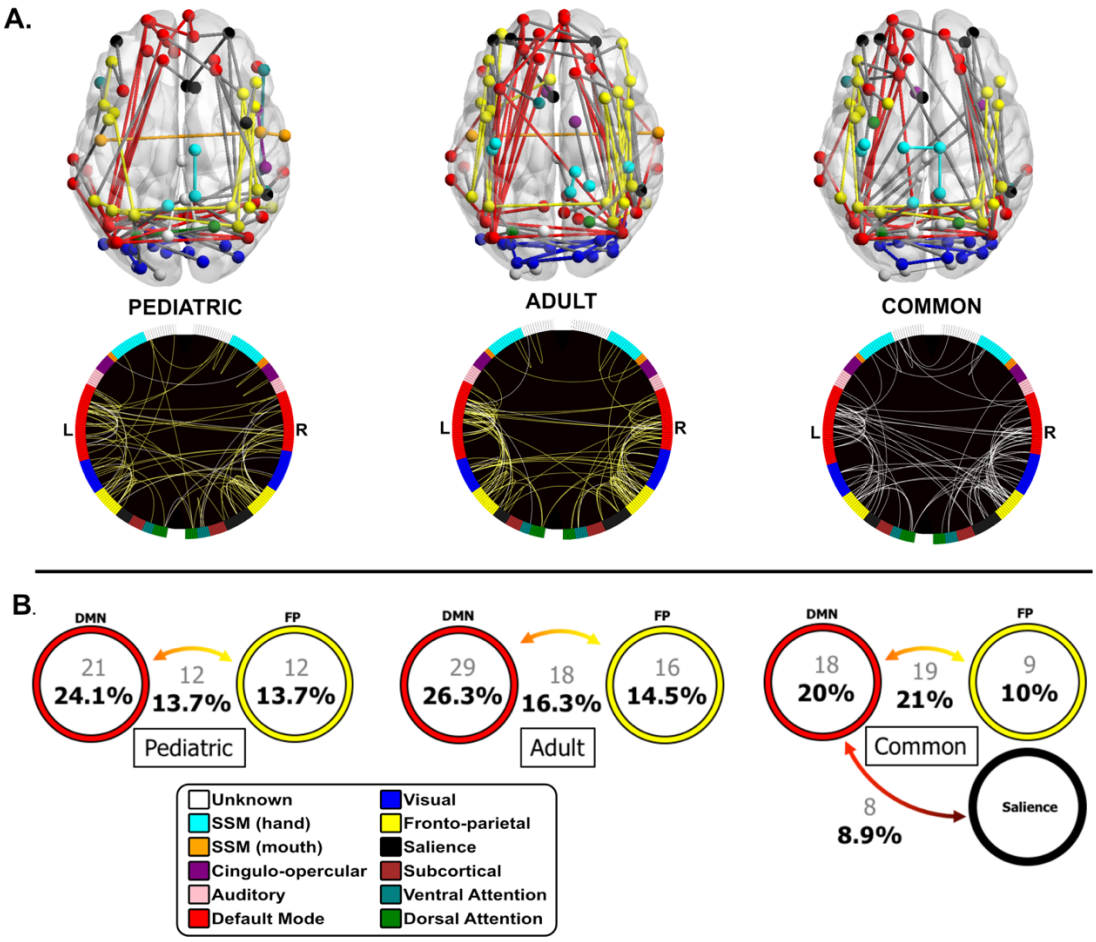

Note: (A.) Pediatric and adult functional fingerprint mask connections are displayed. Out of a possible 32,385 unique functional connections, 87 pediatric and 110 connections survived at this threshold. A common set mask was created that represented connections that were chosen at least once within all six subgroups in the pediatric and adult groups. 90 functional connections survived this threshold in the common mask. (See also Study 1, Figures S2, S3, and S4.)

(B.) Ranking connections in each mask based on their network representation revealed the largest percentage of connections were within the DMN network, followed by between the DMN and FP network, and within FP network. The common set mask revealed connections representing between FP and DMN, within DMN, within FP, and between the DMN and salience (SAL) network connections.

Next, we examined the common set rank matrix (all connections chosen for at least one fold across all pediatric and adult subgroups) using the same steps outlined above. The data revealed a nearly identical representation of network assignment across the functional connections (Study 1, Figure 3b). Out of a total 90 connections in the common set rank matrix, 19 (21%) represented between FP and DMN network connections, 18 (20%) represented within DMN

connections, 9 (10%) represented within FP connections, and 8 (9%) represented connections between the DMN and salience (SAL) networks. The same 10,000 simulated feature sets were created with 90 connections to compare to this common set rank matrix. The simulated sets showed an average of 3.9 (4.36%) between FP and DMN, 4.4 (4.92%) within DMN, 0.8 (0.09%) within FP, and 2.8 (3.16%) between DMN and SAL connections.

Common feature sets have classification utility for opposite age group:

In an effort to quantify the similarity of pediatric- vs adult-specific connections chosen as features, we used the summed fold-rank matrices as feature masks on the original timeseries and re-ran the SVM classifier permutation analysis. All connections with a value of five or six, after thresholding, were used as features. The pediatric groups were run with the adult feature mask (110 features) and the adult groups were run with the pediatric feature mask (87 features). There were 13 identical features that overlapped the pediatric and adult feature sets. Using the opposite age group's top-ranking features mask resulted in significant, although reduced, classifier accuracy for all groups except the MSC Repeats and resulted in non-significant accuracy for the HCP DZ twin subgroup (Study 1, Figure 2a).

When the adult subgroups were trained using the pediatric-specific feature mask (Study 1, Table 2), classifier accuracies were: MSC Repeats (accuracy=1.0, chance= 0.1, $p<.001$); HCP MZ Twins (accuracy=0.35, chance=0.04, $p<.001$); HCP DZ Twins (accuracy=0.11, chance=0.04, $p=.065$). When the pediatric subgroups were trained using the adult-specific feature mask, classifier accuracies were: UT Repeats (accuracy=0.92, chance= 0.06, $p<.001$); UT MZ Twins (accuracy=0.32, chance=0.06, $p<.001$); UT DZ Twins (accuracy=0.24, chance=0.05, $p<.001$); UT Same-sex Sibling Pairs: (accuracy=0.23, chance=0.06, $p=.015$).

Study 1, Table 2: Mean Classifier Accuracies per Group

	Group Chance	Mean Accuracy	Lower 95% CI	Upper 95% CI	Mean Accuracy (Opposite Age Mask)	Lower 95% CI	Upper 95% CI
UT Repeat	0.063	1.00**	-	-	0.92**	0.919	0.922
MSC Repeat	0.100	1.00**	-	-	1.00**	-	-
UT MZ Twins	0.066	0.52**	0.518	0.525	0.32**	0.322	0.327
HCP MZ Twins	0.041	0.57**	0.565	0.571	0.35**	0.353	0.359
UT DZ Twins	0.053	0.24**	0.242	0.247	0.24**	0.243	0.248
HCP DZ Twins	0.039	0.22**	0.218	0.222	0.11	0.108	0.112
UT SS Siblings	0.057	0.35**	0.349	0.354	0.23*	0.232	0.236

Note: Group chance values are empirical chance and are calculated by running the classifier after randomly shuffling scan pair labels (scan pairs were no longer correctly labeled with their matching scan). The left side of the table is running the classifiers normally and the right side is running the classifier with the opposite age-group's feature mask.

* = p<.05, ** = p<.001 - Classifier Performance vs. Chance

DISCUSSION

In the current work, we address the stability and similarity of the functional fingerprint within pediatric and adult samples. Further, we directly tested the ability of a functional fingerprint identified in our developmental sample to successfully identify adults, and vice-versa. These results provide initial evidence that the functional fingerprint found in pediatric samples is remarkably similar to the functional fingerprint found in adulthood and contributes to a better understanding of the stability of the brain's functional fingerprints over age.

First, we identified the specific functional connections that were most consistently representative of an individual across multiple subgroup comparisons and tested their utility to predict individuals in the opposite-age datasets with substantial success. We then used SVM classifiers to identify an individual based on a previous scan or the scan of a genetic relative, across multiple pediatric and adult neuroimaging datasets. We also provided evidence that segmentation of resting state timecourses is a viable means to provide multiple samples for ANOVA feature selection. We believe this type of feature selection can identify highly individualized functional connections within a "functional fingerprint" of an individual. This process results in a more accurate characterization of functional connectivity within an individuals' resting state signal and

can identify a more discriminating set of functional connections than averaging the full timecourse during feature selection.

Our results also replicate and extend the generalizability of previous work that assessed fMRI-based functional fingerprints in adults, by highlighting the role of genetic similarity on functional fingerprinting. MZ twins in both the pediatric and adult subgroups exhibited similar and higher classifier accuracy of rs-fcMRI data than DZ twins. Including only same-sex siblings in our pediatric subgroup significantly improved classifier accuracy of ~50% genetically similar individuals, but the classifier still did not reach the level of MZ classification accuracy. This suggests an influence of biological sex on functional fingerprint similarity.

SVM Classifier Accuracy Reveals a Genetic Impact on Functional Fingerprint

We observed higher classification accuracy for MZ co-twins than DZ co-twins in both the pediatric (MZ=0.52; DZ=0.24) and adult (MZ=0.57; DZ=0.22) subgroups. These results provide evidence of a genetic influence on the organization of highly individualized resting state functional connections. SVM classifier accuracy scores supported our prediction that classifier performance would be highest in subgroups with greater genetic similarity. It is notable that classifier accuracy was greater for repeat scans than for MZ twin subgroups, given that both groups include scans that share 100% genetic similarity. One possible explanation for reduced classifier accuracy (compared to repeat scan individuals) in both MZ twin subgroups is an increase of individual differences in network organization emerging with age (Freund et al., 2013). However, neither environmental influence nor age could be directly and accurately tested in the current dataset. The observed decrease in classifier accuracy from MZ to DZ twins also aligns with previous work that used the model-based connectotyping method (Miranda-Dominguez et al., 2018). Although the connectotyping method differs from our approach, our results provide corroborating evidence from a different methodology that a functional fingerprint in resting state network organization is, in fact, impacted by genetic similarity. Further, the current work emphasizes that this genetic impact

is found in direct measures of resting state functional connectivity in both pediatric and adult participants. This similarity across age groups provides initial evidence that the pattern of organization within a functional fingerprint may be established early in life and is similar to that found in adulthood.

We expected the pediatric groups to exhibit overall lower classifier prediction accuracy due to ongoing organization of resting state functional networks throughout adolescence (Cai, Dong, & Niu, 2018; Fair et al., 2007; Grayson & Fair, 2017; Power et al., 2010; Satterthwaite et al., 2013). Somewhat surprisingly, adult and pediatric twin groups showed similar prediction accuracy on the basis of zygosity. During development, individuals may share a level of common developmental change as a result of age-related stages of network organization, regardless of genetic similarity. One possible reflection of this common change can be seen in distribution of classifier sensitivity scores (Study 1, Figure 2c).

Sensitivity scores were derived using area under the receiver operating characteristic curve (AUC) which were calculated from each scan pair's true positive and false positive classifications. While both adult twin groups showed higher average group accuracy scores than the pediatric twin groups, the adult MZ twins showed significantly higher AUC scores than the adult DZ twins ($p<0.0001$). However, the pediatric MZ twins did not show significantly different AUC scores than the pediatric DZ twins. Qualitatively, the larger spread of AUC scores within both DZ groups is more pronounced in the adult DZ group and highlights a higher rate of classifier confusion for adult DZ twin pairs. This increase in classifier confusion between adult scan pairs may be due to a reduction of shared developmental changes in functional network organization and increased environmental discrepancy between co-twins that is amplified as they age.

Top Predictive Features Reveal Similar Key Network Representation

Mapping the top features repeatedly chosen across subgroups revealed that connections in the DMN and FP networks most consistently differentiated individuals, facilitating correct SVM

classifier identification. It is important to note that the DMN is the most highly represented in our ROI set (57 out of a total 255). However, we find the high similarity in percentage and type of connection between the pediatric and adult groups (Study 1, Figure 3b) is informative in regard to the stability of individually unique connections. Indeed, using the features from one age group (e.g. top features from the adult sample) to predict the other age group (e.g. the pediatric subgroups) was significantly greater than chance in all but the adult DZ group, though less optimal than features derived from one's same age group (Study 1, Figure 2a). Further, feature set simulations choosing the same number of connection types at random highlighted the unique nature of the network representation and type of connections within both age groups' feature sets. The similarity of network representation of chosen functional connections across pediatric and adult groups contradicted our hypothesis that children and adolescents would have a different pattern of chosen connections relative to adults. Higher-order cognitive functions such as problem solving (Fedorenko, Duncan, & Kanwisher, 2013; Hearne, Mattingley, & Cocchi, 2016; Price, Yeo, Wilkey, & Cutting, 2018), task switching (Church, Bunge, Petersen, & Schlaggar, 2017; Cole et al., 2013; Loose, Wisniewski, Rusconi, Goschke, & Haynes, 2017), and sustained attention (Crittenden, Mitchell, & Duncan, 2016; Lawrence, Ross, Hoffmann, Garavan, & Stein, 2003; Marek & Dosenbach, 2018) rely on putative control networks such as the FP and CO networks, and behaviorally show substantial differences between children and adults. The essential nature of these networks for human functioning is likely highly individualized in their specific instantiation and therefore likely to be included in the functional fingerprint. This study demonstrates potential age invariance in these networks' contributions.

Previous work exploring functional fingerprints also implicate the FP and DMN networks as highly predictive of an individual (Finn et al., 2015; Horien et al., 2019; Miranda-Dominguez et al., 2018), though consistency of specific connections across age groups was not fully explored. Our results expand and clarify these previous findings, suggesting that although these systems are

still maturing and integrating throughout adolescence, the individualized aspects of these core connections may be established early on. However, some age-unique connectivity effects are likely embedded within these connections, as swapping the feature sets between age groups produced lower, though still significant, accuracy across nearly all groups. Based on the successful classification performance after swapping feature sets, one critical interpretation is that the inclusion of specific types of connections, at a specific ratio or count, may hold a high level of importance in identifying individuals from their functional fingerprint. More work exploring the developmental trajectory of functional connections that form a generalizable functional fingerprint is necessary, but our initial findings suggest a unique pattern is established, stable, and useful for identifying individuals even before whole-brain functional network organization is fully solidified in early adulthood.

Motion Artifacts Unlikely Contributor to Classifier Accuracy

It is well established that motion contributes substantially to noise and rs-fcMRI results (Laumann et al., 2016; Power, Barnes, Snyder, Schlaggar, & Petersen, 2012; Power et al., 2014; Van Dijk, Sabuncu, & Buckner, 2012). In-scanner motion is linked to distance-dependent artifacts that especially impact measurement of long-range connections (Satterthwaite et al., 2012; Van Dijk et al., 2012). Our fold-rank matrices (Study 1, Figure S2 & Figure S3) revealed that the majority of chosen features for both age groups came from longer, ipsilateral connections between anterior and posterior ROIs, as well as short-range, contralateral connections within posterior parietal DMN and VIS network ROIs. Critically, these results were consistent across age groups, suggesting that age-related differences in scanner motion did not drive the contribution of long-range connections to classifier accuracy. In an effort to directly test the ability of motion to drive our classifier accuracies, the classifiers were trained on FD values in place of functional connectivity values. However, FD motion calculations provide only one value per TR, in contrast to the 32,385 possible unique functional connections, and therefore the feature selection step could

not be realistically performed. The reduced amount of data is under-powered for this type of analysis. Although testing classifier accuracies with the single vector of FD values is not an accurate comparison to our main methods, classifier accuracies using FD values did not approach significance for any group.

Moreover, our current work rigorously followed current best practices in neuroimaging data preprocessing and motion correction, in an effort to mitigate the influence of motion on classifier accuracy. The mean FD for all individuals and groups were well within the normative range for both pediatric and adult resting state analyses, no major motion outliers were included in our groups, and the chosen FD of .25mm is at or below commonly accepted motion censoring thresholds. Taking each of these motion considerations into account, we believe the influence of motion on our classifier results is minimal. However, future approaches can possibly put this presumption to the test.

Limitations of the Study

Although this study expands upon recent findings in functional fingerprinting and genetic influences on rs-fcMRI organization, the following limitations must be considered. One limitation is the size of the pediatric twin sample. It is difficult to recruit and successfully retain pediatric neuroimaging participants. At the time of analysis, the neuroimaging branch of the Texas Twin Project was one of the largest pediatric twin resting state datasets, but did not provide a sufficient number of scans to fully explore analyses such as the effect of same-sex DZ pairs. Soon after completion of the current study's analyses, raw imaging data and genetic information necessary to calculate zygosity has been released from The Adolescent Brain Cognitive Development Study dataset (Casey et al., 2018; Volkow et al., 2018). This multi-site dataset includes a large number of MZ and DZ pediatric pairs, and inclusion of these data should be included in future analyses to better explore group differences. Additionally, many unknowns are introduced in the realm of functional organization during development. Currently, the exact developmental trajectory of

functional network organization is unknown. Incorporating future methods that quantify and account for age-related changes in network organization would further clarify the accuracy of the SVM classifier results in our pediatric subgroups.

Future analyses should explore other potential influences on classifier accuracy, such as same-sex vs opposite-sex sibling pairs. We indirectly investigated the impact of sex on identification accuracy within families by including a same-sex sibling group and comparing that to the MZ and DZ twin groups. However, siblings in this group necessarily differed by age, thus introducing a separate confound. Matching declared sex for sibling pairs did, in fact, result in higher SVM classifier accuracy of the same-sex sibling pairs than the pediatric DZ twin pairs (which was not sex-matched), suggesting a notable impact of sex variance on identification of individuals through this approach. There are limited rs-fcMRI studies that directly address sex differences in healthy twin populations and the precise source of sex differences on functional network organization is still not fully understood (Hjelmervik, Hausmann, Osnes, Westerhausen, & Specht, 2014; Satterthwaite et al., 2015). Future analyses on larger twin datasets can better parse out and control for sex differences between genetically related individuals.

CONCLUSIONS

The ability of rs-fcMRI pattern classifiers to identify matched pairs of participants in pediatric and adult samples decreased as genetic similarity decreased. This suggests a genetic influence on the pattern of highly individualized functional connections within a functional fingerprint. Connections within the identified functional fingerprint were dominated by regions in the DMN and FP networks, suggesting that integration of higher order functional networks plays a key role in establishing the organization of individualized functional fingerprints. This pattern of connections appears to be established early in life and, importantly, is similar enough in children and adults to often allow for significant classification of individuals using the opposite age group's selected features.

Study 2: Quantifying Patterns of Resting State fMRI Associated with EF Task Performance in Youths

INTRODUCTION

Executive functions (EFs) are a set of complex cognitive processes that guide goal-directed behaviors, and are related to both academic and life success (Best et al., 2011; Jacob & Parkinson, 2015). Behaviors that rely on EFs engage higher-level cognitive processes, such as the ability to switch between a set of rules or tasks (cognitive flexibility), to control or stop actions or thoughts (inhibition), or to maintain and update a number of items in memory (working memory/updating). During childhood and adolescence, the development of EF skills is especially important, as this period of life is a time of both social and skill-based growth. Difficulty with control over one's behavior can impact everything from interacting with peers or learning a new hobby, to recruiting and maintaining the attention and cognitive abilities required to succeed at academic goals. While outcomes of EF skills exhibit great improvement during childhood, previous work has found that not only is EF task performance highly heritable (Engelhardt et al., 2015), but that the neural architecture that is essential for successful EF task performance is already established by mid-childhood (Engelhardt et al., 2019). This work suggests that brain network dynamics that are essential for EF task performance can be identified early in life, even though significant maturation of EF task performance is observed to continue through childhood, adolescence, and into young adulthood (Best & Miller, 2010; Ferguson, Brunsdon, & Bradford, 2021).

The neural activity responsible for EF is not isolated to one distinct area of the cortex; EFs demand the successful integration and recruitment of multiple brain regions (Church et al., 2017; Dosenbach et al., 2006; Engelhardt et al., 2019; Nowrangi et al., 2014). Further, previous work has shown that the cortical representation of brain activity associated with individual tasks within three domains of EF (cognitive flexibility, inhibition, and working memory/updating) is overlapping in children (Engelhardt et al., 2019; Nugiel et al., 2020) and similar overlap in control-

demanding tasks is observed in adults (Crittenden et al., 2016; Dosenbach, Fair, Cohen, Schlaggar, & Petersen, 2013; Nowrangi et al., 2014). Not surprisingly, the majority of overlap across EF task brain activity is predominantly in cortical areas associated with resting state functional networks attributed to attention-based or control-based behaviors, such as the fronto-parietal and cingulo-opercular networks (Fiske & Holmboe, 2019; McKenna, Rushe, & Woodcock, 2017).

These prior findings suggest that EF task performance is dependent on the successful and efficient integration of cortical activation in regions classically assigned to "higher level" or "cognitive control" functional brain networks. Previous work expands this idea of integration further, and states that successful attention and cognitive control is dependent on the efficient integration of sensory systems, which guide the input and output of task behavior, to cognitive control systems necessary for successful task performance (Petersen & Posner, 2012). Deficits that young children experience in the successful navigation of EF-related behaviors may therefore be as strongly associated with individual differences in brain network integration, as they are with the anatomical development of these regions. Given the need for cross-network integration in successful EF task performance, a deeper understanding of the patterns of organization that may impact information flow within these networks, and the relationship of that organization to EF task performance, is important for understanding cognitive development in youths.

One set of tools for quantifying functional brain network organization is termed graph metrics (GMs). GMs provide a deeper understanding of the organizational structure of a network (or graph) by quantifying specific traits of that network, such as ease of information flow from one region in the network to all others (Sporns, 2018; Wang, 2010). When calculating GMs, we define a network as a series of nodes (regions of interest) that are connected by edges (a value quantifying the strength of the relationship between two nodes). For resting state functional connectivity (RSFC), we define these edge values as the pairwise correlation of the average brain activity of a pair of nodes over time. By calculating GMs from RSFC data, we are able to quantify specific

traits of functional network organization, absent of a specific task, that may be associated with a behavior. This type of multivariate and integrated viewpoint on brain activation and communication can provide an alternate viewpoint of how an individual's functional brain network organization may support or hinder behavioral outcomes, such as EF task performance.

Previous work has shown that graph metrics can help identify some brain network organizational properties that are related to either intelligence, or EF tasks (such as the n-back working memory task) that are often used to calculate IQ or fluid intelligence. One set of findings associated shorter path lengths between cortical regions to better intellectual performance in individuals (Hilger, Ekman, Fiebach, & Basten, 2017b; Langer et al., 2012; van den Heuvel, Stam, Kahn, & Hulshoff Pol, 2009). More specifically, stronger integration between cortical areas represented in the fronto-parietal, cingulo-opercular, and salience networks (commonly labeled as "control" networks) were associated with measures of intelligence. Global efficiency, which is directly related to characteristic path length (a measure of the shortest paths across a network) has been shown to be directly related to the n-back working memory task. Previous work found that higher global efficiency (stronger levels of full-network integration) is related to greater performance on the n-back task (Stanley et al., 2015). However, previous results in the literature are somewhat inconsistent. While measures of shortest paths have been related to measures of intelligence in adults, other work did not find significant relationships between tested global network parameters (which included characteristic path length and global efficiency) and IQ (Wu et al., 2013).

Previous research also provides evidence that methodological neuroimaging decisions, such as scan length (Birn et al., 2013; Whitlow, Casanova, & Maldjian, 2011) or sample size (Kruschwitz et al., 2018; Marek et al., 2020), may be a significant impacting factor when associating whole-brain GMs to behavior. In fact, recent work that used a large sample (n=1,096) from the human connectome project (HCP) public release, were unable to replicate previous results

relating global efficiency to measures of intelligence (Kruschwitz et al., 2018). Another important aspect to consider is that the majority of extant literature focusing on the brain-behavior associations of RSFC-derived GMs and EF task performance used adult samples. Thus, the extent that these relationships between graph metrics and EF can be accurately identified during development is not wholly explored.

The current study tested the ability of GMs to quantify specific traits of resting state functional network organization in youths, and successfully predict EF task performance. We tested the impact of scan length and network components on our GM-focused results, using a large dataset combined across locally collected and publicly released neuroimaging datasets. Additionally, we addressed concerns over the minimum sample size needed to accurately identify brain-wide associations of behavioral outcomes (Dick et al., 2021; Marek et al., 2020), and the potential impact of resting state preprocessing decisions (Gargouri et al., 2018; Liang et al., 2012) with the inclusion of a unique set of 2,000 preprocessed scans from the curated Collection 3165 - DCAN Labs ABCD-BIDS release (https://collection3165.readthedocs.io/). Combined, these analyses provide a greater understanding of not only the association of patterns of functional network connectivity to EF task performance in youths, but the extent to which methodological decisions with resting state functional connectivity may impact the ability to identify valid associations of GMs to EF task performance.

METHODS AND MATERIALS

Participant Demographics

Participants in this combined dataset (Study 2, Table 1) of 567 (284 F) youths were recruited either at the University of Texas at Austin (UT) (n=67) or as part of the publicly available Adolescent Brain Cognitive Development (ABCD) study (n=500). All participants included in this study were required to have at least 5-minutes of post-processed resting state scan data, after

motion censoring using a .25 framewise displacement (FD) threshold (see post-motion censored time distribution in supplement (Study 2, Figure S1A)). Participants from the UT dataset were recruited for either a longitudinal, multidimensional study of executive function (e.g., (Nugiel et al., 2020); JAC start-up funds), or as part of the Texas Twin Project (Engelhardt et al., 2019) (NICHD R21HD081437; MPI J.A. Church, E.M. Tucker-Drob). This combined dataset is comprised of youths ages 8.5-17.2 (M=10.3) years-old at the time of scan, and only one twin sibling (pseudo-randomly selected) was included from any family pair to minimize the influence of genetic similarity on our results. The UT sample included 3 participants that had ever received an ADHD diagnosis and the ABCD sample included 77 participants that had ever been diagnosed with ADHD, depression, bipolar disorder, anxiety, or a phobia, per parent report. Exclusion criteria for these datasets included a reported history of epilepsy, head trauma, or any non-removable metal implant that would prevent participation in the MRI portion of the study. Participants in the preprocessed Collection 3165 - DCAN Labs ABCD-BIDS release (DCAN) comparison set (n=2,000) were also collected for the ABCD study under the same inclusion criteria (see Study 2, Table 1 for demographic information). Participants from the DCAN release used within this current study did not overlap with participants in our locally processed ABCD set.

Study 2, Table 1: Participant Demographics

Group Demographics				
	UT	**ABCD**	**COMBINED**	**DCAN**
Participants	67 (30 F)	500 (254 F)	567 (284 F)	2,000 (963 F)
Age Range (years)	8.5 - 17.2	9.0 - 11	8.5 - 17.2	9 – 10.9
Age (M ± SD)	11.8 ± 2.1	10.1 ± 0.63	10.3 ± 1.1	9.9 ± 0.63
Mean Scan Length	9:07	14:30	13:52	15:05
Race/Ethnicity				
Asian	2	7	9	14
Black	5	48	53	284
Hispanic	4	63	67	202
Multiracial or Other	15	38	53	228
White	41	344	385	1272

Note: Mean scan length is minutes and seconds of fully pre-processed resting state scan time, concatenated across all available runs, and post-motion censoring at .25 framewise displacement (FD).

Executive Function Tasks

The current study focused on tasks designed to target cognitive flexibility and working memory/updating EF abilities. Tasks were matched as closely as possible between the University of Texas at Austin (UT) and the ABCD dataset, although slight differences in the presented tasks are noted in the task details section. Further, in an effort to mitigate the influence of setting (tasks completed inside or outside of MRI scanner) on task performance, task setting was matched between the two datasets. Therefore, the cognitive flexibility task scores were collected from tasks performed outside of the scanner, while the working memory/updating task was performed within the scanner. Similarly, we either normalized or matched the task scoring method reported for the ABCD dataset to mitigate differences between reported scores within the two datasets (see Study 2, Figure 1E & F for distribution of task scores across collections).

Cued Task Switching/Cognitive Flexibility Task

Participants in the UT dataset completed 46 trials of a cued rule matching task aimed to assess cognitive flexibility (Church et al., 2017; Engelhardt et al., 2019) while outside of the

scanner (Study 2, Figure 1A). For each trial, participants were cued to match a target stimulus based on one of two possible rules (match the shape or color). Response choices were displayed for the duration of the trial. For the first 1.5 seconds of each trial a red box would indicate the rule to follow. The target stimulus then appeared .5 seconds after the red box indicating the rule had disappeared and the stimulus remained on screen for 2 seconds. During this time, the participant would indicate which response choice matched the target, according to the rule. After each response period, a fixation cross was displayed for 1-4 seconds. All participants completed a brief practice example set to confirm they understood the task. Z-scores calculated from task accuracy scores (correct/total trials) were used for our analyses.

Participants in the ABCD dataset completed a similar switching task from the NIH Toolbox Cognition Battery; the Dimensional Change Card Sort (DCCS) test (Luciana et al., 2018; Zelazo, 2006; Zelazo et al., 2013) while outside of the scanner (Study 2, Figure 1C). During the DCCS, participants are presented with two objects at the bottom of the screen. A third object is then presented in the middle of the screen and the participant is asked to match it to one of the two objects on the bottom of the screen, either by shape or color. All participants are first given a practice set, followed by a block of trials where they match based on one rule, a block where they match on the other rule, and then a block where the rule is pseudo-randomly alternated between the shape and color rules. The DCCS provides a standard score metric (normative mean=100, SD=15) that is not age corrected, and is provided to gauge a participant's overall level of functioning on the task. This score was then converted to z-scores for appropriate use with the UT dataset. This non-age-corrected score was used as age correction is done later in our analyses.

Working Memory/Updating Task

Participants in the UT dataset completed up to two versions of a block design, n-back task (Engelhardt et al., 2019) while inside the scanner (Study 2, Figure 1B). At the start of each scan, the participants were verbally reminded of the rules of the task by the scan operator. The n-back

task was adapted from (Jaeggi et al., 2010) and is used to assess an individual's working memory or updating ability. Each task run consisted of 64 shape stimuli in a fixed block design that were evenly divided into a 1-back and 2-back block. At the start of each block, participants were shown instructions for 4 seconds that indicated if they should look for shapes shown one shape prior (1-back) or two shapes prior (2-back). Each stimulus was shown for 1.5 seconds with a 1 second inter-stimulus interval. Participants were instructed to push a button when they believed the shape they were currently viewing matched a shape either one or two shapes previous, based on the instructions. Each block was followed by a 20 second fixation cross, and a total of 7 matches were shown in each block (21.0% of trials). The correct rate was calculated (total correct / total stimuli shown) for only the 2-back trials, and this measure of task performance was used in our analyses.

Participants in the ABCD dataset completed up to two runs of an emotional n-back (EN-back) (Study 2, Figure 1D) task while in the scanner (Barch et al., 2013; Casey et al., 2018; Cohen et al., 2016). The EN-back task is a variant of the Human Connectome Project n-back task (Barch et al., 2013) and measures working memory processes. The task includes two runs of eight blocks where participants are asked to indicate if an image matches or does not match based on a 0-back or a 2-back rule. In the EN-back, trials consist of both emotional faces (such as happy or fearful) and neutral faces or places. During the 2-back section participants are asked to indicate "match" when the current stimulus matches a target presented two trials back. Each block consists of 10 trials displayed for 2.5 seconds each and 4 fixation blocks displayed for 15 seconds each. Each stimulus was presented for two seconds followed by a 500ms fixation cross. During each block, two of the trials are targets, 2-3 are non-target lures, and the remaining trials are non-lures. To match the UT dataset, our analyses only included task performance on the 2-back, non-emotional segments of the task, which was 4 blocks. We then calculated the correct rate (matching the UT dataset task performance measure) and this measure was used for our analyses.

Study 2, Figure 1: Executive Function Tasks

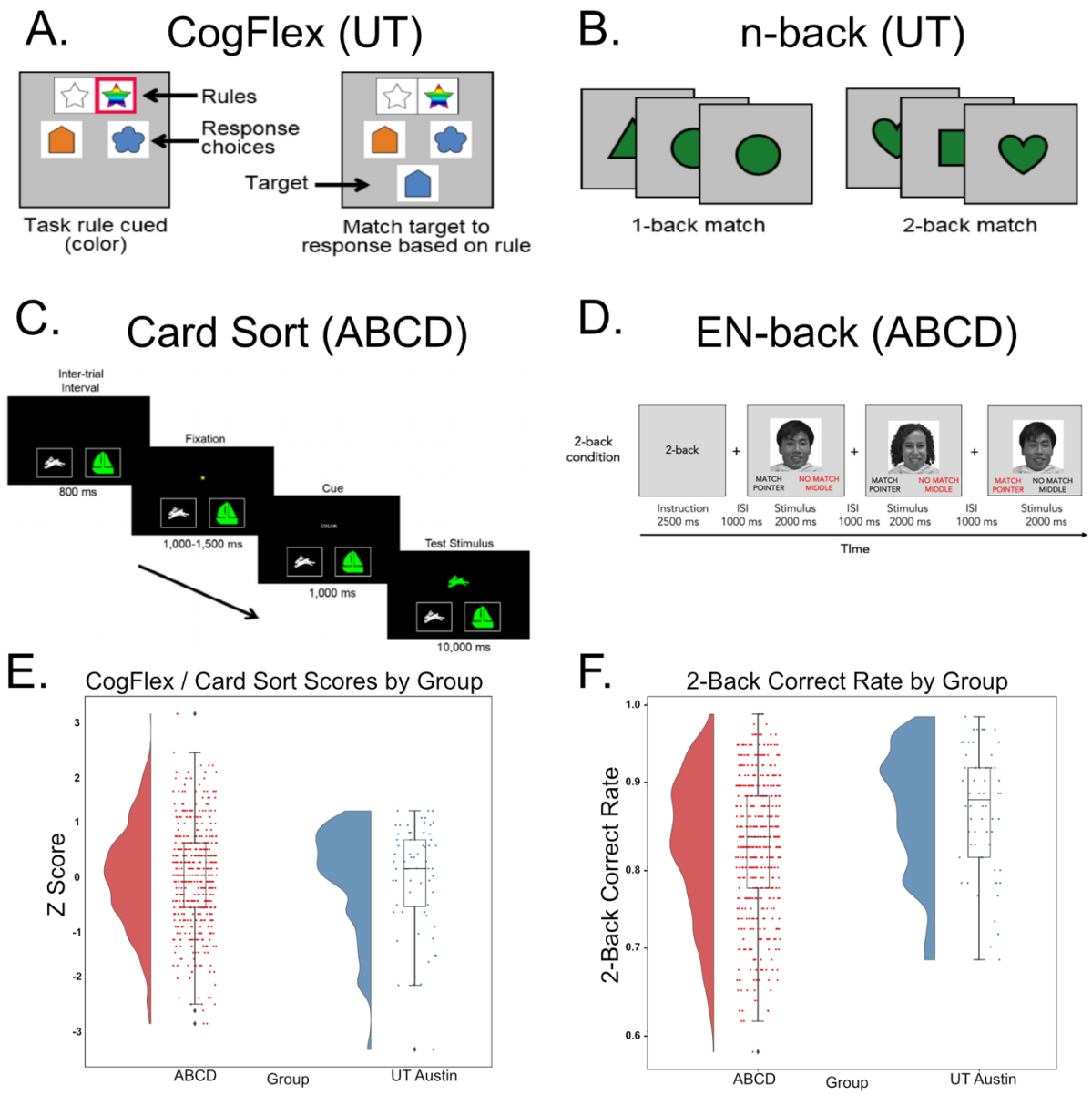

Note: Examples of the cognitive flexibility tasks administered at the UT site (A. CogFlex) and the ABCD sites (C. Dimensional Change Card Sort (image: NIH Toolbox)). Examples of the working memory tasks administered at the UT site (B. n-back) and the ABCD sites (D. Emotional n-back, (image: Casey et al., 2018)). To match between sites, only trials containing neutral faces and places were used from the EN-back (D.) task. Task score distributions are also shown, separated by participants group, for the cognitive flexibility (E.) and working memory (F.) tasks.

Neuroimaging Acquisition

The University of Texas at Austin

All participants scanned at the University of Texas at Austin (UT) were scanned in the Biomedical Imaging Center on a Siemens Skyra 3 Tesla scanner, with a 32-channel head coil. Foam padding was used around the head for comfort and to reduce head motion, and verbal feedback on body motion and to ensure participant comfort was provided between scans. One T1-weighted structural MPRAGE sequence (TR=2530ms, TE=3.37ms, FOV=256x256, voxel resolution=1x1x1mm) scan and one T2-weighted structural image using a turbo spin echo sequence (TR=3200ms, TE=412ms, FOV=256x256, voxel resolution=1x1x1mm) were collected and included in the preprocessing steps for this study.

Up to two, 6-minute echo-planar sequence functional resting state scans (TR=2000ms, TE=30ms, flip angle=60°, MB factor=2, 48 axial slices, voxel resolution=2x2x2mm) were collected. All resting state scans were acquired with the participant instructed to view a white fixation cross on a black background. Participants were instructed to simply stay awake and lie still. Up to two working memory task functional scans were collected (see n-back description above) using the same acquisition settings reported for the resting state scans. All tasks were run using PsychoPy version 1.8 (Peirce, 2007) with stimuli projected behind the scanner that participants viewed using a mirror attached to the head coil. Participants recorded their responses during this task using a two-button response pad.

Adolescent Brain Cognitive Development (ABCD) Study

In an effort to avoid any unknown scanner manufacturer confounds (Noble et al., 2017; Zhao et al., 2018), only participant scans collected on a 3T Siemens Prisma scanner were included in this dataset. All ABCD participant scans were downloaded in their unprocessed form from the NIH Data archive (https://nda.nih.gov/abcd) and preprocessed using our in-house preprocessing pipeline. One T1-weighted structural scan (TR=2500ms, TE=2.88ms, FOV=256x256, voxel

resolution=1x1x1mm) and one T2-weighted structural scan (TR=3200ms, TE=565ms, FOV=256x256, voxel resolution=1x1x1mm) were used for our pre-processing. Up to four, 5-minute resting state scans (TR=800ms, TE=30ms, flip angle=52°, MB factor=6, 60 axial slices, voxel resolution=2.4x2.4x2.4mm) and up to two working memory functional scans (see EN-back description above) were collected and used in this study. For complete information on the ABCD scan protocol, see Casey et al., 2018.

Collection 3165 – DCAN Labs ABCD-BIDS Release

The DCAN dataset - used for the preprocessing and sample size comparisons – was collected as part of the ABCD release and followed the fMRI acquisition protocol described above. fMRI preprocessing steps (DCAN-Labs, 2019) for this set are outlined briefly below.

Resting State Preprocessing

In-house Preprocessing Pipeline

To mitigate confounds to analyses that stem from preprocessing decisions, all participants' scans (other than those in the DCAN Labs ABCD-BIDS release) were preprocessed using our in-house pipeline comprised of FMRIB Software Library (Smith et al., 2004), Freesurfer (Dale, Fischl, & Sereno, 1999), and Connectome Workbench (Marcus et al., 2011) commands, along with custom Matlab (www.mathworks.com) computational scripts. The pipeline follows the first three steps of the Human Connectome minimal preprocessing pipeline (Glasser et al., 2013), followed by volume and surface preprocessing steps developed in-house, informed by current best practices for resting state analyses (Caballero-Gaudes & Reynolds, 2017; Dipasquale et al., 2017; Hallquist, Hwang, & Luna, 2013; Lindquist, Geuter, Wager, & Caffo, 2019; Power et al., 2012, 2014).

Volume resting state preprocessing steps included: (1) motion correction and registration to 2mm MNI atlas space; (2) mode 1k normalization; (3) temporal band-pass filtering (0.009 Hz $< f <$ 0.08 Hz); (4) demeaning and detrending of fMRI data; and (5) regression of band-pass filtered

nuisance signals including six directions of motion plus their derivatives, cerebral spinal fluid, white matter, and whole brain signal. To reduce the reintroduction of noise that occurs with multiple transformations, all registration steps were done in one single transform. Similarly, all nuisance signal regression and temporal filtering was performed simultaneously (Lindquist et al., 2019).

Surface resting state preprocessing steps work on the unsmoothed, but fully preprocessed volume scans from the volume preprocessing stage and maps those outputs to 32k fs_LR surface space using the following steps: (1) creation of grey matter ribbon using the white and pial boundaries previously created during the HCP steps; (2) downsampling of grey matter ribbon to functional scan dimensions; (3) exclusion of voxels with high coefficient of variation to improve SNR (following the HCP pipeline's "fMRISurface" procedure); (4) mapping of volume functional data to 32k fs_LR surface mesh; (5) spatial smoothing (2mm FWHM); (6) and creation of CIFTI dense timeseries file.

DCAN Labs Preprocessing Pipeline

The DCAN comparison set was downloaded in its fully preprocessed form as a curated release of the ABCD study. This set was preprocessed using the ABCD-HCP pipeline created by DCAN-Labs (DCAN-Labs, 2019). The DCAN-Labs pipeline generally follows the steps outlined in the Human Connectome minimal preprocessing pipeline (Glasser et al., 2013). However, the following BOLD signal processing steps are applied: (1) Standard pre-processing; (2) Respiratory motion filter application; (3) Motion censoring; (4) Parcellated time series creation. (See https://collection3165.readthedocs.io/en/stable/pipeline/ for detailed explanations of each pipeline step.) The current study used the framewise displacement (FD) values and dense timeseries files provided in the DCAN set, and parcellated timeseries were extracted and motion censored locally.

Graph Metrics

Four main graph metrics (GMs) of interest were chosen to test the relationship of patterns of functional network organization and EF task performance. The chosen GMs have previously been associated with EF task performance or measures of general intelligence that incorporate working memory tasks (Cole, Yarkoni, Repovs, Anticevic, & Braver, 2012; Hilger, Ekman, Fiebach, & Basten, 2017a; Stanley et al., 2015; van den Heuvel et al., 2009) and provide a literature-informed starting point.

Characteristic Path Length (CPL) (Study 2, Figure 2A) is an average of all shortest path lengths within a network. An individual path length is defined as the minimum number of edges that must be traveled to connect two nodes. CPL is the average number of edges contained within the shortest path lengths between all possible connection pairs in a network. CPL can quantify overall network integration, thus highlighting the ability of a network to quickly and efficiently integrate information across subnetworks. A system with a shorter characteristic path length suggests faster propagation of information across the global system or network. Previous work has found a shorter characteristic path length is associated with better intellectual performance (Hilger et al., 2017b; Langer et al., 2012; van den Heuvel et al., 2009).

$$L = \frac{1}{\| N(G) \| (\| N(G) \| - 1)} \sum_{ij \in i \neq j} L_{ij}$$

Global Efficiency *(GE)* (Study 2, Figure 2B) is the average inverse shortest path length in a network and quantifies the average efficiency of all nodes within a network. GE is regarded as a measure of "information flow" and quantifies how efficiently a network may exchange information. Previous work has indicated that higher global efficiency is better for working memory tasks, such as the n-back (Stanley et al., 2015).

$$F_{glob} = \frac{1}{\| N(G) \| (\| N(G) \| - 1)} \sum_{i \neq j \in G} 1/L_{ij}$$

Betweenness Centrality *(BC)* (Study 2, Figure 2D) is quantified as the fraction of shortest paths within a network that pass through the node of interest. BC quantifies how much a node acts

as a connection between other nodes. Nodes with a high BC, that are also connected to multiple subnetworks, are typically labeled as "connector hubs". Connector hubs are thought to allow subnetworks to easily integrate and pass information back and forth. Previous work suggests that greater levels of integration between areas of the front-parietal, cingulo-opercular, and salience networks are associated with intellectual performance (Hilger et al., 2017a, 2017b; Jung & Haier, 2007). BC is one metric that allows us to quantify levels of integration between functional networks.

$$B(u) = \sum_{u \neq v \neq w} \sigma_{v,w}(u)/\sigma_{v,w}$$

Rich-Club Coefficient *(RCC)* (Study 2, Figure 2C) is a GM that quantifies the extent that highly connected nodes within a network are also connected to one another. RCC identifies densely, interconnected hubs and can indicate how easily information can flow between subnetworks in a larger system. Networks that have a higher RCC are expected to have many connections between nodes with a high degree (or number of connected edges). Previous work has indicated that improved network integration, especially between frontal and parietal areas, may lead to better intellectual performance (Hilger et al., 2017b; Jung & Haier, 2007; Langer et al., 2012) and RCC can quantify network integration through interconnected hubs. Below, N(G,k) are the set of nodes with a degree of k or greater and E(G,k) are the set of edges that connect two nodes in the N(G,k) set.

$$R(G,k) = \frac{\| E(G,k) \|}{\| N(G,k) \| (\| N(G,k) \| - 1)}$$

Study 2, Figure 2: Graph Metrics

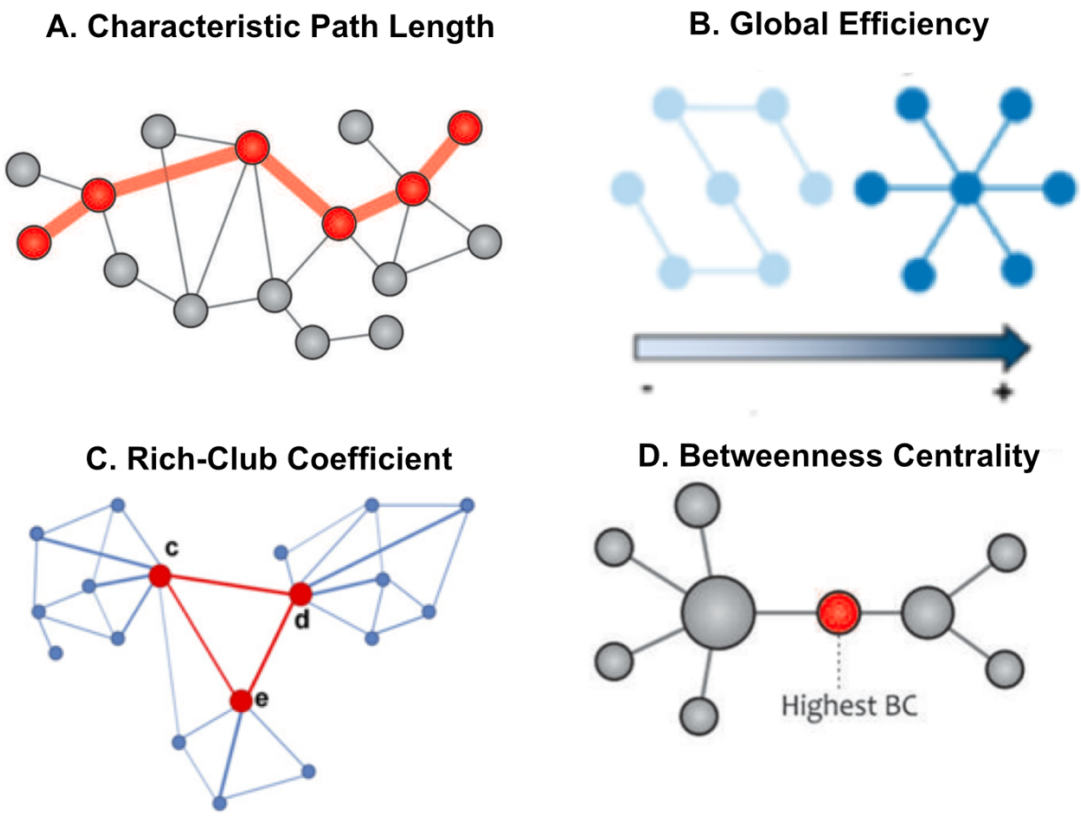

Note: (A.) Characteristic Path Length is the average shortest paths between all possible nodes of a network and represents information flow within a network. An example of the shortest path length between two nodes is displayed here. (B.) Global Efficiency is the average inverse shortest path length in a network and quantifies the average efficiency of information flow across nodes in a network (C.) The Rich-Club Coefficient identifies densely interconnected hubs and quantifies the extent that highly connected nodes are connected to other highly connected nodes. The Rich-Club Coefficient is a measure of how easily information can flow between subnetworks of a system. (D.) Betweenness Centrality is a measure of "hubness" and identifies how much one node acts as a connector between other nodes. Betweenness Centrality is quantified as the fraction of a network's shortest paths that pass through the node of interest.
Figures adapted from (A & D) (Farahani et al., 2019), (B) (Conti et al., 2019), and (C) (Cao et al., 2014)

Graph Metrics Calculations

All graph metrics (GMs) were calculated by: (1) extracting resting state timeseries using a 333 cortical surface parcellation set (Gordon et al., 2016); (2) motion censoring timeseries data using a .25mm framewise displacement (FD) threshold (Power et al., 2012, 2014); (3) creation of a 333x333 connectivity matrix using pairwise correlations of parcellated timeseries; (4) calculating GMs from connectivity matrices using NetworkX (Hagberg, Schult, & Swart, 2008) and Brain Connectivity Toolbox (BCT) (Rubinov & Sporns, 2010) functions.

Previous work with GMs suggests that metrics should be calculated with a range of connection densities applied to the connectivity matrix. Thresholding is suggested due to the fact that a network with a large number of connections with low weights may overly influence graph metric calculations and network features will vary as the number of connections in a network changes (Duda, Cook, & Gee, 2014; van Wijk, Stam, & Daffertshofer, 2010). The current study's GMs were calculated after applying a range of connection densities from 5-30% to our connectivity matrices.

Normalization of GMs is also suggested (Paldino, Golriz, Zhang, & Chu, 2019; Rubinov & Sporns, 2011). Normalization of GMs is thought to remove the influence of low-level connectivity attributes, such as degree distribution on the calculated metrics. GM scores were normalized by dividing the raw GM score by an average score for each metric. Average scores were obtained by calculating the metric of interest on a set of 20 randomized graphs. Randomized graphs were created by taking the individual's original connectivity matrix and shuffling the edge values. This practice ensures that the randomized graph has the same degree distribution, number of nodes, and connection density as the original, but provides a null hypothesis reference (Sinclair et al., 2015) that is devoid of the original graph's potentially unique topological features. Normalized GM values were used for all regression analyses.

Statistical Analyses

Ordinary Least Squares regression analyses were conducted to test the relationship between our four chosen GMs and performance scores in the cognitive flexibility and working memory tasks. Since performance on EF tasks improves as individuals get older, task performance measures were controlled for age. Models predicting either correct rate (working memory task) or Z-scores (cognitive flexibility task) tested characteristic path length, global efficiency, rich-club coefficient, and betweenness centrality (all metrics normalized).

One significant methodological decision that may impact replication in resting state analysis is the amount of time included per participant. Historically, due to the cost of fMRI data collection, relatively short amounts of resting state data were often used in analyses. However, as these costs have come down and the field has focused on the importance of collecting longer scans in order to achieve a more precise representation of an individual's RSFC and to improve reliability (Anderson, Ferguson, Lopez-Larson, & Yurgelun-Todd, 2011; Birn et al., 2013; Laumann et al., 2015; Murphy, Bodurka, & Bandettini, 2007). To test the influence of scan time on our results, models were run using GMs calculated from connectivity matrices derived from: (1) the full available resting state scan time for all individuals, (2) a 5-minute pseudo-random crop of resting state data for all individuals, (3) a subset of resting state scans from individuals with 10-minutes or greater scan data.

Another significant methodological decision is the choice of brain networks. Previous results have highlighted cortical activation related to EF task performance in brain regions belonging to parcels in classic resting state "control" networks (Fiske & Holmboe, 2019; Ullman, Almeida, & Klingberg, 2014). We thus tested the influence of functional network makeup by running the same models on connectivity matrices that only included nodes from commonly-labeled "control" networks; The cingulo-opercular, dorsal attention, fronto-parietal, salience, and ventral attention networks, and comparing results to nodes across the whole brain (333 surface parcel set from (Gordon et al., 2016)).

Finally, in order to test the possible impact of both sample size and fMRI preprocessing pipeline decisions on our results, we re-ran our models using the already pre-processed DCAN comparison set, including full available resting state scan time and full network for all individuals (n=2000).

RESULTS

Graph metrics related to EF task performance measures

We tested the ability of our GMs of choice to successfully predict EF task performance, while focusing on the influence of three different methodological factors: (1) length of resting state data, (2) functional brain network makeup, (3) sample size, and (4) fMRI preprocessing pipeline. Of note, Characteristic Path Length (CPL) and Betweenness Centrality (BC) values (both metrics calculated off the shortest paths between nodes in the graph) were highly correlated in our sample (R=0.98) for whole brain nodes, and results with these two GMs were highly similar across all tests. Therefore, only CPL was tested. (See Study 2, Figure S1B for correlation of GM values). All significance statistics were Bonferroni corrected for multiple comparisons (correction for three tests). See Study 2, Table 2 for complete Cognitive Flexibility task results and Study 2, Table 3 for complete Working Memory task results.

Metrics calculated across scan time thresholds in main sample

In our main sample of 567 youths, varying the amount of resting state data that was used to calculate our GMs of interest impacted our results. When CPL was calculated on all available resting state data per individual, CPL significantly predicted cognitive flexibility task performance ($p<0.01$) after Bonferroni correction for three tests. Similarly, CPL calculated only for individuals with 10-minutes or greater resting state data (n=461) significantly predicted cognitive flexibility task performance ($p=0.01$) after Bonferroni correction (Study 2, Table 2). CPL did not successfully predict cognitive flexibility task performance when all resting state data was limited to 5-minutes for all participants. Additionally, both Global Efficiency (GE) and Rich-club Coefficient (RCC) did not successfully predict cognitive flexibility task performance in any time sub-group.

In the models predicting working memory task performance from GMs calculated from our different time sub-groups (Study 2, Table 3), none of the chosen GMs were able to successfully

predict task performance after Bonferroni correction, regardless of the amount of resting state data used to calculate GMs.

Metrics calculated using control network parcels in main sample

Next, we tested if GMs calculated using only parcels commonly assigned to putative resting state EF networks would act as a form of feature selection that improved prediction to task performance on EF tasks. We calculated GMs on networks reduced to include only parcels belonging to the cingulo-opercular, dorsal attention, fronto-parietal, salience, and ventral attention networks. All models using these GMs could not successfully predict task performance outcomes for either the cognitive flexibility or working memory tasks in our main analysis group (Study 2, Table 2 & Table 3).

Metrics calculated using the full DCAN comparison set (n=2,000)

The publicly available DCAN dataset was used as a comparison set to help identify the influence of sample size and fMRI preprocessing decisions on our results. To assess sample size, all previous tests were also run on this larger sample of 2,000 youths. All reported results were Bonferroni correction for three tests.

All GMs calculated using all available resting state data significantly predicted cognitive flexibility task performance (CPL and GE $p<0.001$; RCC $p=0.01$). In models using these same GMs to predict working memory task performance, CPL ($p=0.02$) and GE ($p<0.001$) successfully predicted task outcomes, while RCC did not. (Study 2, Table 4 & Table 5)

GMs calculated for individuals with 10-minutes or more resting state data (n=1,752) significantly predicted cognitive flexibility task performance ($p<0.01$) in all models (Study 2, Table 4). Alternatively, only GE calculated on 10-minutes or greater resting state data significantly ($p<0.001$) predicted working memory task performance in the DCAN comparison set (Study 2, Table 5).

Next, we tested the impact of shorter scan times on our results in the DCAN group by calculating all GMs on a pseudo-randomly selected crop of resting state data for each participant. For models predicting the cognitive flexibility task outcomes (Study2, Table 4), CPL ($p=0.003$) and GE ($p<0.001$) successfully predicted task performance, while RCC did not. Alternatively, for the working memory task (Study 2, Table 5), CPL did not predict task performance, but GE ($p=0.03$) and RCC ($p=0.002$) did successfully predict working memory scores.

In tests using GMs calculated from a reduced network consisting of just control network parcels, only CPL ($p=0.001$) and GE ($p=0.003$) predicted cognitive flexibility task performance. This same pattern of results was seen for the working memory task, with CPL ($p=0.037$) and GE ($p=0.002$) predicting task performance, while RCC did not predict either task performance in this control network limited sub-group (Study 2, Table 4 & Table 5).

DCAN 500 (n=500) and Main Analysis ABCD-only (n=500) comparisons

In order to address fMRI preprocessing decisions, a subset of 500 participants from the DCAN sample was pseudo-randomly selected and compared to results calculated from only the 500 ABCD subjects in our main sample. The main analysis group was reduced to only ABCD participants as the age range of our locally collected data extended further than the age range collected in the first wave of the ABCD collection. Further, using only the ABCD participants matched MRI exact scanner model for both groups. (These comparison groups hereafter referred to as "Main 500" and "DCAN 500".) Task performance measures did not significantly differ between the Main 500 and DCAN 500 sub-sets (cognitive flexibility: $p=0.273$; working memory: $p=0.857$).

Results using GMs calculated from all available resting state data in these n=500 comparison groups, differed across groups on CPL and GE for cognitive flexibility tasks, and in GE for the working memory task (see Study 2, Table 6).

Study 2, Table 2: OLS Regression table for predicting cognitive flexibility task performance from graph metrics. (Main Analysis Group)

Cognitive Flexibility Task					
Main Analysis Group (n=567)					
Full Network – Full Time					
Graph Metric	**B**	**SE B**	**R^2**	**F**	**p**
CPL	2.49	0.84	0.02	8.79	**0.003****
GE	-2.89	1.33	0.01	4.71	0.030
RCC	0.25	1.67	< 0.01	0.02	0.881
5-min Crop					
Graph Metric	**B**	**SE B**	**R^2**	**F**	**p**
CPL	1.33	0.85	< 0.01	2.47	0.117
GE	-3.05	1.41	0.01	4.67	0.031
RCC	0.81	1.76	< 0.01	0.21	0.644
10-min or More					
Graph Metric	**B**	**SE B**	**R^2**	**F**	**p**
CPL	2.76	0.95	0.02	8.55	**0.004***
GE	-1.30	1.68	< 0.01	0.60	0.439
RCC	-1.04	1.77	< 0.01	0.34	0.558
Control Networks Only (n=461)					
Graph Metric	**B**	**SE B**	**R^2**	**F**	**p**
CPL	2.04	0.89	0.01	5.23	0.023
GE	-1.43	1.34	< 0.01	1.13	0.289
RCC	1.81	1.94	< 0.01	0.87	0.350

Note: Main Analysis Group. Results for all models predicting cognitive flexibility task outcomes from graph metric values. Results that remained significant after Bonferroni correction for multiple comparisons for three tests are denoted as * = p < .05, ** p < .01, and *** = p < .001.
CPL = Characteristic Path Length, GE = Global Efficiency, RCC = Rich-club Coefficient. All outcomes reported for normalized graph metrics calculated at 10% density threshold.

Study 2, Table 3: OLS Regression table for predicting working memory task performance from graph metrics. (Main Analysis Group)

Working Memory (N-Back) Task					
Main Analysis Group (n=567)					
Full Network – Full Time					
Graph Metric	**B**	**SE B**	**R^2**	**F**	**p**
CPL	-0.10	0.07	< 0.01	2.18	0.140
GE	-0.01	0.11	< 0.01	0.004	0.953
RCC	-0.26	0.14	0.01	3.60	0.058
5-min Crop					
Graph Metric	**B**	**SE B**	**R^2**	**F**	**p**
CPL	-0.01	0.07	< 0.01	0.001	0.971
GE	-0.09	0.12	< 0.01	0.60	0.438
RCC	-0.17	0.15	< 0.01	1.28	0.258
10-min or More					
Graph Metric	**B**	**SE B**	**R^2**	**F**	**p**
CPL	-0.09	0.08	< 0.01	1.17	0.281
GE	0.02	0.15	< 0.01	0.02	0.879
RCC	-0.34	0.15	0.01	4.98	0.026
Control Networks Only (n=461)					
Graph Metric	**B**	**SE B**	**R^2**	**F**	**p**
CPL	-0.16	0.07	0.01	4.40	0.036
GE	0.11	0.11	< 0.01	0.95	0.330
RCC	-0.15	0.16	< 0.01	0.81	0.369

Note: Main Analysis Group. Results for all models predicting working memory (N-Back) task outcomes from graph metric values. Results that remained significant after Bonferroni correction for multiple comparisons for three tests are denoted as * = p < .05, ** p < .01, and *** = p < .001.
CPL = Characteristic Path Length, GE = Global Efficiency, RCC = Rich-club Coefficient. All outcomes reported for normalized graph metrics calculated at 10% density threshold.

Study 2, Table 4: OLS Regression table for predicting cognitive flexibility task performance from graph metrics. (DCAN Comparison Groups)

Cognitive Flexibility Task					
DCAN Comparison Group (n=2,000)					
Full Network – Full Time					
Graph Metric	**B**	**SE B**	**R^2**	**F**	**p**
CPL	2.19	0.59	< 0.01	13.59	**< 0.001*** **
GE	-5.53	0.90	0.02	37.62	**< 0.001*** **
RCC	2.57	0.88	< 0.01	8.52	**0.004***
5-min Crop					
Graph Metric	**B**	**SE B**	**R^2**	**F**	**p**
CPL	1.53	0.47	< 0.01	10.65	**0.001****
GE	-3.70	0.91	< 0.01	16.66	**<0.001*** **
RCC	-1.47	0.96	< 0.01	2.335	0.127
10-min or More					
Graph Metric	**B**	**SE B**	**R^2**	**F**	**p**
CPL	1.71	0.61	<0.01	7.90	**0.005***
GE	-4.44	1.00	0.01	19.74	**<0.001*** **
RCC	2.21	0.92	<0.01	5.81	**0.016***
Control Networks Only (n=1,752)					
Graph Metric	**B**	**SE B**	**R^2**	**F**	**p**
CPL	2.53	0.72	<0.01	12.23	**<0.001****
GE	-2.77	0.84	<0.01	10.82	**0.001****
RCC	0.03	0.90	<0.01	0.001	0.970

Note: DCAN Comparison Groups. Results for all models predicting cognitive flexibility task outcomes from graph metric values. Results that remained significant after Bonferroni correction for multiple comparisons for three tests are denoted as * = p < .05, ** p < .01, and *** = p < .001.
CPL = Characteristic Path Length, GE = Global Efficiency, RCC = Rich-club Coefficient. All outcomes reported for normalized graph metrics calculated at 10% density threshold.

Study 2, Table 5: OLS Regression table for predicting working memory task performance from graph metrics. (DCAN Comparison Group)

Working Memory (N-Back) Task					
DCAN Comparison Group (n=2,000)					
Full Network – Full Time					
Graph Metric	**B**	**SE B**	**R^2**	**F**	**p**
CPL	0.24	0.09	< 0.01	7.19	**0.007***
GE	-0.81	0.13	0.02	36.22	**< 0.001*****
RCC	-0.04	0.13	< 0.001	0.10	0.753
5-min Crop					
Graph Metric	**B**	**SE B**	**R^2**	**F**	**p**
CPL	0.10	0.07	< 0.01	1.85	0.174
GE	-0.36	0.14	< 0.01	6.96	**0.008***
RCC	-0.49	0.14	< 0.01	11.78	**<0.001****
10-min or More					
Graph Metric	**B**	**SE B**	**R^2**	**F**	**p**
CPL	0.18	0.09	<0.01	3.91	0.048
GE	-0.80	0.15	0.02	27.98	**<0.001*****
RCC	-0.05	0.14	<0.01	0.10	0.747
Control Networks Only (n=1,752)					
Graph Metric	**B**	**SE B**	**R^2**	**F**	**p**
CPL	0.27	0.11	<0.01	6.25	**0.012***
GE	-0.35	0.13	<0.01	7.68	**<0.001*****
RCC	-0.01	0.13	<0.01	0.005	0.946

Note: DCAN Comparison Groups. Results for all models predicting working memory (N-Back) task outcomes from graph metric values. Results that remained significant after Bonferroni correction for multiple comparisons for three tests are denoted as * = p < .05, ** p < .01, and *** = p < .001.
CPL = Characteristic Path Length, GE = Global Efficiency, RCC = Rich-club Coefficient. All outcomes reported for normalized graph metrics calculated at 10% density threshold.

Study 2, Table 6: OLS Regression table for predicting cognitive flexibility and working memory task performance from graph metrics. ("Main 500" and "DCAN 500" Comparison Groups)

Cognitive Flexibility Task (Full Network – Full Time)					
"Main 500" Comparison Group					
Graph Metric	**B**	**SE B**	**R^2**	**F**	**p**
CPL	2.65	0.94	0.02	7.90	**0.005***
GE	-1.50	1.47	<0.01	1.05	0.307
RCC	-0.20	1.79	<0.01	0.01	0.909
"DCAN 500" Comparison Group					
Graph Metric	**B**	**SE B**	**R^2**	**F**	**p**
CPL	0.75	1.18	<0.01	0.40	0.525
GE	-5.70	1.83	<0.01	9.71	**0.002****
RCC	-0.31	1.71	0.02	0.03	0.857
Working Memory (N-Back) Task (Full Network – Full Time)					
"Main 500" Comparison Group					
Graph Metric	**B**	**SE B**	**R^2**	**F**	**p**
CPL	-0.06	0.08	<0.01	0.56	0.454
GE	-0.04	0.12	<0.01	0.11	0.740
RCC	-0.32	0.15	<0.01	4.73	0.030
"DCAN 500" Comparison Group					
Graph Metric	**B**	**SE B**	**R^2**	**F**	**p**
CPL	0.14	0.11	<0.01	1.70	0.193
GE	-0.60	0.17	<0.01	13.32	**<0.001*****
RCC	-0.21	0.15	0.03	1.79	0.181

Note: "Main 500" and "DCAN 500" comparison group results. These groups were used to test fMRI preprocessing decisions on regression results. Both groups included only ABCD participants from either the main or DCAN comparison groups and groups did not significantly differ on task performance measures (cognitive flexibility: $p = 0.273$; working memory: $p = 0.857$).

Results that remained significant after Bonferroni correction for multiple comparisons for three tests are denoted as
* = $p < .05$, ** $p < .01$, and *** = $p < .001$.
CPL = Characteristic Path Length, GE = Global Efficiency, RCC = Rich-club Coefficient. All outcomes reported for normalized graph metrics calculated at 10% density threshold.

Study 2, Figure 3: Graph metrics regression plots

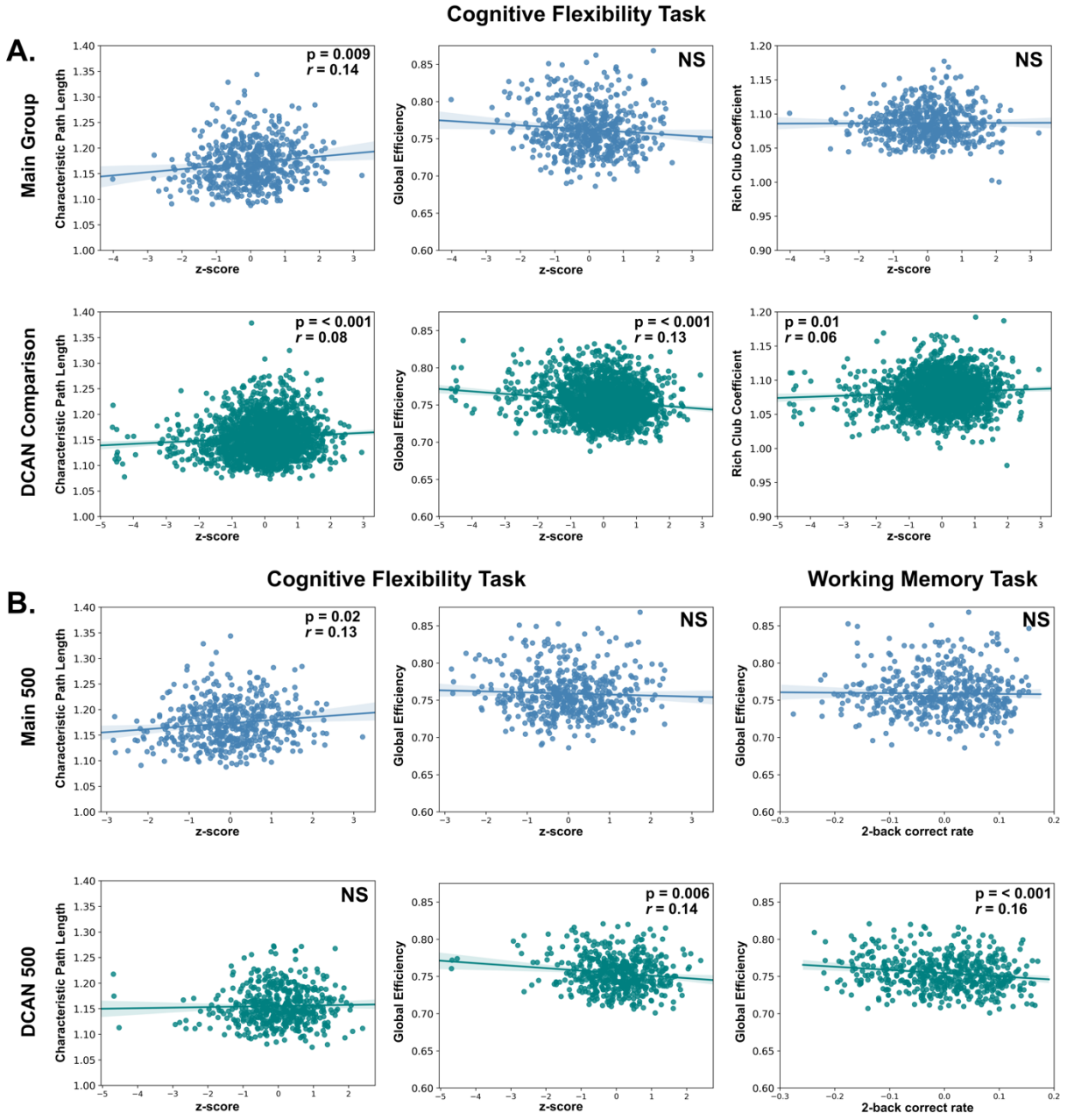

Note: (A.) Main analysis group and DCAN comparison group regression plots for the cognitive flexibility task. Only CPL was significant in the main analysis group. All three GMs were significant in the DCAN comparison group. (B.) Regression plots for the "Main 500" and "DCAN 500" fMRI processing comparison groups. CPL and GE showed differences between the two groups for the cognitive flexibility task. Only GE showed differences between the two groups for the working memory task. (CPL = characteristic path length, GE = global efficiency, NS = not significant. All GM values are for normalized graph metrics calculated at 10% density threshold. All p-values are Bonferonni corrected for 3 tests.)

DISCUSSION

The current work sought out to test the ability of four graph metrics chosen from previous literature (characteristic path length, global efficiency, betweenness centrality, and rich-club coefficient) to successfully predict executive function (EF) task performance in a large, youth neuroimaging sample. Two EF tasks were chosen; one cognitive flexibility and one working memory task. In order to address variables that may contribute to the inconsistency of extant work using graph metrics (GMs) to predict behavioral outcomes, we tested GMs calculated from resting state data that was grouped in four different sub-groups: (1) all resting state data that included all cortical parcels, (2) a pseudo-randomly selected sample of 5-min of resting state data that included all cortical parcels, (3) only subjects that had 10-min or more resting state data that included all cortical parcels, and (4) all resting state data, but limiting the network to parcels within commonly deemed "control" networks (cingulo-opercular, dorsal attention, fronto-parietal, salience, and ventral attention). Additionally, we tested the influence of sample size and fMRI preprocessing pipeline by using a large sample of 2,000 youths that were preprocessed and made publicly available as part of the Collection 3165 - DCAN Labs ABCD-BIDS release. Although we hypothesized that differences in amount of resting state data used to calculate graph metrics would have the largest impact on results, sample size was the greatest impacting factor across all GMs and both tasks. Additionally, this work provides evidence that measures of network organization alone account for very little variance in behavioral measures. These results suggest that GMs be paired with other measures to more accurately identify brain-wide associations of EF task performance and functional network organization.

Amount of resting state data does not linearly influence results

The amount of resting state data required for precise and replicable outcomes is a topic of much debate in the field of neuroimaging research. While general guidelines for the minimum amount of fMRI data required for analyses has been examined (Anderson et al., 2011; Birn et al.,

2013; Whitlow et al., 2011; Xu et al., 2016), a broadly accepted minimum has not been established. While previous work suggests that calculating GMs using as little as 2-minutes of resting state data may be accurate (Whitlow et al., 2011), using longer scans is considered a better option (Anderson et al., 2011; Birn et al., 2013; Laumann et al., 2015; Murphy et al., 2007). A few limiting factors are that fMRI data collection is still expensive, and resting state data is challenging for participants. As researchers push to collect larger datasets or include more scan types in their collections, a compromise is often forced between affordability and the amount of data collected. Additionally, research that focuses on populations that historically are less tolerant of long scanning sessions (e.g., younger children, individuals diagnosed with ADHD, or older participants who may experience discomfort while lying in the scanner for long periods of time), often aim to reduce the amount of time a participant is in the scanner. Given these considerations on fMRI data collection, we assessed the impact of scan length on GM calculations.

We hypothesized that longer scan times would provide a clearer representation of an individual's functional network, and therefore a stronger pattern would emerge in the relationship between the GMs and task outcomes when applying these time cutoffs. Surprisingly, we did not see a clear linear difference from the main analysis group and the 10-minutes or greater group. Models only including participants with 10-minutes or more resting state data, while statistically significant, did a slightly worse job at predicting cognitive flexibility EF task performance from CPL in our main analysis group. This same pattern in the cognitive flexibility task was found in the DCAN comparison group for all GMs. However, for the working memory task, in the DCAN comparison group, the models including CPL no longer significantly predicted task outcomes in the 10-minute plus group, when they had in the main group that included scans at our minimum inclusion cutoff of 5-minutes. This difference also can't be explained simply from differences in sample size or a significant loss of power, as both 10-minutes or more sub-groups were approximately 80% of their full group (Main analysis group: n=461; DCAN group: n=1,752).

While limiting inclusion to only participants with 10-minutes or greater did not reveal a clear benefit of longer scans, our tests reducing all 2,000 DCAN scans to 5-minutes suggest that datasets only including scans at this minimum threshold may not provide accurate results. Assuming that the large sample size of this DCAN comparison set is accurately revealing small brain-behavior effects that our main sample missed due to number of participants, when scan time was reduced, the ability of our models to predict task scores was also reduced. In the DCAN 5-minute crop tests, RCC no longer successfully predicted cognitive flexibility outcomes and CPL no longer successfully predicted working memory outcomes. However, RCC did predict working memory task scores in the 5-minute cut off group, where it had not previously in the main DCAN group tests. These results suggest that inclusion of shorter scans in analysis groups may not have an obvious impact on results (assuming your sample size large enough to identify small effects), but that only including subjects with a minimum of acceptable scan time may provide results that are inconsistent at best, and incorrect at worst.

Although a clear pattern of the influence of scan time across did not emerge for all GMs in all tests, these data suggest that the impact of scan time on the calculation of GMs is not linear. Importantly, we provide evidence that scan time is one of a number of factors impacting our results, and that longer scan collections are not a singular "fix-all" for improving the accuracy of brain-behavior tests using GMs. Although early studies relating GMs to behavioral outcomes suffered from shorter scan times (per current attitudes toward minimal collection cut-offs), shorter resting state scan times are only one factor contributing to the inconsistency of previous results.

Reduction of functional network representation for graph metrics negatively impacts prediction strength

Previous work has highlighted the role of the dorsolateral prefrontal cortex (DL-PFC) and the superior parietal cortex as key neural substrates of task performance in the three main domains of executive functions: working memory, inhibitory control, and cognitive flexibility performance

(Fiske & Holmboe, 2019; Gao et al., 2013; Nowrangi et al., 2014). Cortical parcels within these cortical regions are often labeled as belonging to the fronto-parietal, dorsal attention, and ventral attention networks. Additionally, there is evidence that as the brain matures toward young adulthood, connections between regions in attention networks (such as the fronto-parietal network) are refined and specialized, and may be one key element to performance on EF tasks that improves and becomes more "adult-like" (Buss & Spencer, 2018; Mehnert et al., 2013). Based on this evidence, we questioned whether brain-wide GMs would provide a less focused representation of functional network organization that is associated with EF task performance, than GMs calculated from only parcels assigned to functional "control" networks. This idea was tested by reducing the graphs used to calculate our GMs of interest to include only parcels assigned to the fronto-parietal, cingulo-opercular, dorsal attention, ventral attention, and salience networks.

To the contrary, across both tasks, all GMs calculated on this reduced network representation were worse at predicting EF task performance than those calculated using the whole brain data. In our main analysis group, none of the GMs of interest could successfully predict task performance for either task. In the DCAN comparison group CPL and GE still predicted both tasks (though to a lesser significance), but RCC no longer predicted either the cognitive flexibility or working memory task.

These results suggest that connections between parcels within control networks may be equally as important as connections between those networks and parcels across the entire cortex, when predicting EF task outcomes. It is interesting to note that peak neural activity during EF task performance is located in putative control network parcels. However, individual differences in resting state functional network organization that is associated with EF task performance may not only reflect connectivity within control networks. Rather, successful task performance may be equally dependent on how efficiently parcels in control networks integrate information from other functional networks. These results support theories stating that the systems of cognitive control

that support higher-order processes necessary for EF task performance may rely equally on the efficient communication between sensory regions for task input and output, as well as the flexible integration classic "control" networks (Petersen & Posner, 2012).

fMRI preprocessing choices show smaller than expected impact

Previous work investigated the role of fMRI preprocessing choices on the stability of GMs calculated from functional connectivity (Gargouri et al., 2018). The authors found that fMRI preprocessing decisions, most notably the order of preprocessing steps, impact the reliability of GM calculations. The current work provides support for these extant findings. We hypothesized that the differences between choices of our in-house preprocessing pipeline and those of the publicly released Collection 3165 - DCAN Labs ABCD-BIDS dataset would result in different subgroup results across all GM measures. However, the associations of our GMs of interest and our EF task performance measures were similar for half of the tests (one cognitive flexibility and two working memory), when the DCAN dataset was matched in sample size (Study 2, Table 6).

Although the two collections were preprocessed using different fMRI preprocessing pipelines, our results suggest a more nuanced effect of preprocessing on our outcomes than initially expected. We hypothesize that this is because the our in-house and the DCAN Labs preprocessing pipelines, while different, run similar key resting state preprocessing steps (such as regression of "nuisance" signals, surface smoothing), both are expanded from the same HCP pipeline, and both run all major steps in the same order and using the same software functions. Indeed, preprocessing step order is the main highlight in the previous work (Gargouri et al., 2018). These results provide evidence that differences in preprocessing pipelines may have an apparent impact on replicability of GM calculations, but this effect may be mitigated if the order of the major steps are similar, and the sample size is substantial.

Larger sample sizes are needed to identify small brain-behavior association effects

In the current study, we created a main analysis group that consisted of 567 individuals from both internally-collected and publicly available data. This combined dataset is significantly larger than the average sample size for modern neuroimaging studies. Even in the last few years, the average sample for fMRI studies was less than 100 participants (Szucs & Ioannidis, 2020). However, there is evidence that much larger datasets ($N \gtrapprox 2{,}000$) are needed for reproducible and accurate associations of brain-wide activation and behavioral outcomes (Marek et al., 2020). To test this issue in our analyses, we ran all of our models using 2,000 individuals from the publicly available preprocessed DCAN Labs dataset.

By increasing the sample size to 2,000 with the DCAN dataset, all GMs, except for RCC, significantly predicted both cognitive flexibility and working memory task performance after Bonferroni correction. However, the validity of these results cannot focus solely on statistical significance and must be carefully interpreted. For any statistical test using OLS regression, statistical significance values will become more significant as the sample size increases. Although we feel that this larger sample was able to identify much smaller effects than our main sample of 567 youths – a result that follows and supports recent findings (Marek et al., 2020) - the relative amount of variance explained by our models is less than approximately 2% in all tests (see r2 column in table).

A more complete picture of individual variance associated with EF task performance is needed

While GMs alone do not uniquely account for much variance in EF task performance, the statistical significance found for all tests, except RCC predicting working memory, in the larger DCAN sample, indicates that our GMs of interest account for a piece of the EF performance puzzle. Even though our main analysis group (n=567) would be considered a large sample in the field of fMRI research, the majority of GM associations with the working memory task were

missed. This is due to their small effects not being statistically identified without a much larger sample. We interpret these results as an indication that to best understand the association of functional network organization and EF task performance in our samples, GMs should be paired with other measures for a more complete picture of the variables that describe individual differences in task performance. Previous work has shown that genetics, sleep habits, socioeconomic status, and exercise all impact EF task performance (Holanda Júnior & Almondes, 2016; Last, Lawson, Breiner, Steinberg, & Farah, 2018; Micalizzi, Brick, Flom, Ganiban, & Saudino, 2019; Salas-Gomez et al., 2020). Inclusion of such variables may reveal interactions with GMs that increase the amount of explained variance within a dataset. Additionally, these results also highlight the need to carefully separate statistical significance from clinical significance when modelling brain-behavior associations in large fMRI samples.

LIMITATIONS AND FUTURE DIRECTIONS

This current work focused on a set of chosen graph metrics (GMs) that was informed by previous literature. While this method of GM selection was chosen to mitigate over-testing (using all possible GMs) or "result fishing", issues with previous samples highlighted in this current study indicate that this may not have been the best method of choosing the most relevant GMs. The work that informed our GM choice not only suffered from shorter scan lengths and smaller sample sizes (seen here to have a significant impact on the consistency of our results) but was also primarily conducted with adult samples. Future work that aims to test the brain-behavior association of GMs to executive function task performance in youths would benefit from a purely data-driven approach to GM selection.

Additionally, future work associating GMs to EF task performance should take into account the low amount of variance explained by GMs alone and either: (1) pair GMs with other variables shown to impact EF performance such as genetics, sleep habits, socioeconomic status,

or exercise, or (2) pair GMs up with other neuroimaging methods such as task contrast maps to focus or reduce the functional network used to calculate GMs.

CONCLUSIONS

The ability of graph metrics - calculated from resting state functional connectivity - to predict EF task performance is impacted by multiple factors, such as scan time, network size, fMRI preprocessing decisions, and sample size. Across all of our tests associating our graph metrics of interest to both cognitive flexibility and working memory task outcomes in youth, sample size was the largest impacting factor, followed by the length post-motion censored scan time. Longer scan time did not consistently alter our results over both tasks, and the impact of differences in scan time was not linear. However, reducing all participants' scan time to the minimum study threshold resulted in inconsistent results and reduced statistical significance. Reducing the network makeup to only include parcels in "control" networks resulted in all models unsuccessfully predicting task outcomes in our main sample. fMRI preprocessing decisions (comparing the main analysis set to an externally preprocessed DCAN set) appeared to have an impact on our results; however, we hypothesize the impact was mitigated by the fact that both preprocessing pipelines used the same main steps that follow the HCP pipeline's suggested order. Finally, sample size was the largest impacting factor on our results, with our 2,000-participant DCAN comparison set revealing significant associations of all GMs with performance measures on both tasks, except for RCC predicting working memory task performance. These results support the need for larger datasets in tests of brain-wide associations to behavioral measures. Additionally, we highlight that graph metrics alone account for very little of the variance observed in EF task performance in youths, but are a piece of the brain-behavior association puzzle. This emphasizes the need for GMs to be paired with other measures to better capture the variance in task outcomes, and is a reminder of the careful consideration of statistical vs. clinical significance.

Study 3: Resting State Hub Node Identification in Youths and their Association with EF Task Performance

INTRODUCTION

Childhood and adolescence marks a period of rapid growth and brain development (Barnea-Goraly et al., 2005; Giedd et al., 1999; Houston et al., 2014; Mills et al., 2016; Stiles & Jernigan, 2010). During this time, many neural systems within the brain are being refined and integrated, as children learn and perfect complex behaviors. Specifically, the refinement of neural systems that support behaviors related to executive functions (EFs) such as memory, attention, and cognitive flexibility are increasingly important, as children begin to perfect the skills that are essential to academic and general life success (Best et al., 2011; Jacob & Parkinson, 2015). Although the behaviors linked to EF are established early in life, EF abilities show significant refinement through young adulthood (Best & Miller, 2010; Ferguson et al., 2021). A similarly accelerated period of anatomical brain growth is seen during childhood and adolescence (Brown & Jernigan, 2012; Lenroot & Giedd, 2006). However, cortical development that supports high-level cognitive processes is not confined to any one specific brain region (Fiske & Holmboe, 2019). Rather, the link between brain and behavioral development is better understood using a network view (Byrge, Sporns, & Smith, 2014; Mišić & Sporns, 2016; Pessoa, 2014) that interprets brain function as neural activation that's interconnected across many cortical regions. This viewpoint raises two questions: (1) How does the complex integration of cortical regions emerge during development? and (2) Does a higher level of brain network integration result in a greater ability in high-level cognitive processes?

Neuroimaging analysis methods, such as resting state functional coactivation or "connectivity" (RSFC), allow us to view brain function as a large network of integrated activity between cortical brain regions, absent of a specific task state. RSFC networks are defined as a group of nodes (cortical areas of the brain) that are connected by edges (the correlation of brain

activity, over time, between any two nodes). This larger, whole-brain network of RSFC is further organized into a set of sub-networks (Doucet et al., 2011; Gordon et al., 2016; Power et al., 2011; Thomas Yeo et al., 2011), that are reliably observed in adult populations. One method for quantifying between-region integration and the capacity for efficient exchange of information across sub-networks is the identification of nodes that are highly connected to multiple sub-networks. This type of highly connected brain region that connects and integrates sub-networks are referred to as 'hub' regions (Power et al., 2013; van den Heuvel & Sporns, 2013).

Previous work identifying cortical hubs in adults has not only identified specific cortical surface sections (parcels) as connector hubs, but has also identified three distinct categories of connector hubs based on functional connectivity profiles of parcels (Gordon et al., 2018). These categories were named "control-default", "cross-control", and "control-processing" connector hubs due to the cortical areas they primarily connected. "Control-default" hubs are localized primarily in the dorsal angular gyrus, superior and inferior frontal gyrus, retrosplenial cortex, precuneus, and ventromedial prefrontal cortex, and display a majority of their connections to parcels within the fronto-parietal (FPN) and default mode (DMN) networks. "Cross-control" hubs are located in the inferior parietal lobule, supramarginal gyrus, middle and superior frontal gyrus, and posterior precuneus, and primarily functionally relate to correlations between the cingulo-opercular (CON), dorsal attention (DAN), and FPN networks. "Control-processing" hubs are located in the pre and postcentral gyrus, lateral occipital cortex, dorsomedial prefrontal cortex, and posterior insula, and are primarily connected to the lateral visual (lVis), auditory (AUD), premotor (PMot), hand somatomotor (hSM), CON, and DAN networks. Further, network simulations that removed edges of these hubs from adult whole-brain functional networks resulted in significantly altered brain-wide functional network organization (Gordon et al., 2018). These results suggest that not only are distinct hub types present in the adult functional brain network, but that these

specific hub regions play a potentially crucial role in the integration and flow of information between sub-networks.

Gordon and colleagues further explored the role of these hub regions in adults by quantifying the activation within these hub regions across three task vs baseline contrasts (Gordon et al., 2018). The analysis included one motor task, a mixed block event-related task that included spatial coherence discrimination and verbal discrimination conditions, and an implicit memory task. They found that cortical regions identified as "control-default" hubs deactivated during all tasks, but that "control-processing" hubs activated during all tasks. Most interesting, "cross-control" hubs deactivated during the motor task but activated during the implicit memory and the mixed block event-related task, suggesting that "cross-control" hub regions may play a larger role in tasks that specifically engage higher-order processes.

Given the fact that RSFC networks appear relatively adult-like in childhood (Grayson & Fair, 2017; Thornburgh et al., 2017), the current study tested whether the three distinct sets of hubs found in adults can be replicated in a large-scale youth sample, using a predefined cortical parcellation set. Further, given that the different hub types showed task-specific dynamics in adults (Gordon et al., 2018), this study also tested whether any hub types found in youths related to EF task performance outcomes. To this end, the current study aimed to answer two main questions: (1) Are the same three distinct hub categories found in youths, or are one or more of these hub types not developed until young adulthood? and (2) Does a higher nodal strength (the average value of all edges connected to that node) of cortical hubs identified in youths relate to better EF task performance? Specifically, the current study tested the hypothesis that, if resting state cortical hubs can be identified in a youth sample, stronger hubs will reflect better integration of the brain's sub-networks, which will relate to better outcomes on measures of EF task performance.

METHODS AND MATERIALS

The dataset used for the current study is the same main 567 participant dataset used in Study Two of this dissertation. Details on demographic information, fMRI preprocessing, and executive function tasks are copied below for ease of reference.

Participant Demographics

Participants in this combined dataset (Study 3, Table 1) of 567 (284 F) youths were recruited either at the University of Texas at Austin (UT) (n=67) or as part of the publicly available Adolescent Brain Cognitive Development (ABCD) study (n=500). All participants included in this study were required to have at least 5-minutes of post-processed resting state scan data, after motion censoring using a .25 framewise displacement (FD) threshold (see post-motion censored time distribution in supplement (Study 3, Figure S1A)). Participants from the UT dataset were recruited for either a longitudinal, multidimensional study of executive function (e.g., (Nugiel et al., 2020); JAC start-up funds), or as part of the Texas Twin Project (Engelhardt et al., 2019) (NICHD R21HD081437; MPI J.A. Church, E.M. Tucker-Drob). This combined dataset is comprised of youths ages 8.5-17.2 (M=10.3) years-old at the time of scan, and only one twin sibling (pseudo-randomly selected) was included from any family pair to minimize the influence of genetic similarity on our results. The UT sample included 3 participants that had ever received an ADHD diagnosis and the ABCD sample included 77 participants that had ever been diagnosed with ADHD, depression, bipolar disorder, anxiety, or a phobia, per parent report. Exclusion criteria for these datasets included a reported history of epilepsy, head trauma, or any non-removable metal implant that would prevent participation in the MRI portion of the study.

Study 3, Table 1: Participant Demographics

Group Demographics			
	UT	**ABCD**	**COMBINED**
Participants	67 (30 F)	500 (254 F)	567 (284 F)
Age Range (years)	8.5 - 17.2	9.0 - 11	8.5 - 17.2
Age (M ± SD)	11.8 ± 2.1	10.1 ± 0.63	10.3 ± 1.1
Mean Scan Length	9:07	14:30	13:52
Race/Ethnicity			
Asian	2	7	9
Black	5	48	53
Hispanic	4	63	67
Multiracial or Other	15	38	53
White	41	344	385

Note: Mean scan length is minutes and seconds of fully pre-processed resting state scan time, concatenated across all available runs, and post-motion censoring at .25 framewise displacement (FD).

Executive Function Tasks

The current study focused on tasks designed to target cognitive flexibility and working memory/updating EF abilities. Tasks were matched as closely as possible between the University of Texas at Austin (UT) and the ABCD dataset, although slight differences in the presented tasks are noted in the task details section. Further, in an effort to mitigate the influence of setting (tasks completed inside or outside of MRI scanner) on task performance, task setting was matched between the two datasets. Therefore, the cognitive flexibility task scores were collected from tasks performed outside of the scanner, while the working memory/updating task was performed within the scanner. Similarly, we either normalized or matched the task scoring method reported for the ABCD dataset to mitigate differences between reported scores within the two datasets (see Study 3, Figure 1E & F for distribution of task scores across collections).

Cued Task Switching/Cognitive Flexibility Task

Participants in the UT dataset completed 46 trials of a cued rule matching task aimed to assess cognitive flexibility (Church et al., 2017; Engelhardt et al., 2019) while outside of the

scanner (Study 3, Figure 1A). For each trial, participants were cued to match a target stimulus based on one of two possible rules (match the shape or color). Response choices were displayed for the duration of the trial. For the first 1.5 seconds of each trial a red box would indicate the rule to follow. The target stimulus then appeared .5 seconds after the red box indicating the rule had disappeared and the stimulus remained on screen for 2 seconds. During this time, the participant would indicate which response choice matched the target, according to the rule. After each response period, a fixation cross was displayed for 1-4 seconds. All participants completed a brief practice example set to confirm they understood the task. Z-scores calculated from task accuracy scores (correct/total trials) were used for our analyses.

Participants in the ABCD dataset completed a similar switching task from the NIH Toolbox Cognition Battery; the Dimensional Change Card Sort (DCCS) test (Luciana et al., 2018; Zelazo, 2006; Zelazo et al., 2013) while outside of the scanner (Study 3, Figure 1C). During the DCCS, participants are presented with two objects at the bottom of the screen. A third object is then presented in the middle of the screen and the participant is asked to match it to one of the two objects on the bottom of the screen, either by shape or color. All participants are first given a practice set, followed by a block of trials where they match based on one rule, a block where they match on the other rule, and then a block where the rule is pseudo-randomly alternated between the shape and color rules. The DCCS provides a standard score metric (normative mean=100, SD=15) that is not age corrected, and is provided to gauge a participant's overall level of functioning on the task. This score was then converted to z-scores for appropriate use with the UT dataset. This non-age-corrected score was used as age correction is done later in our analyses.

Working Memory/Updating Task

Participants in the UT dataset completed up to two versions of a block design, n-back task (Engelhardt et al., 2019) while inside the scanner (Study 3, Figure 1B). At the start of each scan, the participants were verbally reminded of the rules of the task by the scan operator. The n-back

task was adapted from (Jaeggi et al., 2010) and is used to assess an individual's working memory or updating ability. Each task run consisted of 64 shape stimuli in a fixed block design that were evenly divided into a 1-back and 2-back block. At the start of each block, participants were shown instructions for 4 seconds that indicated if they should look for shapes shown one shape prior (1-back) or two shapes prior (2-back). Each stimulus was shown for 1.5 seconds with a 1 second inter-stimulus interval. Participants were instructed to push a button when they believed the shape they were currently viewing matched a shape either one or two shapes previous, based on the instructions. Each block was followed by a 20 second fixation cross, and a total of 7 matches were shown in each block (21.0% of trials). The correct rate was calculated (total correct / total stimuli shown) for only the 2-back trials, and this measure of task performance was used in our analyses.

Participants in the ABCD dataset completed up to two runs of an emotional n-back (EN-back) (Study 3, Figure 1D) task while in the scanner (Barch et al., 2013; Casey et al., 2018; Cohen et al., 2016). The EN-back task is a variant of the Human Connectome Project n-back task (Barch et al., 2013) and measures working memory processes. The task includes two runs of eight blocks where participants are asked to indicate if an image matches or does not match based on a 0-back or a 2-back rule. In the EN-back, trials consist of both emotional faces (such as happy or fearful) and neutral faces or places. During the 2-back section participants are asked to indicate "match" when the current stimulus matches a target presented two trials back. Each block consists of 10 trials displayed for 2.5 seconds each and 4 fixation blocks displayed for 15 seconds each. Each stimulus was presented for two seconds followed by a 500ms fixation cross. During each block, two of the trials are targets, 2-3 are non-target lures, and the remaining trials are non-lures. To match the UT dataset, our analyses only included task performance on the 2-back, non-emotional segments of the task, which was 4 blocks. We then calculated the correct rate (matching the UT dataset task performance measure) and this measure was used for our analyses.

Study 3, Figure 1: Executive Function Tasks

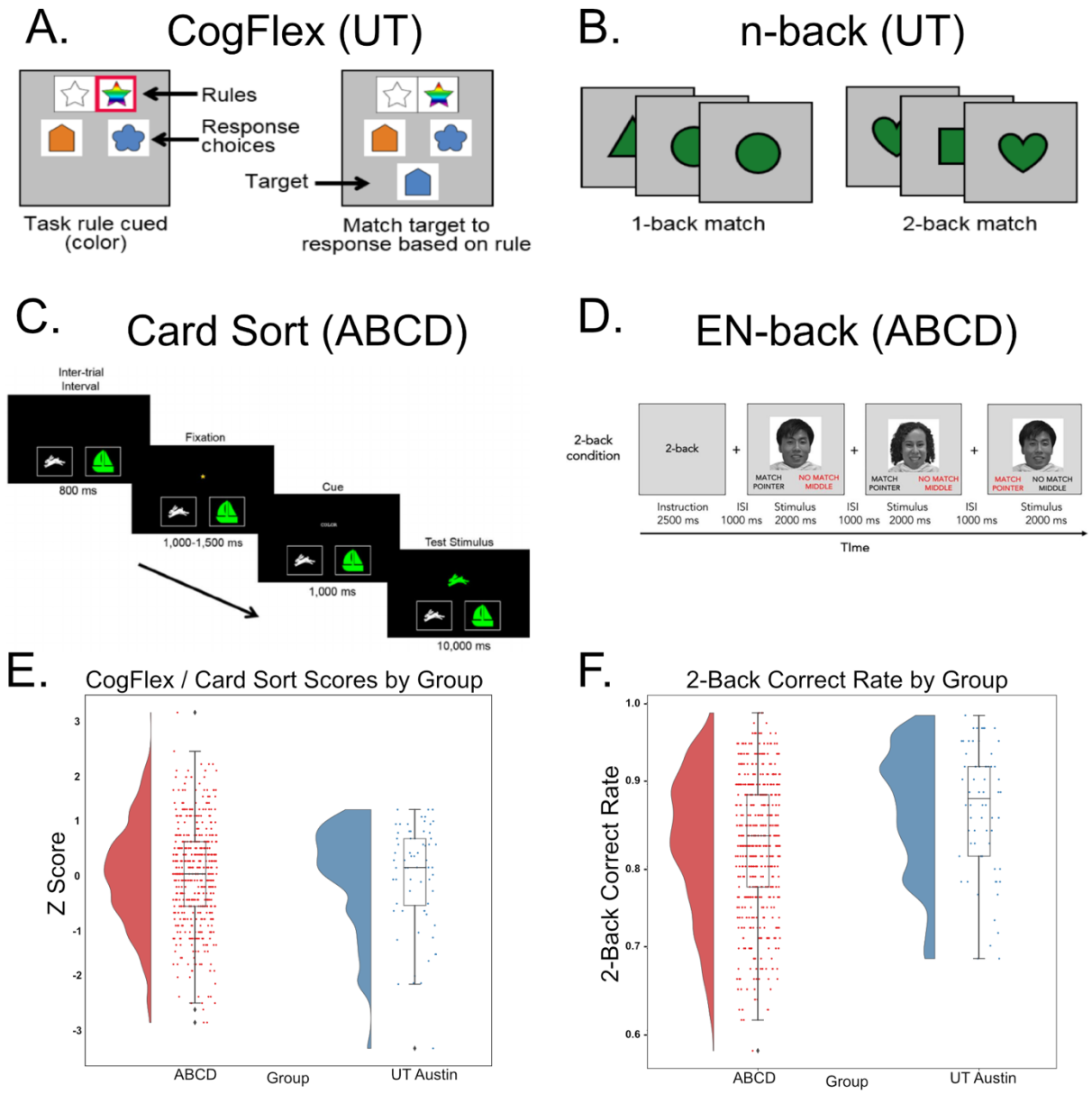

Note: Examples of the cognitive flexibility tasks administered at the UT site (A. CogFlex) and the ABCD sites (C. Dimensional Change Card Sort (image: NIH Toolbox)). Examples of the working memory tasks administered at the UT site (B. n-back) and the ABCD sites (D. Emotional n-back, (image: Casey et al., 2018)). To match between sites, only trials containing neutral faces and places were used from the EN-back (D.) task. Task score distributions are also shown, separated by participants group, for the cognitive flexibility (E.) and working memory (F.) tasks.

Neuroimaging Acquisition

The University of Texas at Austin

All participants scanned at the University of Texas at Austin (UT) were scanned in the Biomedical Imaging Center on a Siemens Skyra 3 Tesla scanner, with a 32-channel head coil. Foam padding was used around the head for comfort and to reduce head motion, and verbal feedback on body motion and to ensure participant comfort was provided between scans. One T1-weighted structural MPRAGE sequence (TR=2530ms, TE=3.37ms, FOV=256x256, voxel resolution=1x1x1mm) scan and one T2-weighted structural image using a turbo spin echo sequence (TR=3200ms, TE=412ms, FOV=256x256, voxel resolution=1x1x1mm) were collected and included in the preprocessing steps for this study.

Up to two, 6-minute echo-planar sequence functional resting state scans (TR=2000ms, TE=30ms, flip angle=60°, MB factor=2, 48 axial slices, voxel resolution=2x2x2mm) were collected. All resting state scans were acquired with the participant instructed to view a white fixation cross on a black background. Participants were instructed to simply stay awake and lie still. Up to two working memory task functional scans were collected (see n-back description above) using the same acquisition settings reported for the resting state scans. All tasks were run using PsychoPy version 1.8 (Peirce, 2007) with stimuli projected behind the scanner that participants viewed using a mirror attached to the head coil. Participants recorded their responses during this task using a two-button response pad.

Adolescent Brain Cognitive Development (ABCD) Study

In an effort to avoid any unknown scanner manufacturer confounds (Noble et al., 2017; Zhao et al., 2018), only participant scans collected on a 3T Siemens Prisma scanner were included in this dataset. All ABCD participant scans were downloaded in their unprocessed form from the NIH Data archive (https://nda.nih.gov/abcd) and preprocessed using our in-house preprocessing pipeline. One T1-weighted structural scan (TR=2500ms, TE=2.88ms, FOV=256x256, voxel

resolution=1x1x1mm) and one T2-weighted structural scan (TR=3200ms, TE=565ms, FOV=256x256, voxel resolution=1x1x1mm) were used for our pre-processing. Up to four, 5-minute resting state scans (TR=800ms, TE=30ms, flip angle=52°, MB factor=6, 60 axial slices, voxel resolution=2.4x2.4x2.4mm) and up to two working memory functional scans (see EN-back description above) were collected and used in this study. For complete information on the ABCD scan protocol, see Casey et al., 2018.

Resting State Preprocessing

In-house Preprocessing Pipeline

To mitigate confounds to analyses that stem from preprocessing decisions, all participants' scans were preprocessed using our in-house pipeline comprised of FMRIB Software Library (Smith et al., 2004), Freesurfer (Dale et al., 1999), and Connectome Workbench (Marcus et al., 2011) commands, along with custom Matlab (www.mathworks.com) computational scripts. The pipeline follows the first three steps of the Human Connectome minimal preprocessing pipeline (Glasser et al., 2013), followed by volume and surface preprocessing steps developed in-house, informed by current best practices for resting state analyses (Caballero-Gaudes & Reynolds, 2017; Dipasquale et al., 2017; Hallquist et al., 2013; Lindquist et al., 2019; Power et al., 2012, 2014).

Volume resting state preprocessing steps included: (1) motion correction and registration to 2mm MNI atlas space; (2) mode 1k normalization; (3) temporal band-pass filtering (0.009 Hz $< f <$ 0.08 Hz); (4) demeaning and detrending of fMRI data; and (5) regression of band-pass filtered nuisance signals including six directions of motion plus their derivatives, cerebral spinal fluid, white matter, and whole brain signal. To reduce the reintroduction of noise that occurs with multiple transformations, all registration steps were done in one single transform. Similarly, all nuisance signal regression and temporal filtering was performed simultaneously (Lindquist et al., 2019).

Surface resting state preprocessing steps work on the unsmoothed, but fully preprocessed volume scans from the volume preprocessing stage and maps those outputs to 32k fs_LR surface space using the following steps: (1) creation of grey matter ribbon using the white and pial boundaries previously created during the HCP steps; (2) downsampling of grey matter ribbon to functional scan dimensions; (3) exclusion of voxels with high coefficient of variation to improve SNR (following the HCP pipeline's "fMRISurface" procedure); (4) mapping of volume functional data to 32k fs_LR surface mesh; (5) spatial smoothing (2mm FWHM); (6) and creation of CIFTI dense timeseries file.

Resting state cortical hub parcels in youths

Identification of hub parcels

Identification and categorical labeling of cortical hub nodes largely followed the methods outlined by Gordon and colleagues using an adult sample (Gordon et al., 2018). We identified hub nodes by first extracting resting state timeseries for each individual, using a predefined cortical surface parcellation set (Gordon et al., 2016) consisting of 333 unique parcels. Values for all vertices within each parcel were averaged and then cross-correlated to create a 333x333 connectivity matrix, which was then Fisher-transformed. The spatial relationship of parcels was taken into consideration by setting correlations of parcels that are within 30mm geodesic distance of one another to zero (Study 3, Figure 2A). Next, community detection was applied to each individual's matrix using the Infomap algorithm (Rosvall & Bergstrom, 2008) across a set of edge density thresholds ranging from 0.3% to 5%. At each density threshold, the Infomap algorithm was run using a random seed and 1k iterations. This method provided individually-specific community labels, for all parcels, at each matrix density threshold.

The participation coefficient (PC) metric was then calculated for each parcel, across all density thresholds, using the previously defined individually-specific community labels provided

by Infomap. PC for any parcel with a degree (the number of connections to other parcels in the network) in the bottom 25th percentile of all parcels was set to zero. This degree censoring step is performed due to parcels with a low degree providing unstable or inflated PC values (Gordon et al., 2018). Finally, PC values were then converted to percentiles. This percentile value, averaged across all thresholds, was used for hub identification. For our analyses, the top 20% of parcels for a given individual (calculated from the percentile values of the previous step) was labeled as a hub; following the threshold suggested by Gordon and colleagues. While there is no established cutoff for labeling a parcel a hub vs a non-hub, nearly identical results were found previously using cutoffs from the 75th to 95th percentile (Gordon et al., 2018) and the 80th percentile cutoff is also reported in the previous adult work. Using the 80th percentile cutoff resulted in 67 hubs for each participant.

Study 3, Figure 2: Distance Masks and Cortical Hub Profiles

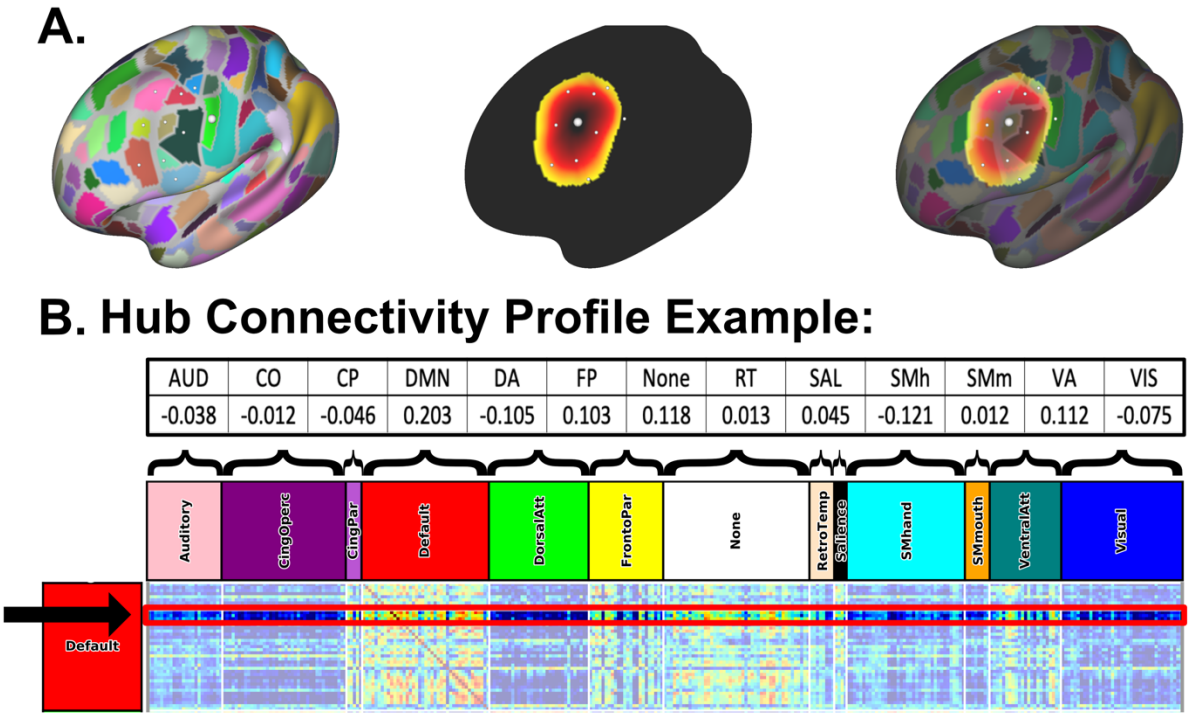

Note: Correlations between cortical parcels less than 30mm geodesic distance of one another were set to zero. This mitigates the impact of spatially-close parcels exhibiting higher functional connectivity due to BOLD signal overlap, rather than parcel coactivation. One parcel centroid is highlighted (A) and neighboring parcels within and beyond the 30mm geodesic distance are shown. An example of a hub connectivity profile is illustrated here (B). Profiles are calculated by averaging the connectivity between an identified hub parcel, and its connectivity to all parcels within each functional network. This created a profile of 13 values; one average correlation value for each of the predefined functional networks.
(Network abbreviations: AUD: auditory, CO = cingulo-opercular, CP = cingulo-parietal, DMN = default mode, DA = dorsal attention, FP = fronto-parietal, NA = unassigned, RT = restrosplenial-temporal, SMh = somatomotor hand, SMm = somatomotor mouth, VA = ventral attention, VIS = visual)

Hub parcel categorization

Following hub identification, a connectivity profile was calculated for each hub. Hub connectivity profiles are created by calculating the functional connectivity strength between each hub and all other parcels (excluding the hub's self-correlation). Connectivity strengths are then averaged across all within-network parcels to create a connectivity profile consisting of 13 averaged connectivity strengths (one for each of the 13 independent networks in the Gordon parcellation) for each hub (Study 3, Figure 2B).

Once hub connectivity profiles were created for all identified hubs, hub category types were assigned by clustering together hubs that displayed a similar connectivity profile. We pseudo-randomly split our main sample into three groups of 189 participants (with equal representation from the UT and ABCD datasets) to assess the stability of clusters found within our dataset. For each of these three groups of 189 participants, the following steps were completed: (1) First, we cross-correlated all identified hubs for all 189 group participants to create a correlation matrix of hub profiles (12,663 x 12,663 matrix). (2) This correlation matrix was then used to identify clusters within the set of hub profiles using the Louvain algorithm function (Rubinov & Sporns, 2010) from the brain connectivity toolbox. The Louvain algorithm was applied to this signed matrix 1,000 times, using the asymmetric negative weight argument which preserves, but down-weights negative connections as suggested for functional brain networks (Rubinov & Sporns, 2011). (3) An "association-recluster" strategy was used to address the concern that modularity-based clustering is often non-deterministic, and each iteration can result in different community assignments, despite the same input matrix. A consensus clustering assignment was created by calculating the frequency, across the 1,000 Louvain iterations, that nodes co-occurred in the same community (Lancichinetti & Fortunato, 2012). (4) This final consensus community assignment vector was used to group together hubs with similar connectivity profiles, and categorize each group based on the average connectivity profile of all cortical hubs clustered into that group. (5) Each of these cluster groups were then qualitatively compared to the three cortical hub categories described in the adult literature (Gordon et al., 2018). Hub category names were then assigned to each cluster group based on the average connectivity profile for all hubs in that group.

Cortical hub brain-behavior analyses

After hub categories were assigned for all cortical hubs, we then assessed the relationship of resting state functional connectivity (RSFC) of cortical hub types with EF task performance. First, the brain-wide average value of all connected edges (across the whole-brain network) was

calculated for all cortical hubs within each hub category, for all participants. This provided one average connectivity value, for each hub category, for each participant. The average connectivity values were then correlated with both the cognitive flexibility and working memory task performance measures. Second, we tested the association of "within hub-category" connectivity to our chosen task performance measures. For this step, average connectivity values were again calculated for all hubs within each category, for each participant. However, the average connectivity for this analysis was calculated using only connectivity from each hub to parcels within the functional networks assigned to hub category. This provided one average connectivity value for each participant that represented the of parcels within the functional networks of a given hub category, to all participants hubs belonging to that hub category. For all tests, the cognitive flexibility and working memory task scores were corrected for participant age, and significance values were false discovery rate (FDR) corrected for two tests.

RESULTS

Cortical hub parcels identified in youths

Across our full 567 participant dataset, parcels that were identified as hubs spanned across the majority of the cortex. However, consistent hub locations were observed when hub parcels were aggregated across all participants (Study 3, Figure 3A). Peak hub locations were observed in the bi-lateral supramarginal gyrus, precuneus, superior parietal lobule, and posterior cingulate, the right superior medial frontal gyrus, and the left inferior temporal gyrus, inferior frontal gyrus, superior frontal gyrus, prefrontal gyrus, and superior parietal lobule. These peak parcels are assigned to the cingulo-opercular, cingulo-parietal, fronto-parietal, default mode, dorsal attention, and somatomotor hand resting state networks.

Categories of youth cortical hub parcels

Across the three sub-groups created for hub categorization (n=189 participants and 12,633 hub profiles in each group), either six or seven clusters were identified from the hub profiles within each group (Study 3, Figure 3B). Out of these results, the first four clusters in each group contained enough hub profiles to be considered a hub category and was assigned a qualitative label. A fifth common and stable cluster was found (cluster 5 in group 1 & 2 and cluster 6 in group 3), however the number of hub profiles in this cluster represented less than 1% of the total. As a result, this cluster was not considered for the main hub categories. The remaining clusters contained only one or two hub profiles, and were thus not considered stable clusters and removed from further analyses.

Additionally, we checked for any possible influence of participant dataset on each group's identified clusters (i.e., if clusters represented dataset rather than unique hub connectivity profiles). Hub connectivity profile correlation matrices were ordered according to their Louvain cluster assignment and then each participant hub was color labeled according to the dataset of origin. Across all three groups, the identified Louvain clusters showed a relatively equal representation of participants from each fMRI collection (Study 3, Figure S1B).

The four main clusters were similar in all three of our sub-groups (Study 3, Figure 3B), and were merged across all 567 participants. Hub connectivity profiles for each of these clusters were then averaged across all participants and four final hub categories were created (Study 3, Figure 4). Hub categories were named based on their connectivity profiles and their resemblance to hub categories found in adults (Gordon et al., 2018).

The first category (12,983 profiles, 34% of total) contained connections primarily to parcels within the cingulo-parietal, default mode, fronto-parietal, unassigned, salience, and ventral attention networks, and was named "youth control-default" hubs (Study 3, Figure 4A). The second category of hubs (10,406 profiles, 27.4% of total) contained connections primarily in the cingulo-opercular, cingulo-parietal, dorsal attention, retrosplenial-temporal, somatomotor hand, and visual

networks. This second category was named “youth control-processing (VIS)” hubs (Study 3, Figure 4B). The third category, named “youth control-processing (AUD + SM)” hubs (10,464 profiles, 27.5% of total) contained parcels with connections primarily in the auditory, cingulo-opercular, somatomotor hand, and somatomotor mouth functional networks (Study 3, Figure 4C). The fourth hub category (4,069 profiles, 10.7% of total) contained parcels with connections primarily in the auditory, cingulo-opercular, dorsal attention, fronto-parietal, salience, and ventral attention networks, and was named “youth cross-control” hubs (Study 3, Figure 4D).

Study 3, Figure 3: Cortical Hub Identification & Categorization

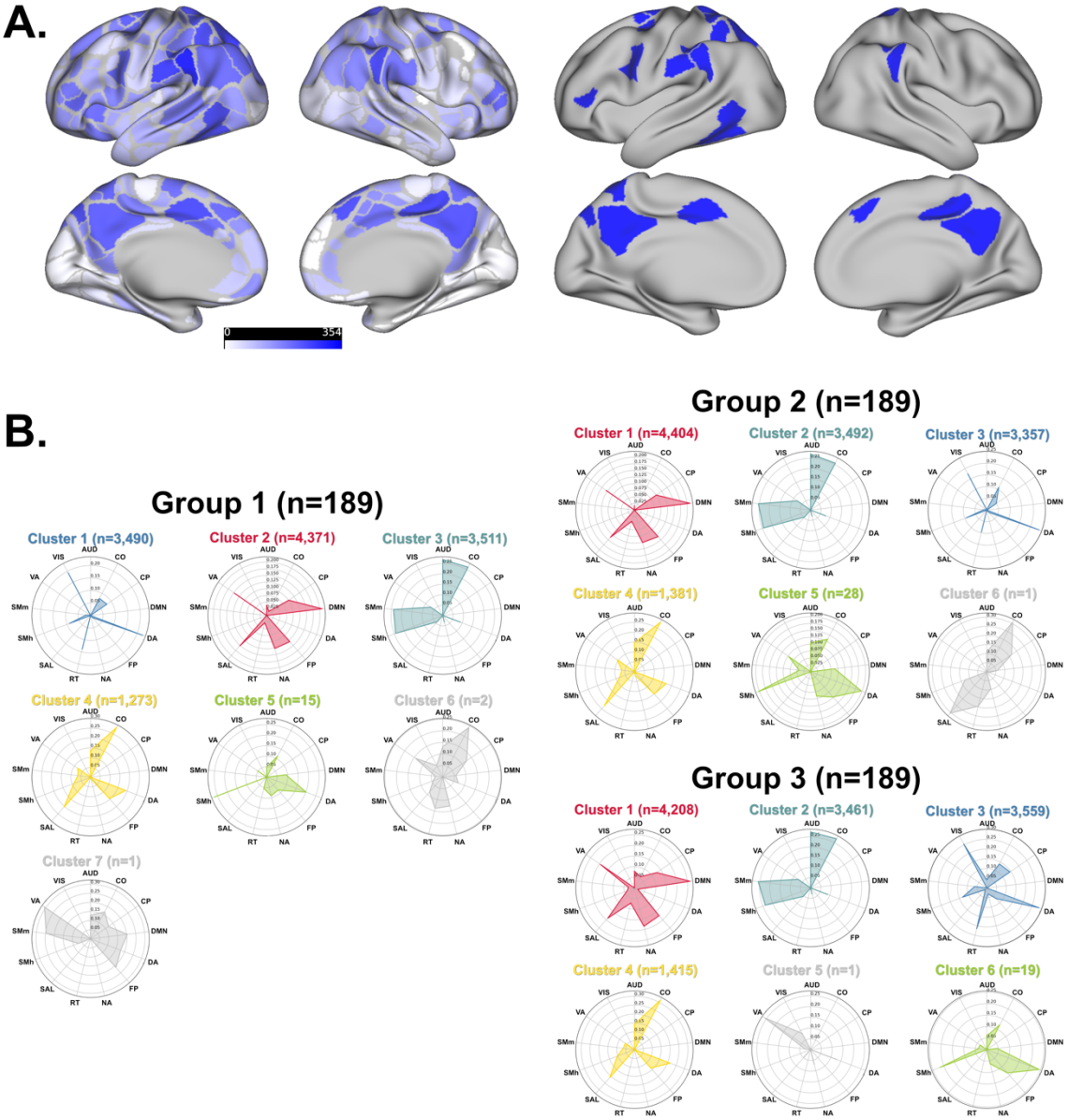

Note: (A.) Left: Density map of cortical parcels that were labeled as hubs across the full group of 567 participants. This density map illustrates the distribution of hub parcels across the cortex. Right: Parcels above a 70% threshold on the full group density map are highlighted. (B.) Raw radar plots for three sub-groups of participants used for hub profile clustering. The Louvain algorithm does not assign cluster numbers in any stable order. Therefore, clusters have been assigned colors based on their final full-group categorization for easier comparison at the group level.
(Network abbreviations: AUD: auditory, CO = cingulo-opercular, CP = cingulo-parietal, DMN = default mode, DA = dorsal attention, FP = fronto-parietal, NA = unassigned, RT = restrosplenial-temporal, SMh = somatomotor hand, SMm = somatomotor mouth, VA = ventral attention, VIS = visual)

Study 3, Figure 4: Youth Cortical Hub Categories

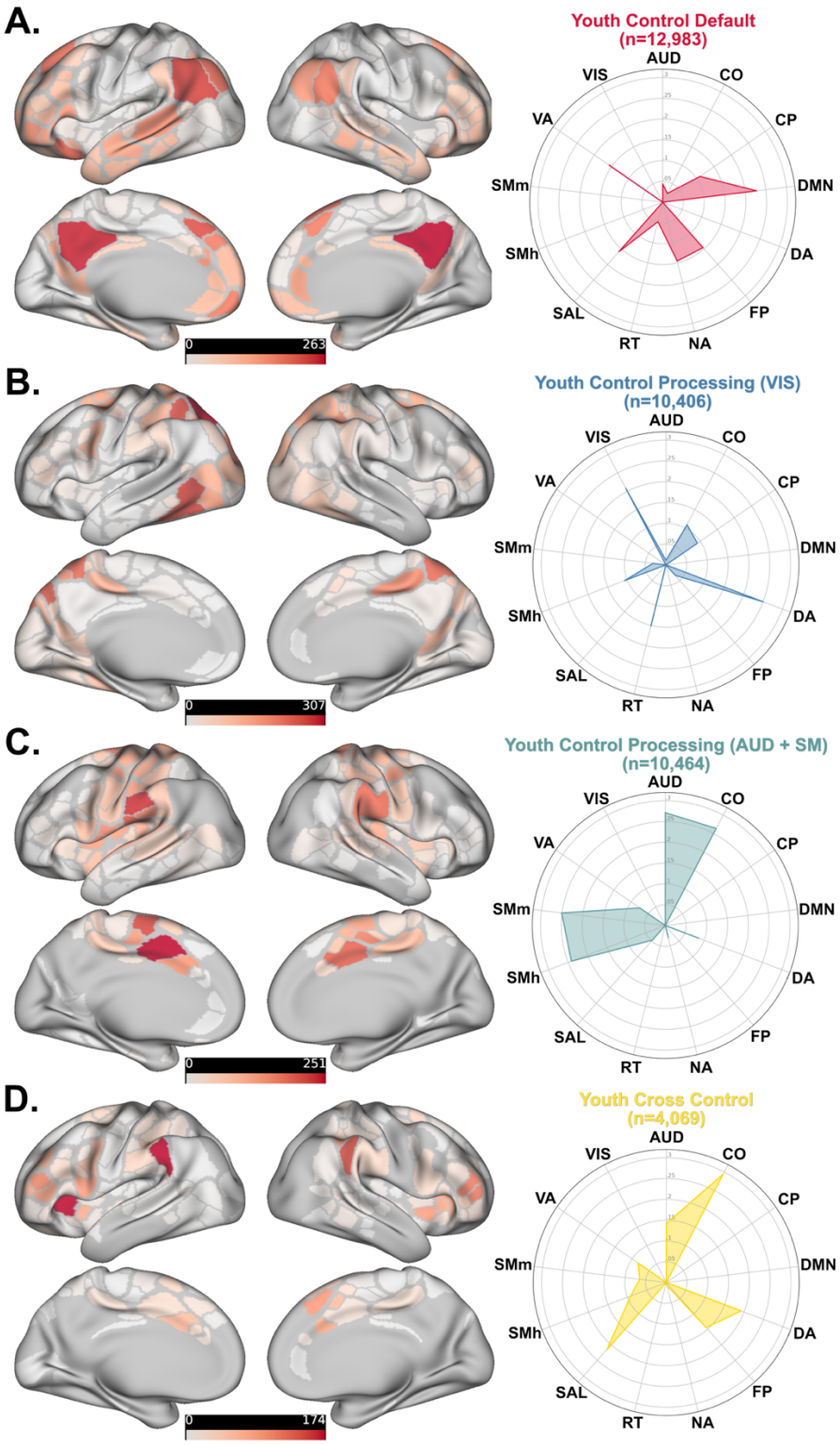

Note: Four primary cortical hub categories were identified in youths: (1) youth control-default (A) with connectivity primarily in the cingulo-parietal, default mode, fronto-parietal, unassigned, salience, and ventral attention functional networks; (2) youth control-processing (VIS) (B) with connectivity primarily in the cingulo-opercular, cingulo-parietal, dorsal attention, retrosplenial-temporal, somatomotor hand, and visual functional networks; (3) youth control-processing (AUD + SM) (C) with connectivity primarily in the auditory, cingulo-opercular, somatomotor hand, and somatomotor mouth functional networks; (4) youth cross-control (D) with connectivity primarily in the auditory, cingulo-opercular, dorsal attention, fronto-parietal, salience, and ventral attention functional networks.
(Network abbreviations: AUD: auditory, CO = cingulo-opercular, CP = cingulo-parietal, DMN = default mode, DA = dorsal attention, FP = fronto-parietal, NA = unassigned, RT = restrosplenial-temporal, SMh = somatomotor hand, SMm = somatomotor mouth, VA = ventral attention, VIS = visual)

Executive function task performance associated with cortical hub connectivity

We tested the role of cortical hubs identified in youths on EF task performance by associating the connectivity of hub parcels, within each of the four identified categories, with EF task outcomes. For each participant, we calculated the correlation of both the brain-wide average and the within hub category average connectivity of all hubs within each of the four hub categories. We then correlated these average hub connectivity values with age-corrected scores on the cognitive flexibility and working memory tasks.

Across all hub categories using the brain-wide average connectivity values, connectivity of hubs did not significantly correlate with either EF task performance measures ($r < 0.07$ and $p > 0.1$ in all tests). However, when using the within hub category average connectivity, both youth control-processing (AUD + SM) and youth control-processing (VIS) were significantly correlated with the cognitive flexibility task scores ($r = 0.13$, $p = 0.004$ and $r = 0.09$, $p = 0.03$, respectively) after FDR correction for two tests (Study 3, Figure 5). Working memory performance was not significant with any within-hub category.

Study 3, Figure 5: Hub Connectivity Associated with EF Task Performance

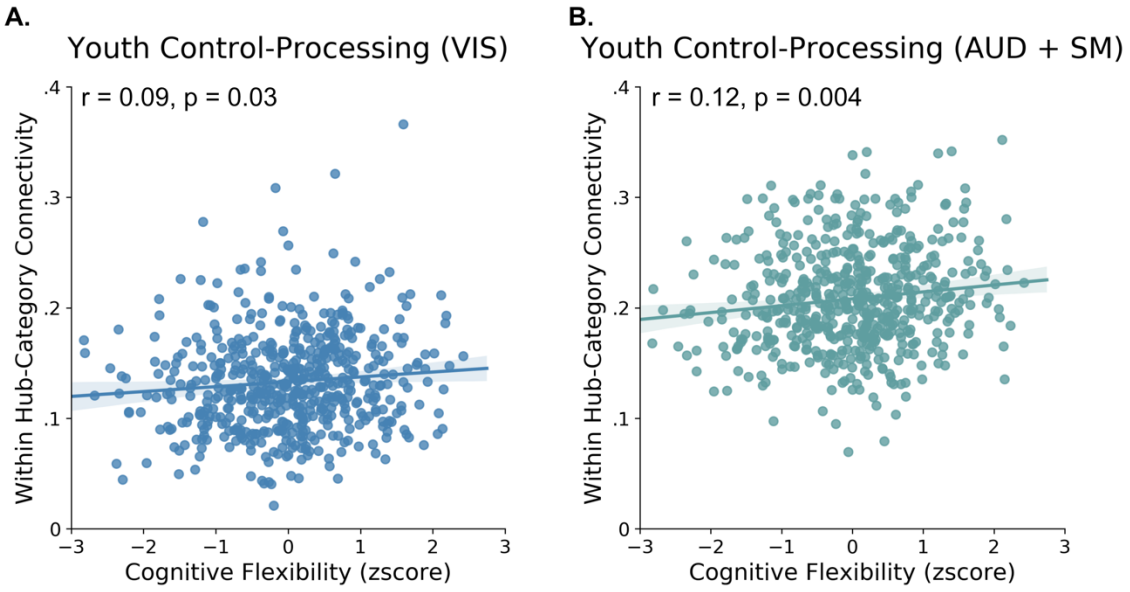

Note: Average within hub category connectivity correlated with cognitive flexibility task scores. Significant associations were observed for the average (A) Youth Control-Process (VIS) hub connectivity and the average (B) youth control-processing (AUD + SM) hub connectivity. Cognitive flexibility scores were age corrected and then Z-scored. Significance values were false detection rate (FDR) corrected for two groups.

DISCUSSION

During childhood and adolescence, neural systems within the brain are undergoing rapid growth and refinement (Barnea-Goraly et al., 2005; Lenroot & Giedd, 2006; Mills et al., 2016; Stiles & Jernigan, 2010). As the brain structure becomes more refined during development, the interaction between specialized cortical regions becomes increasingly important (Fair et al., 2009; Grayson & Fair, 2017) and cognitive control and decision-making abilities are supported by the successful coordination of cortical activity in multiple brain regions (Dwyer et al., 2014; Petersen & Sporns, 2015). One type of cortical node vital for successful integration of brain regions, the connector hub, provides a means for the efficient and flexible integration of information between functionally segregated neural systems (Bertolero, Yeo, & D'Esposito, 2017; Gratton et al., 2018b). The current work sought to identify and categorize resting state cortical hub parcels in a large neuroimaging dataset of youths. By replicating the general methods of hub identification and

categorization previously applied to adults, we aimed to qualitatively compare the similarity of hubs identified in youths, with those found in adults (Gordon et al., 2018). Additionally, we tested the role of cortical hub connectivity, across the four hub categories identified in youths, on outcomes for two EF tasks; one cognitive flexibility and one working memory task.

We found that cortical hub parcels identified using resting state functional coactivation/connectivity (RSFC) from youths, generally resembled those identified in adults, though similar 'control-default' and 'cross-control' categories show additional functional network inclusion relative to what was observed in adults. Additionally, we saw a split in control-processing hubs (visual and auditory/somatomotor), such that one adult hub cluster was found to be similar to two hub clusters in our youth sample (Study 3, Figure 4). Further, the average within hub category RSFC strength of these split control-processing hubs was correlated to the cognitive flexibility EF task in our sample, while the other two hub categories were not. The results from this work suggest that adult-like hub parcels can be clearly identified by mid-childhood, but that hub category profiles may still be developing, especially in how control networks interface with input and output processors; this developmental configuration may also be influencing performance of some cognitive-control demanding tasks.

Youth control-default and cross-control hubs show more diverse connectivity than in adults

In the current work, we provide evidence that cortical hub categories resembling those found in adults are established in mid-childhood. However, we see the impact of ongoing functional network refinement and segregation in our "youth control-default" and "youth cross-control" categories as well (Study 3, Figure 4A & D) in these categories' connectivity profiles. In these two categories, we observe an inclusion of connections to functional networks, not found in their analogous adult hub category. In our youth control-default hubs (Study 3, Figure 4A), we see strong connectivity in the default mode and fronto-parietal networks as was found in adults.

The youth hub category, however, also includes strong cingulo-parietal, salience, and ventral attention connections, as well as connections to parcels that were not assigned to a functional network in the predefined parcellation set. Similarly, the youth cross-control hubs (Study 3, Figure 4D) exhibit strong connectivity to the cingulo-opercular, dorsal attention, and fronto-parietal networks (as seen in the adult categories), but also include ties to the salience and auditory networks.

These two hub categories were observed across all three of the participant subgroups (n=189 each) used for the hub categorization step (Study 3, Figure 3B), suggesting that around 10 years of age, these youth-specific hub categories are stable across individuals. However, their inclusion of functional networks not found in the adult categories may be due to non-linear developmental trajectories of functional network integration and specialization. While the current work used participation coefficient (PC) to identify individual parcels exhibiting hub-like connectivity across functional networks, PC has also been used to quantify the overall average integration of resting state functional networks. Previous work tracked fluctuations in PC within common resting state functional networks from early adolescence to young adulthood (Marek et al., 2015). From ages 12 to 22, PC values in the default mode network showed a U trajectory that decreased until around 18 years old and then increased through 22 years old. Alternatively, PC values in the fronto-parietal network increased from 12 to 14 years old, decreased until around 20 years old, and then increased again through 22 years old. These previous results suggest that, during development, parcels in functional networks fluctuate between connections dominantly within their "home" network to connections dominantly outside of their "home" network.

Although the majority of participants in our sample are younger than the age-range this previous work tested, these previous results offer a possible explanation for the increased connectivity profile diversity of youth control-default and cross-control hub categories, compared to adults. Indeed, the cortical hub categories found in adults begin organizing in middle-childhood,

but developmental influences on functional network organizational trajectories may cause a pattern of inclusion of additional network representation in the makeup of these hub categories in youths.

Two distinct types of youth control-processing hubs

Contrary to the single adult "control-processing" hub category that integrates sensory networks with the cingulo-opercular and dorsal attention networks (Gordon et al., 2018), we found that youth control-processing hubs were split into two distinct categories. The two hub categories that we identified and labeled as "youth control-processing (VIS)" and "youth control-processing (AUD + SM)" hubs (Study 3, Figure 4B & C), present strong connectivity between sensory networks, such as the somatomotor hand and mouth, visual, and auditory networks, with control networks such as the cingulo-opercular and dorsal attention control networks. The cingulo-opercular (and to a lesser extent dorsal attention) network is represented in both categories. This evidence of two distinct control-processing hub types in youth may highlight the developmental need for differentiated integration of sensory inputs and outputs to cognitive-control focused networks.

Cortical activation related to cognitive control during task engagement is anatomically separate from those directly involved in sensory processing and motor actions, but must coordinate these incoming perceptions and outgoing responses for successful task performance (Petersen & Posner, 2012). One theory of cognitive control processes outlines a function where control-processing parcels may act as intermediaries that route sensory information to and from cognitive-control specialized networks (Petersen & Posner, 2012; Power & Petersen, 2013). This processing system is responsible for processing incoming stimuli, routing this information to networks that make decisions based on that incoming information, and then routing those decisions back to the appropriate outputs for the specific task.

We posit that the control-processing hubs found in youths are differentiated based on sensory input, where the control-processing (VIS) hubs primarily route visual stimuli to the dorsal

attention network, and the control-processing (AUD + SM) primarily routes auditory and somatomotor stimuli to the cingulo-opercular network. The cingulo-opercular and dorsal attention networks, which are also primary networks within the youth cross-control hubs, then process the information and make decisions based on the task, before passing information back to one or both of the control-processing hubs for output. This observed split in control-processing hub categories provides evidence that the functional networks that support this type of cognitive-control demanding task completion are not yet integrated to the degree seen in an adult sample (Gordon et al., 2018).

Youth control-processing hubs are related to cognitive flexibility

Based on previous work highlighting the role of connector hubs in EF processes (Dwyer et al., 2014; Gratton et al., 2018b), we tested the relationship between youth cortical hub categories and EF task performance in youths. We found that, for the two separate youth control-processing categories, greater average connectivity of hubs within that category to all parcels within that category's assigned networks, correlates with better performance on the cognitive flexibility task (Study 3, Figure 5). These results support the theory outlined above that both types of control-processing hubs in youths may act as intermediaries; routing sensory information to and from specialized cognitive-control networks. However, given that the network organization tested in this current work is derived from resting state data, we posit that the increased average connectivity of youth control-processing hubs at rest may reflect the necessary connectivity of these hubs while youths are engaged in a task state. Further, the association we see in the current study may, in fact, be highlighting cortical areas previously found to exhibit significant age-related differences in cognitive flexibility tasks (Church et al., 2017).

In this previous work, cortical regions within the fronto-parietal, default mode, dorsal attention, and cingulo-opercular functional networks showed significant age effects between adults and youths, during the preparatory control period of a similar cognitive flexibility (switching) task

(Church et al., 2017). The regions with the greatest difference between youths and adults during the cue period of the task, line up with our youth control-processing (VIS) and control-processing (AUD + SM) categories. In fact, cortical areas in the superior and inferior parietal, inferior temporal, and lateral visual cortex show a large amount of overlap between the peak age differences in that work and our youth control-processing hub peak hub counts. We hypothesize that the similarity of results in these cortical regions may be evidence that youth control-processing hubs are heavily involved in the preparatory control phase of the cognitive flexibility task, and are undergoing substantial developmental change in this age range.

Together, these results suggest that individual differences in youth control-processing hubs connectivity may impact the successful relay of sensory input to more cognitive-control specialized networks, like those in the cross-control hub category. During development, this routing of information may be especially important as these control-processing hubs are not yet consolidated as has been observed in adults.

LIMITATIONS AND FUTURE DIRECTIONS

In the current work, we used an establish, predefined cortical parcel set (Gordon et al., 2016) to identify cortical hubs in youths. While the use of a predefined parcel set demonstrates the generalizability of hub identification in youths and provides a less computationally intensive method for this work, our future work should quantitatively test the difference of hubs defined with pre-established parcels vs. individual-specific parcels (as used in the adult work (Gordon et al., 2018)). Additionally, recent work has established probabilistic maps of functional brain networks (Dworetsky et al., 2021) and, although these maps were defined using adult data, the use of these high consensus regions would provide a computationally reasonable alternative to defining hubs using individual-specific maps.

To fully understand the development of cortical hub parcels in youths, the developmental trajectory of cortical hubs defined by PC should be carefully considered. It is important that future

work incorporate a longitudinal fMRI dataset that follows individuals from youth to adulthood (e.g., the ABCD study) and tracks how the non-linear change of average PC of functional networks impacts cortical hubs as children age. Of note, many hub regions defined in our youth set belong to resting state functional networks, such as the default mode and fronto-parietal networks, that have been shown to exhibit vast changes in coactivation of both within and between network parcels during this period of life (DeSerisy et al., 2021; Rubia, 2013; Sherman et al., 2014). Such work would add valuable knowledge of how hubs organize, longitudinally, from youth into adulthood.

Lastly, the brain-behavior associations of cortical hubs to EF task performance that we have highlighted in our youth dataset are specific to functional network organization during resting state. The connectivity profiles of cortical hubs may significantly change while youths are actively engaged in a task state. Our future work plans to quantify the shift in hub connectivity profiles from resting state to task state, by replicating these hub identification methods on fMRI data collected while youths were actively engaged in the two EF tasks. We can then test the influence of hub connectivity on task outcomes to begin to separate the influence of cortical hubs during rest vs while engaged in EF tasks.

CONCLUSIONS

Four main categories of cortical hub parcels can be identified in youths using a pre-established cortical parcellation set. These four hub categories – "youth control-default", "youth control-processing (VIS)", "youth control-processing (AUD + SM)", and "youth cross-control" – strongly resemble the three hub categories found in previous adult work and provide evidence that hub categories found in adults are established in their "developmental form" by middle-childhood. However, the adult "Control-Processing" category is split into two distinct hub categories in youths, and youth "Control-Default" and "Cross-Control" hubs exhibit connectivity profiles that include more "control" network connections than similar hubs identified in adults. We propose

this is evidence of ongoing or "incomplete" developmental refinement and segregation of resting state functional networks during middle childhood and adolescence. Lastly, whole-brain resting state connectivity of cortical hub parcels in youths, was not associated with our cognitive flexibility or working memory task performance scores. However, stronger within hub category connectivity in the two "Control-Processing" categories was associated with cognitive flexibility task performance. We posit that Control-Processing hubs act as input/output controllers of sensory information in youths, and thus may relate to coordinating complex behaviors in development.

General Discussion

The development of higher-order cognitive processes in youth is not a homogenous process. Identifying unique differences in brain activation, and their association with behavior, can offer valuable insights to brain development during this period of life. This dissertation reports a body of work that investigated three methods for quantifying individual differences in the organization of networks derived from resting state functional connectivity/coactivation (RSFC). This work then proceeds to relate these measures of network organization to two cognitive tasks related to executive functions (EFs) in youths. Quantified individual differences in RSFC network organization can offer many insights into the development and specialization of cortical coactivation from birth to adulthood (De Asis-Cruz et al., 2016; Fair et al., 2009; Fransson et al., 2011; Gao et al., 2011; Power et al., 2010). Many higher-order cortical processes depend on this refinement of functional networks, and disruptions in the normative organizational trajectory of these networks may result in clinically diagnosed mental states or physiological disease (Cordova et al., 2020; Craddock et al., 2009; Fair et al., 2010; Liu et al., 2020; Ma et al., 2019). Further, even individual differences in functional network organization that don't result in clinical diagnoses may impact the normative development of behavioral skills such as those of EFs (Reineberg, Gustavson, Benca, Banich, & Friedman, 2018). Such disruptions in the development of EFs may result in substantial negative academic outcomes and general life success (Best et al., 2011; Jacob & Parkinson, 2015). This dissertation sought out to investigate three methods for quantifying RSFC functional network organization - the functional fingerprint, graph metrics, and cortical hubs - and then test the relationship of two of those methods with working memory and cognitive flexibility task performance. As a whole, this work improves our understanding of the organization of individually unique functional coactivation, and of how differences in that organization may impact the higher-order processes related to EF in youths.

In Study 1, we identified a neural fingerprint in RSFC (a unique pattern of functional coactivation that distinguishes one individual from another) using support vector machine (SVM) classifiers (Demeter et al., 2020). Functional fingerprints were identified in both youths and adults, and our large, cross-sectional sample consisted of repeat-scan individuals, monozygotic (MZ) twin pairs, and dizygotic (DZ) twin pairs. The results of this study indicated that functional fingerprints in both youths and adults are dominated by functional coactivation between cortical areas within the default mode and fronto-parietal networks, and result in successful identification of an individual's current scan when SVM classifiers were trained on their pervious scan. Our results also indicated that the RSFC used to calculate functional fingerprints are influenced by genetics, resulting in the successful identification of one twin based on their co-twin's scan. Further, we also showed that classifier accuracies decrease as the genetic similarity of the scans decrease, with repeat scan individuals showing the highest accuracy, followed by MZ twin pairs, and then DZ twin pairs. As a whole, Study 1 found that although common RSFC networks across individuals can be found early in development, a stable pattern of unique functional coactivation, influenced by genetics, exists and can be used to identify individuals.

In Study 2, we took a closer look at the role of specific patterns of RSFC network organization in youths - defined by graph metrics (GMs) - on behavioral performance of cognitive tasks linked to EFs. We tested the ability of two GMs based on the shortest paths within the functional network (characteristic path length (CPL) and global efficiency (GE)) and one GM based on highly interconnected cortical parcels (rich-club coefficient (RCC)), to predict performance on one working memory and one cognitive flexibility task. Further, we included a comparison set of publicly available, preprocessed fMRI data (n=2,000) to investigate the influence of sample size, resting state scan time, functional network makeup, and fMRI preprocessing decisions on our results. Our results indicated that sample size and fMRI preprocessing decisions have the most significant impact on using GMs to predict task

performance in youths. Specifically, we found that even our main sample (n=567), which would be considered relatively large in fMRI research, was not sufficient to consistently identify the small brain-behavior effects that the larger comparison group identified. Further, all successful models accounted for very little variance ($R^2 < 0.02$) across all tests. These results add to the growing literature highlighting the need for very large samples ($N \gtrapprox 2{,}000$) to accurately identify brain-behavior effects using fMRI data. Further, this work emphasizes that GMs are only a piece of the puzzle associating brain-wide RSFC network organization to behavior, and should be combined with other measures to more robustly account for the observed variance in working memory and cognitive flexibility task performance in youths.

Study 3 expanded on the themes of studies 1 and 2, by using the participation coefficient (PC) to identify cortical hubs in youths, categorize stable hub types across individuals using a clustering algorithm, and then associate whole-brain coactivation of hubs with working memory and cognitive flexibility task performance. We found four main hub categories in youths that closely resemble those found in adults, but that are developmentally unique: (1) youth control-default hubs, (2) youth control-processing (VIS) hubs, (3) youth control-processing (AUD + SM) hubs, and (4) youth cross-control hubs. Contrary to the cortical hubs identified in adults, youth hubs exhibited more diverse connectivity to functional networks, and control-processing hubs were split into two distinct categories, as opposed to the single category found in adults. Further, we found that only these two youth control-processing hub categories were significantly associated with cognitive flexibility task performance, while none of the hub categories identified in youths were associated with working memory task performance. These results indicate that the cortical hubs categories found in adults are established in a developmentally-unique form during middle childhood, and the relationship of youth cortical hubs to EF task performance supports previous work highlighting the need for cognitive control processes to flexibly integrate sensory stimuli to and motor outputs from classic cognitive control functional networks (Petersen & Posner, 2012).

Insights on the sources of individualized functional fingerprints

While the main goal of this dissertation was to evaluate multiple methodologies for quantifying unique patterns of RSFC in youths, I believe results across the three studies highlight the importance of a specific element in the organization of RSFC: cortical hub nodes. In Study 1, we found that functional fingerprints in both youths and adults were primarily composed of within- and between-network connections in the default mode (DMN) and fronto-parietal (FP) networks. Previous neuroimaging work has highlighted that cortical regions assigned to the FP and DMN networks are distinctly responsible for conscious processes (Demertzi, Soddu, & Laureys, 2013; Heine et al., 2012). Specifically, the posterior cingulate and medial prefrontal cortex, both regions in the DMN, are found to be important for autobiographical thought and self-reference, respectively (Whitfield-Gabrieli et al., 2011). However, while many of the cortical regions of the DMN and FP exhibit protracted development (Giedd & Rapoport, 2010; Stiles & Jernigan, 2010) compared to rapidly-matured sensory regions, the developmental trajectory of cortical regions that support higher-level processes are most likely not the core of what's driving these functional fingerprints.

This claim is supported by our results using the opposite age-group's features while running the SVM classifiers in Study 1. Had the functional fingerprint been primarily driven by maturation patterns of the DMN and FP networks, we would have seen a larger age effect at best, or a complete failure of the SVM classifiers to classify different ages at worst. In contrast, we saw prediction accuracy go down, but stay significantly better than chance across the all groups except the adult dizygotic twins. This suggests that something besides solely developmental maturation trajectories account for the individually-specific patterns of RSFC network organization identified with functional fingerprints.

In work investigating cortical hubs in adults (Gordon et al., 2018), it was found that the removal of each hub type resulted in dissociable disruption to the whole-brain network, dependent on which type of hub was removed. These results provide some evidence that FP cortical hubs

(included in the control-default hub category in adults, and in the control-default and cross-control categories in youths) have a significant impact on the organizational structure of the whole-brain network. I propose that the essential elements of the functional fingerprints we identified in youths and adults in Study 1, may have been comprised of many cortical hub nodes. The hubs' unique influence on whole-brain functional network integration may have been at least partially driving the individualized connectivity of the functional fingerprints. Further, we found both functional fingerprints (Study 1) and cortical hubs (Study 3) are found to be generally similar over age, which might explain the similarity in functional fingerprint network representation and utility of features in opposite age groups SVM classifiers.

Insights into the neural systems supporting EF development in youths

In Studies 2 and 3, our results provide evidence that the neural systems supporting higher-order processes associated with EF task performance in youths rely on the efficient and flexible integration of sensory networks with cognitive control networks (Petersen & Posner, 2012). Previous work has revealed the role of different cortical regions in the cingulo-opercular, fronto-parietal, dorsal attention, and ventral attention networks – for example, the dorsolateral prefrontal cortex (DL-PFC) and the superior parietal cortex - as neural substrates of task performance in EF domains (Fiske & Holmboe, 2019; Gao et al., 2013; Nowrangi et al., 2014). These prior results prompted us to test the ability of our chosen GMs, calculated from a reduced network only including parcels in these putative functional control networks, to predict working memory and cognitive flexibility task performance (Study 2). While we expected these results to match or exceed results using whole-brain networks to calculate GMs, across both tasks, the GMs calculated form this "control-network focused" set of parcels failed to predict task performance on both tasks in our main analysis group. Similarly, even in the larger DCAN comparison group, characteristic path length (CPL) and global efficiency (GE) predicted both tasks, but to a reduced degree, and rich-club coefficient (RCC) no longer successfully predicted outcomes in either task, relative to

the whole brain set. These results suggested that within cognitive-control network RSFC alone did not best predict EF task performance and, unbeknownst to us at the time, foreshadowed our results in Study 3.

Indeed, in Study 3, one of our main findings was a split between control-processing hub categories in youths; a split not found in adults (Gordon et al., 2018). We identified one youth control-processing hub category (VIS) to exhibit connectivity profiles primarily in the cingulo-opercular, cingulo-parietal, dorsal attention, restrosplenial-temporal, somatomotor hand, and visual networks. The other, youth control-processing (AUD + SM), exhibits connectivity profiles primarily in the auditory, cingulo-opercular, dorsal attention, somatomotor hand, and somatomotor mouth networks. It is important to note that of the four main hub categories identified in youths, connectivity measures of only hubs within these two control-processing categories were associated with either working memory or cognitive control task performance.

These results support the theory of EFs relying on flexible integration of sensory and cognitive control networks, but also provide evidence of ongoing maturation of these hubs during middle-childhood. We posit that these two distinct types of youth control-processing hubs are specialized in the type of sensory stimuli they route to and from primary cognitive control hubs (cross-control hubs), and that this specialization becomes integrated into one control-processing hub in adulthood. Further, the individual differences in how efficiently these stimuli are routed to and from cross-control hubs accounts for some of the individual differences in EF task performance. The importance of control-processing hubs over cross-control hubs in predicting EF task performance may change once control-processing hubs are refined into a single system in adulthood, thus longitudinal studies will be of particular utility into expanding upon our observations.

Benefits of public datasets and combined methodology

Two of the main strengths of this dissertation are the inclusion of both locally collected and publicly available datasets, and the combination of neuroimaging with behavioral data. Throughout all three studies of this dissertation, I sought to include publically available neuroimaging and behavioral data, such as that provided by the Midnight Scan Club (MSC), the Human Connectome Project (HCP), and the Adolescent Brain Cognitive Development Study Club (ABCD) (Casey et al., 2018; Gordon et al., 2017b; Van Essen et al., 2013). This intention was twofold: (1) to create well-powered samples that are extremely difficult and expensive to collect at a single site, and (2) to provide a means of better assessing the generalizability of our findings. With the inclusion of these outside datasets, we were able to investigate the generalizability of our findings across age groups and across fMRI preprocessing methodologies, and also create a combined sample that is more inclusive and representative of the population. For example, in Study 1, while we had a locally collected sample of pediatric twin pairs, without the adult twins included from the HCP dataset and the repeat-scan individuals from the MSC dataset, we would not have been able to perform our age comparisons. The resulting insight into the similarity and stability of the resting state functional fingerprint in both youths and adults is one of the most interesting elements of that study, and would not have been easily accessible to me without the inclusion of open datasets.

Similarly, in Study 3, the combined 567 participant sample of youths that included both resting state fMRI data, as well as both working memory and cognitive flexibility task data may have been key to finding the association between the split control-processing hub group and cognitive flexibility task performance in youths. While 67 participants from the combined sample were collected locally and had both neuroimaging and behavioral task data available, our results on the impact of sample size on brain-behavior associations from Study 2, brings into question if this result would have been found using only those locally collected data. Further, while our lab is very mindful in our attempt to collect data that are well-balanced in regard to race and ethnicity,

we are ultimately limited by the demographics of our geographical location. Inclusion of the 500 ABCD study participants allowed us to create a sample that was closer to representing the larger population of the US, and thus improving the generalizability of our results.

While the current work being done by neuroimaging consortiums to large and diverse datasets publically available is still in its relative infancy, I believe that the availability of these open datasets will have a substantial impact on the neuroimaging research being conducted over the next decade. Not only will the precision and generalizability of brain-behavior associations identified using neuroimaging methods improve, but as longitudinal data (such as that being collected by the ABCD study) become available, many questions will be answered about the stability of our results and the trajectory of brain organization during development. I feel extremely lucky to have completed by graduate studies at a time when these open datasets are being made available to researchers, and look forward to being in a position to contribute to the open data landscape in the years ahead.

Summary

The three studies presented in this dissertation quantified individual differences in resting state functional network organization that are associated with either the functional fingerprint or executive function task performance in youths. Across all three studies, we leveraged large, cross-sectional samples consisting of both locally collected and publicly available neuroimaging data to increase the generalizability of our results. We demonstrated that a functional fingerprint based on resting state functional connectivity/coactivation (RSFC) is stable in both youths and adults, and that the predictive quality of functional fingerprints using support vector machine classifiers is reduced as the genetic similarity of individuals is reduced. We also presented evidence that graph metrics (GMs) calculated from RSFC can predict outcomes on working memory and cognitive flexibility tasks. However, available scan time, network makeup, and preprocessing decisions all impact the stability of results. Most importantly, the brain-behaviors effects are very small, thus

leading to inconsistent results in samples under approximately 2,000 individuals. Lastly, we found that resting state cortical hubs identified in youths closely resemble those found in adults. However, youth cortical hubs show a more diverse range of functional network inclusion, and control-processing hubs are split into two distinct categories; in contrast to the one category found in adults. As a whole, this dissertation provides a nuanced overview of how a small sample of multivariate methods used to quantify resting state functional network organization can provide valuable insight to individual differences in the developing brain.

Appendix

STUDY 1 SUPPLEMENT

Transparent Methods & Supplemental Materials

Supplemental Figures

Study 1, Figure S1: Accuracies Over ANOVA Feature Selection Thresholds, Related to Figure 2

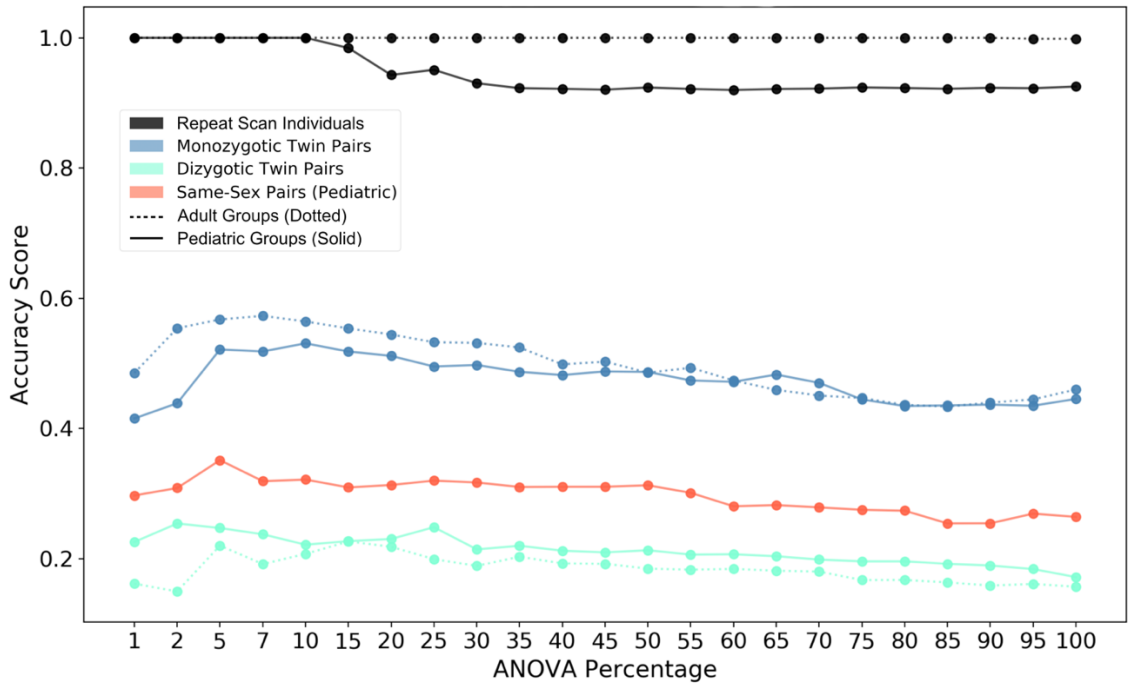

Note: Scikit-learn's default 5% setting for ANOVA feature selection was used for all final analyses. A post-hoc examination of feature selection thresholds was conducted to ensure the main classifier results were not dependent on the a priori 5% feature selection threshold default setting. All ANOVA thresholds from 1-100% were re-run on all subgroups using the SVM classifier method in our main analyses. Prediction accuracy generally peaked around 5-10% and then declined as percentages increased to 100%. These post-hoc accuracy scores suggest our a priori setting is within the optimal range for classification in all groups, that the main results were not driven by the 5% ANOVA threshold, and that using a different threshold would not provide a clear alteration to classifier performance.

Study 1, Figure S2: Pediatric "Fold-Rank" Matrix Features, Related to Figure 3

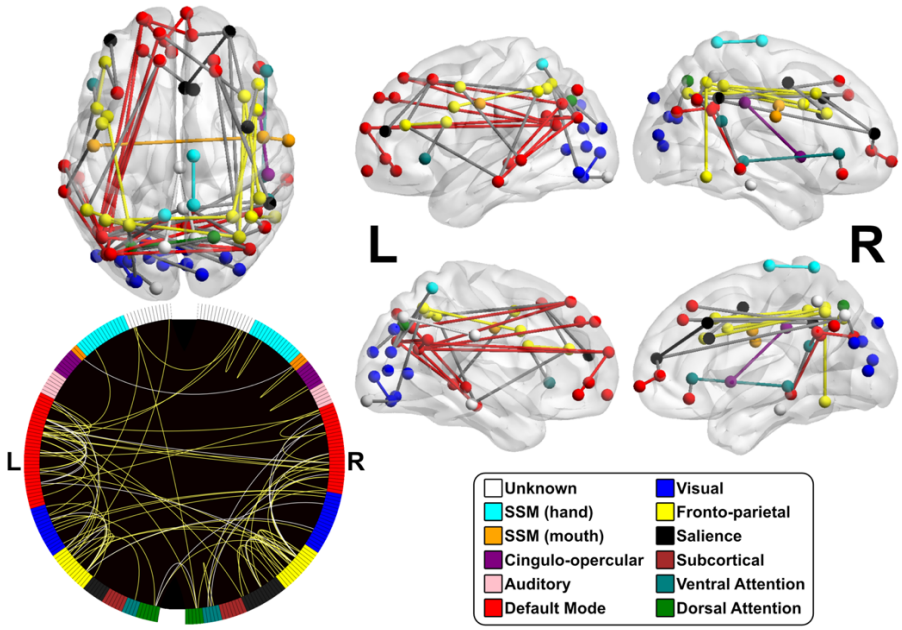

Note: All connections (87) chosen as features for at least 5 (yellow lines in circle graph) or 6 (white lines in circle graph) folds of the pediatric "fold-rank" matrix (total of 3 subgroups) are displayed. On-brain edges that are grey represent a between-network connection. Edges with a color represent a within network connection in the network of that color.

Study 1, Figure S3: Adult "Fold-Rank" Matrix Features, Related to Figure 3

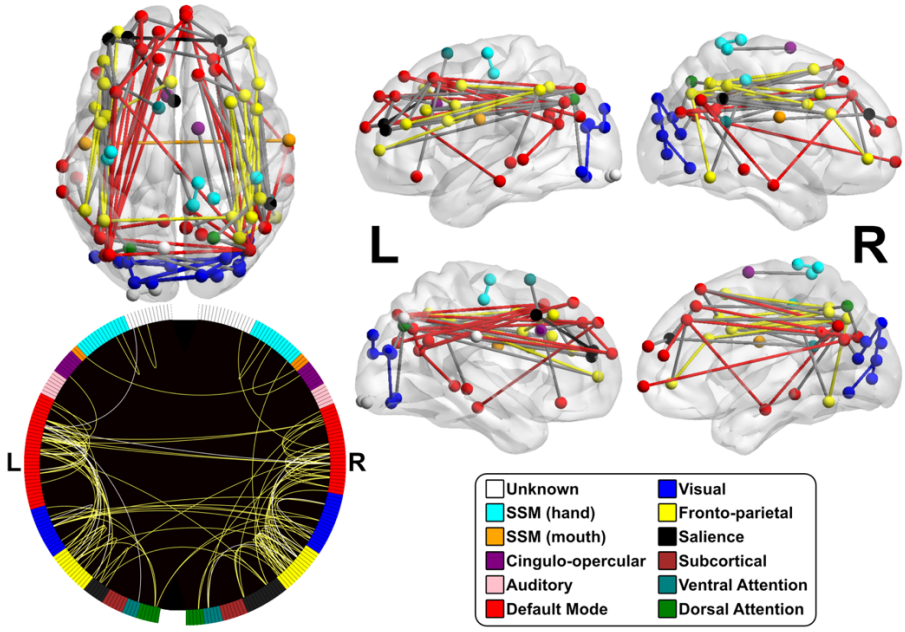

Note: All connections (110) chosen as features for at least 5 (yellow lines in circle graph) or 6 (white lines in circle graph) folds of the adult "fold-rank" matrix (total of 3 subgroups) are displayed. On-brain edges that are grey represent a between-network connection. Edges with a color represent a within network connection in the network of that color.

Study 1, Figure S4: “Common Set” Rank Matrix Features, Related to Figure 3

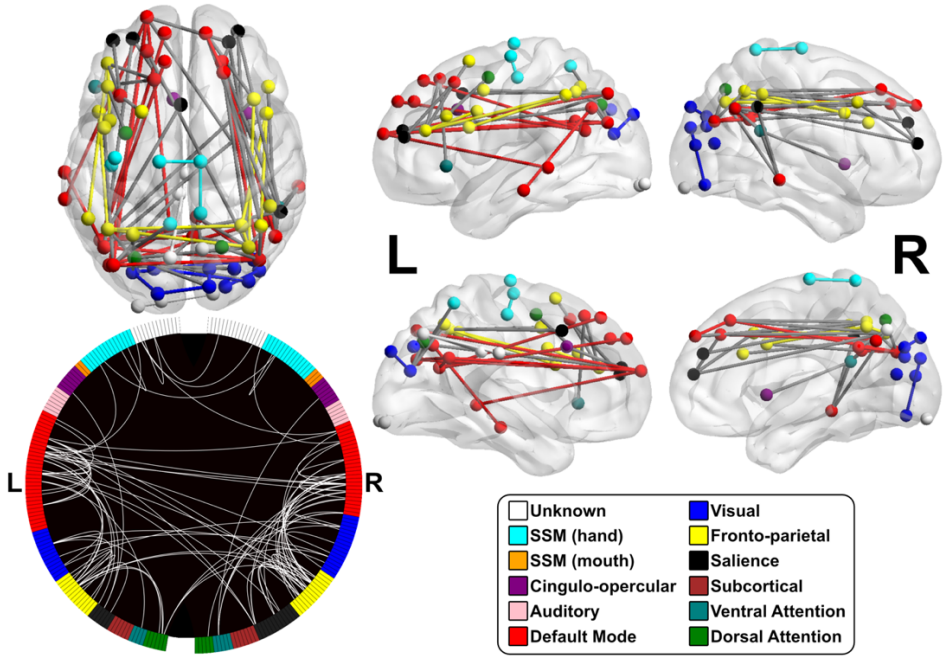

Note: All connections (90 total) chosen for at least one fold across all pediatric and adult subgroups (total of 6 subgroups) are displayed. On-brain edges that are grey represent a between-network connection. Edges with a color represent a within network connection in the network of that color.

Transparent Methods

Participant Demographics

Data from 209 total participants were organized into four pediatric (ages 8-18 years) and three adult (ages 22-35 years) subgroups for analysis. The pediatric groups were collected at The University of Texas at Austin (UT) as part of the Texas Center for Learning Disabilities project (www.texasldcenter.org), the Texas Twin Project (Harden, Tucker-Drob, & Tackett, 2013), or as part of ongoing UT Developmental Cognitive Neuroscience Lab (Church) collections. All UT collections were approved by the Institutional Review Board at either the University of Texas Health Science Center at Houston, or the University of Texas at Austin. Parents provided informed consent and pediatric participants provided informed assent to participate in the study. The adult subgroups were created from two publicly available neuroimaging datasets: the Midnight Scan Club (MSC; (Gordon et al., 2017b) and the Human Connectome Project (HCP; (Van Essen et al., 2013).

The pediatric subgroups included repeat-scanned individuals (spanning 5 to 18 months between scans); monozygotic (MZ) and dizygotic (DZ) twin pairs; and a group of same-sex sibling pairs that, like the DZ twin groups, share ~50% genetic information. The adult subgroups included repeat-scanned individuals (MSC scans were collected on two consecutive days), as well as MZ and DZ twin pairs. Detailed group information, including zygosity for twin pairs, is in Table 2. The similar subgrouping in our two age groups allowed us to test for familial similarities in network organization during both childhood and adulthood, determine whether those results were moderated by sex, and to address possible confounds imposed by MRI acquisition settings and scanner type by using both locally and externally collected datasets.

Pediatric subgroups did not significantly differ from one another in mean IQ ($p>0.32$). Adult twin subgroups did not significantly differ from one another in fluid intelligence ($p=0.19$), as measured by Raven's Progressive Matrices (Raven, 1941). The MSC group exhibited above-average mean IQ but could not be statistically compared to the HCP adult sets due to difference in intelligence measures. Groups did not significantly differ in scanner movement that was quantified by post-motion censoring mean framewise displacement (FD) values (see resting state preprocessing). See Table 2 for detailed subgroup demographics, IQ, and motion information.

Method Details

Neuroimaging Acquisition:

All pediatric participants were scanned at The University of Texas at Austin's Biomedical Imaging Center on a Siemens Skyra 3 Tesla scanner with a 32-channel head coil. Participants were fitted with foam pads around the head to reduce motion and verbal feedback was provided between scans. All resting state scans were acquired after participants were instructed to lie still, stay awake, and keep their eyes open while looking at a white fixation cross on a black background. Resting state scans where participants reported falling asleep were not included in analysis. For each participant, one T1-weighted structural MPRAGE sequence scan (TR=2530ms, TE=3.36ms,

FOV=256x256, voxel resolution=1x1x1 mm) and up to two, six-minute functional resting state scans using a multi-band echo-planar sequence (TR=2000ms, TE=30ms, flip angle=60°, MB factor=2, 48 axial slices, voxel resolution=2x2x2mm) were collected.

All HCP data used in the current analyses were collected on a custom 3 Tesla Siemens Skyra "Connectome scanner" with a Nova Medical 32-channel head coil (Van Essen et al., 2013). At each scanning session, participants underwent at least one T1-weighted structural MEMPRAGE sequence scan (TR=2400ms, TE=2.14ms, FOV=224x224, voxel resolution=0.7x0.7x0.7mm) and one, 14.5 minute functional resting state scan using a multi-band echo-planar sequence (TR=720ms, TE=33.1ms, flip angle=52°, MB factor=8, 72 axial slices, voxel resolution=2x2x2mm).

Data in the MSC dataset was collected on a 3 Tesla Siemens TRIO scanner with a 16-channel head coil (Gordon et al., 2017b). The current analyses include one T1-weighted structural MPRAGE sequence scan (TR=2400ms, TE=3.47ms, voxel resolution=0.8x0.8x0.8mm) and two 30-minute functional resting state scans (TR=2200ms, TE=27ms, flip angle=90°, 36 axial slices, voxel resolution=4x4x4mm) collected over two consecutive visits. Resting state scans for all HCP and MSC sessions were acquired with each participant looking at a white fixation cross on a black background.

Resting State Preprocessing:

In an effort to accurately compare the datasets used in these analyses, all scans were preprocessed identically with an in-house resting state preprocessing pipeline comprised of FMRIB Software Library (Smith et al., 2004) and Freesurfer (Dale et al., 1999) commands, as well as custom Matlab (www.mathworks.com) computational scripts. Adult scans were downloaded from their public database in unprocessed Neuroimaging Informatics Technology Initiative (NIfTI) format. Preprocessing steps followed best practices outlined in the current resting state literature (Hallquist et al., 2013; Power et al., 2012, 2014). The preprocessing steps included: (1)

motion correction and registration to 2mm MNI atlas space; (2) mode 1k normalization; (3) temporal band-pass filtering (0.009 Hz < f < 0.08 Hz); (4) demeaning and detrending of fMRI data; (5) regression of band-pass filtered nuisance signals including six directions of motion plus their derivatives, cerebral spinal fluid, white matter, and whole brain signal; (6) and spatial smoothing (4mm full width at half maximum). To reduce the reintroduction of noise that occurs with multiple transformations, all registration steps were done in one single transform. Similarly, all nuisance signal regression and temporal filtering was performed simultaneously (Lindquist et al., 2019).

Due to the significant negative impact of motion on rs-fcMRI analyses (Power et al., 2012, 2014), all functional scans were analyzed for excess motion and only participants that passed motion criteria were included in analyses. A framewise displacement (FD) threshold of .25mm was used for all datasets, and frames above this threshold were removed. Sections of timecourses without at least 5 contiguous frames post-censoring were also removed. At least 5 minutes of data surviving motion censoring was required for inclusion in all analyses. In an effort to mitigate the influence of varied scan lengths across datasets, fully processed scans included for all analyses were cropped to the first 5 minutes of post-motion censored data. Resting state scans of 5 minutes with a .25mm FD motion censoring threshold allowed us to include the largest number of participants across all datasets, while adhering to suggestions of minimum acceptable scan time (Birn et al., 2013; Whitlow et al., 2011) and an acceptable threshold of head motion (Power et al., 2012, 2014). All scans underwent quality assurance and visual inspection. Any scans that did not successfully align to the MNI atlas, included motion or acquisition artifacts, or did not pass minimum scan length and motion criteria were not included in analyses.

rs-fcMRI Feature Selection:

Features used for SVM classification were chosen from functional connections derived from a pre-defined set of 264 ROIs (Power et al., 2011). Due to inconsistent scan coverage of the

cerebellum across participants, a reduced set of 255 non-cerebellar ROIs was used. Resting state timecourses for each participant were extracted from each ROI (Study 1, Figure 1a). To create the feature mask used by the SVM classifier, each 5-minute timecourse from the training set was divided into 20-second segments (15 total segments) and one pairwise correlation matrix between all 255 ROIs was created for each segment of resting state timecourse (Study 1, Figure 1b). The correlation matrix was then masked to retain only off-diagonal correlation values and was converted into a vector comprised of 32,385 unique correlations for each segment. The segment vectors were then used for ANOVA feature selection (Study 1, Figure 1c) in which the top 5% most variable correlations (1,619) -- representing functional connections -- were retained. The resulting feature mask was then applied to the full 5-minute resting state timecourse for each individual during the SVM classifier steps (Study 1, Figure 1d). The classifier was trained on the same training set used for feature selection, and the held-out datasets (repeat scans for individuals or co-twin scans) were used to test the classifier's accuracy using leave-one-group out cross-validation (see details below).

ANOVA feature selection was set at 5% (the default setting for scikit-learn's (Pedregosa et al., 2011) ANOVA feature selection function) as this default is derived from the traditional minimal p-value threshold for significance tests. Additionally, we conducted a post-hoc examination of the influence of ANOVA thresholds from 1% to 100% to ensure that the a priori 5% threshold was not uniquely driving our results. We used the same classifier methods as used in the main analyses, but tested all feature selection thresholds from 1% to 100%. All ANOVA feature selection thresholds provided accuracies above chance for all of our sub-groups. However, accuracies did peak around the 5-10% range for each group and flattened out before eventually declining (Study 1, Figure S1). Lower scores at percentages below 5% suggest that too few features did not provide the classifier ample information for identification. Alternatively, percentages

nearing 100% may include "noise" which reduces classifier accuracy. We thus found that our 5% feature selection setting choice did not uniquely drive our results.

Similarly, segmenting the full resting state timecourse during feature selection provided a more accurate characterization of functional connectivity that is washed out using the full 5-minute timecourse. We tested feature selection segment lengths ranging from a single TR to one-half of the entire 5-minute timecourse. A reduction of accuracy scores was observed as segment lengths increased, with feature selection including the full 5-minute timecourse producing the lowest classifier performance in all groups. A segment length of 20-seconds was chosen as it identifies a set of connections that are highly discriminating between scan-pairs, provides sufficient samples for ANOVA feature selection, and still adheres to the findings of previous literature addressing the minimal segment length that is needed to capture the resting state functional network structure (Birn et al., 2013; Whitlow et al., 2011).

Quantification and Statistical Analyses

Support Vector Machine Classification:

We used scikit-learn (Pedregosa et al., 2011) to train and test a multi-label classifier for each group, using the rs-fcMRI features chosen during the training step. Prediction accuracy was measured using a SVM classifier and a leave-one-group-out cross-validation scheme. Scan pair classification was achieved with the following steps: (1) Participant scans were organized into two sets: The first set contained one 5-minute scan from each participant and the second set contained either a 5-minute scan of that same participant collected at a different time, or a sibling's scan. Thus, for classifying individuals with repeated scans, this included one set of first-visit scans and one set of second-visit scans. For twin pairs, one set was twin A's scan and the other set was twin B's scan. (2) The first set of scans was then used for feature selection and classifier training, and the second set of scans (held-out data) was used for classifier testing. (3) A prediction accuracy score was calculated for each participant or sibling pair and represented the ratio of correct

predictions that were made to the total number of predictions, thus quantifying how accurately the classifier could label each scan in the testing set, based off the data in the training set. (4) This procedure was then repeated for a cross-validation "fold", where the training/testing scans within sets were swapped. During cross-validation, the second set of scans was used for the feature selection and training steps, and the first set was used for the testing step. (5) In order to address influences on classifier accuracy due to arbitrary grouping of training and testing scan sets, we applied a form of scan-set shuffling to the classification procedure. The feature selection and classification steps (steps 1-4) were run one-thousand times per group while altering which individual's scan was placed in the training set vs the testing set, without shuffling the classifier labels (keeping all participant pair labels correct and intact). In this design, the order of scans did not matter, only that each individual (or twin pair) provides one unique scan in the training set and the other in the testing set. For example, the training set could include all A scans [1A, 2A, 3A…] and the testing set all B scans [1B, 2B, 3B…]. In the next iteration, one or more scan pair's assignment may swap between training [1A, 2B, 3A…] and testing [1B, 2A, 3B…], but all scan pairs are represented only once in each set and the pair labels remain correct. Additionally, no combination of scan pairs was used more than once. Prediction accuracy scores across all scan-set shuffles and folds were then averaged to provide a mean group prediction accuracy score. (6) To quantify whether group classifier performance was above chance, one thousand randomized permutations were conducted for each of the one thousand tests in step 5. In this step the labels in the training and testing sets were shuffled (labels were no longer assigned to the correct scan pairs) and classification accuracy was re-calculated. This resulted in a distribution of one million chance accuracy scores. To assess the significance of the group prediction accuracy score, we calculated p-values as the proportion of chance distribution accuracies that were above the mean group accuracy score. This was achieved by dividing the number of randomized accuracy scores that were greater than our group accuracy score by the number of permutations. (7) Lastly, we assessed

classifier sensitivity by calculating area under the receiver operating characteristic curve (AUC) values for each scan pair within all subgroups.

Functional Fingerprint Mapping:

We examined the specific functional connections that were most different between individuals by identifying connections repeatedly chosen during feature selection across folds and subgroups. Each subgroup's main SVM classifier provided us with two folds, each containing a list of functional connections chosen as features. A matrix was created that tallied the number of times a functional connection was chosen as a feature across folds, which we refer to as a "fold-rank" matrix. Each of these subgroup fold-rank matrices were summed into one pediatric and one adult group matrix that were calculated from the three main subgroups in each age range (excluding the same-sex sibling UT comparison group, as some overlap in sibling pairs existed with the pediatric DZ twin group). The final pediatric (Study 1, Figure S2) and adult (Study 1, Figure S3) fold-rank matrices each contained values ranging from zero to six, and a threshold of five was applied for our final selection of features for each group. Additionally, one "common set" rank matrix was created that combined chosen features across all six pediatric and adult subgroups (Study 1, Figure S4). The common set matrix differs from the fold matrix, in that it is binary, and a connection chosen as a feature for either fold of a subgroup is given a value of one. The resulting matrix included values ranging from zero to six, after summing across all subgroups. We applied a threshold of six to the common set matrix, representing connections chosen as features for at least one fold in all six main subgroups.

STUDY 2 SUPPLEMENT

Supplemental Figures

Study 2, Figure S1: Post Motion Scan Time and Graph Metrics Correlations

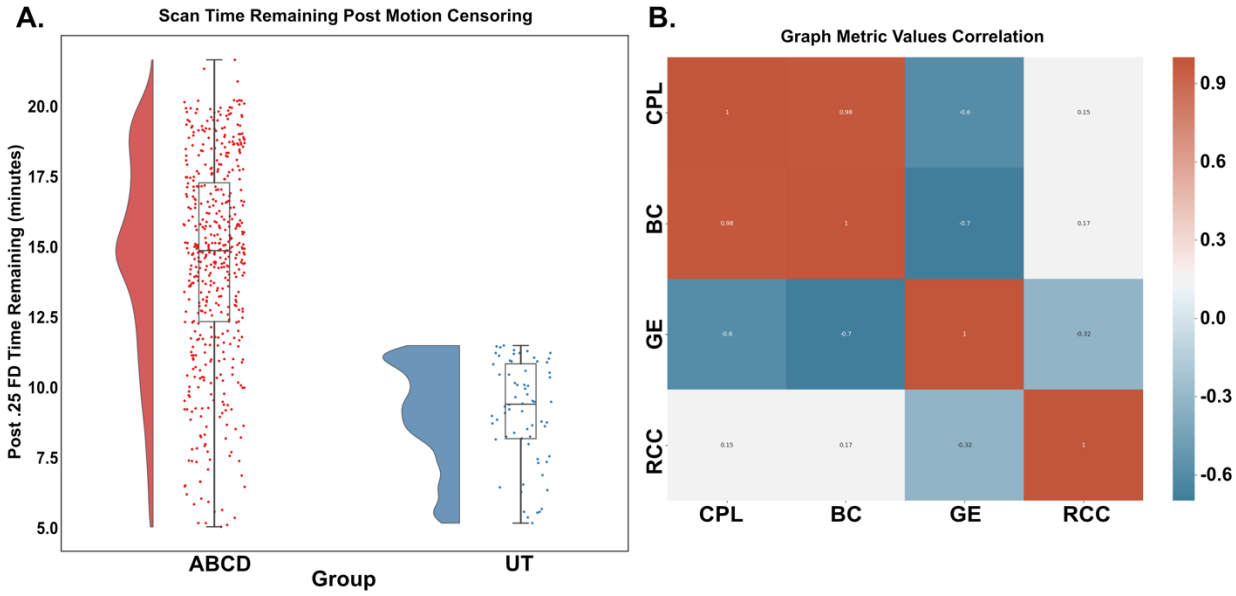

Note: (A) Distribution of resting state scan time, per collection group, after motion censoring at .25 framewise displacement (FD). (B) Correlation of graph metric values calculated from all available resting state data, for all participants in the main analysis group (n = 567). Characteristic Path Length (CPL) and Betweenness Centrality (BC) were highly correlated (r = 0.98) and BC was not reported in our main findings. (GE = Global Efficiency, RCC = Rich-Club Coefficient)

STUDY 3 SUPPLEMENT

Supplemental Figures

Study 3, Figure S1: Post Motion Scan Time and Hub Cluster Participant Distribution

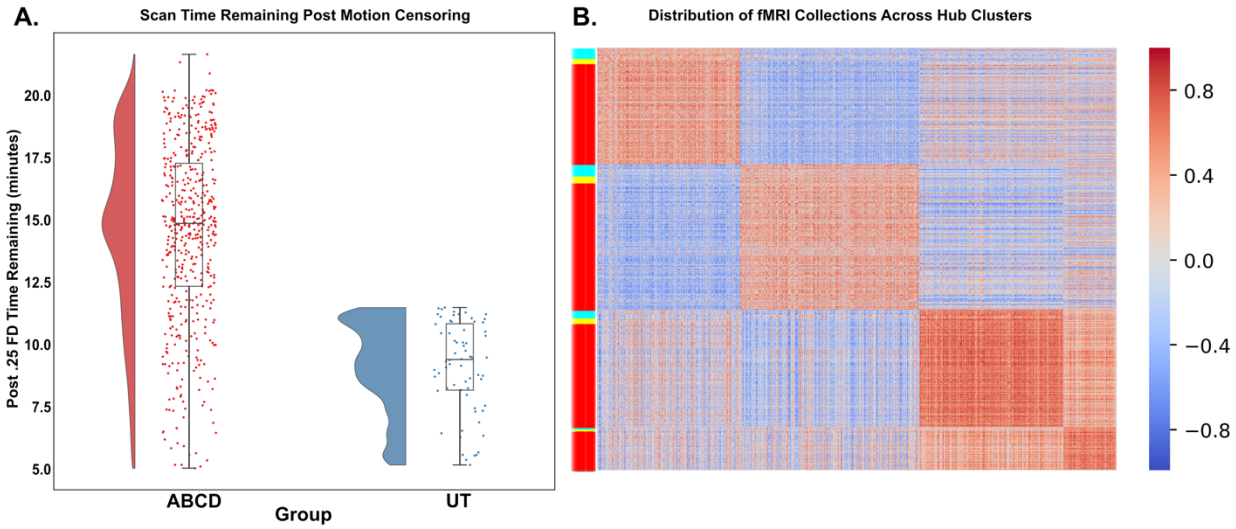

Note: (A) Distribution of resting state scan time, per collection group, after motion censoring at .25 framewise displacement (FD). (B) Correlation matrix of hub connectivity profiles, ordered by Louvain cluster assignment. Participant hubs are color-coded according to their fMRI collection of origin. Group 1 displayed here, but groups 2 and 3 had similar distributions across clusters. (Cyan = UT Austin One; Yellow = UT Austin Two; Red = ABCD)

References

Anderson, J. S., Ferguson, M. A., Lopez-Larson, M., & Yurgelun-Todd, D. (2011). Reproducibility of Single-Subject Functional Connectivity Measurements. *American Journal of Neuroradiology*, *32*(3), 548–555. https://doi.org/10.3174/ajnr.A2330

Balsters, J. H., Mantini, D., & Wenderoth, N. (2018). Connectivity-based parcellation reveals distinct cortico-striatal connectivity fingerprints in Autism Spectrum Disorder. *NeuroImage*, *170*(February 2017), 412–423. https://doi.org/10.1016/j.neuroimage.2017.02.019

Barch, D. M., Burgess, G. C., Harms, M. P., Petersen, S. E., Schlaggar, B. L., Corbetta, M., … Van Essen, D. C. (2013). Function in the human connectome: Task-fMRI and individual differences in behavior. *NeuroImage*, *80*, 169–189. https://doi.org/10.1016/j.neuroimage.2013.05.033

Barnea-Goraly, N., Menon, V., Eckert, M., Tamm, L., Bammer, R., Karchemskiy, A., … Reiss, A. L. (2005). White matter development during childhood and adolescence: A cross-sectional diffusion tensor imaging study. *Cerebral Cortex*, *15*(12), 1848–1854. https://doi.org/10.1093/cercor/bhi062

Bertolero, M. A., Yeo, B. T. T., & D'Esposito, M. (2017). The diverse club. *Nature Communications*, *8*(1), 1277. https://doi.org/10.1038/s41467-017-01189-w

Best, J. R., & Miller, P. H. (2010). A Developmental Perspective on Executive Function. *Child Development*, *81*(6), 1641–1660. https://doi.org/10.1111/j.1467-8624.2010.01499.x

Best, J. R., Miller, P. H., & Naglieri, J. A. (2011). Relations between executive function and academic achievement from ages 5 to 17 in a large, representative national sample. *Learning and Individual Differences*, *21*(4), 327–336.

https://doi.org/10.1016/j.lindif.2011.01.007

Birn, R. M., Molloy, E. K., Patriat, R., Parker, T., Meier, T. B., Kirk, G. R., … Prabhakaran, V. (2013). The effect of scan length on the reliability of resting-state fMRI connectivity estimates. *NeuroImage*, *83*, 550–558. https://doi.org/10.1016/j.neuroimage.2013.05.099

Biswal, B., Zerrin Yetkin, F., Haughton, V. M., & Hyde, J. S. (1995). Functional connectivity in the motor cortex of resting human brain using echo-planar mri. *Magnetic Resonance in Medicine*, *34*(4), 537–541. https://doi.org/10.1002/mrm.1910340409

Brown, T. T., & Jernigan, T. L. (2012). Brain Development During the Preschool Years. *Neuropsychology Review*, *22*(4), 313–333. https://doi.org/10.1007/s11065-012-9214-1

Buckner, R. L., Andrews-Hanna, J. R., & Schacter, D. L. (2008). The brain's default network: Anatomy, function, and relevance to disease. *Annals of the New York Academy of Sciences*, *1124*, 1–38. https://doi.org/10.1196/annals.1440.011

Buss, A. T., & Spencer, J. P. (2018). Changes in frontal and posterior cortical activity underlie the early emergence of executive function. *Developmental Science*, *21*(4), 1–15. https://doi.org/10.1111/desc.12602

Byrge, L., & Kennedy, D. P. (2019). High-accuracy individual identification using a "thin slice" of the functional connectome. *Network Neuroscience*, *3*(2), 363–383. https://doi.org/10.1162/netn_a_00068

Byrge, L., Sporns, O., & Smith, L. B. (2014). Developmental process emerges from extended brain–body–behavior networks. *Trends in Cognitive Sciences*, *18*(8), 395–403. https://doi.org/10.1016/j.tics.2014.04.010

Caballero-Gaudes, C., & Reynolds, R. C. (2017). Methods for cleaning the BOLD fMRI signal.

NeuroImage, *154*(December 2016), 128–149. https://doi.org/10.1016/j.neuroimage.2016.12.018

Cai, L., Dong, Q., & Niu, H. (2018). The development of functional network organization in early childhood and early adolescence: A resting-state fNIRS study. *Developmental Cognitive Neuroscience*, *30*(March), 223–235. https://doi.org/10.1016/j.dcn.2018.03.003

Cao, M., Wang, J.-H., Dai, Z.-J., Cao, X.-Y., Jiang, L.-L., Fan, F.-M., … He, Y. (2014). Topological organization of the human brain functional connectome across the lifespan. *Developmental Cognitive Neuroscience*, *7*(16), 76–93. https://doi.org/10.1016/j.dcn.2013.11.004

Casey, B. J., Cannonier, T., Conley, M. I., Cohen, A. O., Barch, D. M., Heitzeg, M. M., … Dale, A. M. (2018). The Adolescent Brain Cognitive Development (ABCD) study: Imaging acquisition across 21 sites. *Developmental Cognitive Neuroscience*, (May 2017), 0–1. https://doi.org/10.1016/j.dcn.2018.03.001

Church, J. A., Bunge, S. A., Petersen, S. E., & Schlaggar, B. L. (2017). Preparatory Engagement of Cognitive Control Networks Increases Late in Childhood. *Cerebral Cortex*, *27*(3), 2139–2153. https://doi.org/10.1093/cercor/bhw046

Cohen, A. L., Fair, D. A., Dosenbach, N. U. F., Miezin, F. M., Dierker, D., Van Essen, D. C., … Petersen, S. E. (2008). Defining functional areas in individual human brains using resting functional connectivity MRI. *NeuroImage*, *41*(1), 45–57. https://doi.org/10.1016/j.neuroimage.2008.01.066

Cohen, A. O., Breiner, K., Steinberg, L., Bonnie, R. J., Scott, E. S., Taylor-Thompson, K., … Casey, B. J. (2016). When Is an Adolescent an Adult? Assessing Cognitive Control in

Emotional and Nonemotional Contexts. *Psychological Science*, *27*(4), 549–562. https://doi.org/10.1177/0956797615627625

Cohen, J. R., & D'Esposito, M. (2016). The Segregation and Integration of Distinct Brain Networks and Their Relationship to Cognition. *Journal of Neuroscience*, *36*(48), 12083–12094. https://doi.org/10.1523/JNEUROSCI.2965-15.2016

Cole, M. W., Reynolds, J. R., Power, J. D., Repovs, G., Anticevic, A., & Braver, T. S. (2013). Multi-task connectivity reveals flexible hubs for adaptive task control. *Nature Neuroscience*, *16*(9), 1348–1355. https://doi.org/10.1038/nn.3470

Cole, M. W., Yarkoni, T., Repovs, G., Anticevic, A., & Braver, T. S. (2012). Global Connectivity of Prefrontal Cortex Predicts Cognitive Control and Intelligence. *Journal of Neuroscience*, *32*(26), 8988–8999. https://doi.org/10.1523/JNEUROSCI.0536-12.2012

Conti, A., Duggento, A., Guerrisi, M., Passamonti, L., Indovina, I., & Toschi, N. (2019). Variability and Reproducibility of Directed and Undirected Functional MRI Connectomes in the Human Brain. *Entropy*, *21*(7), 661. https://doi.org/10.3390/e21070661

Cordes, D., Haughton, V. M., Arfanakis, K., Carew, J. D., Turski, P. A., Moritz, C. H., … Meyerand, M. E. (2001). Frequencies contributing to functional connectivity in the cerebral cortex in "resting-state" data. *AJNR. American Journal of Neuroradiology*, *22*(7), 1326–1333. Retrieved from http://link.springer.com/10.1007/s10854-014-1833-2

Cordova, M., Shada, K., Demeter, D. V., Doyle, O., Miranda-Dominguez, O., Perrone, A., … Feczko, E. (2020). Heterogeneity of executive function revealed by a functional random forest approach across ADHD and ASD. *NeuroImage: Clinical*, *26*(November 2019), 102245. https://doi.org/10.1016/j.nicl.2020.102245

Craddock, R. C., Holtzheimer, P. E., Hu, X. P., & Mayberg, H. S. (2009). Disease state prediction from resting state functional connectivity. *Magnetic Resonance in Medicine*, *62*(6), 1619–1628. https://doi.org/10.1002/mrm.22159

Crittenden, B. M., Mitchell, D. J., & Duncan, J. (2016). Task Encoding across the Multiple Demand Cortex Is Consistent with a Frontoparietal and Cingulo-Opercular Dual Networks Distinction. *Journal of Neuroscience*, *36*(23), 6147–6155. https://doi.org/10.1523/JNEUROSCI.4590-15.2016

Dale, A. M., Fischl, B., & Sereno, M. I. (1999). Cortical surface-based analysis: I. Segmentation and surface reconstruction. *NeuroImage*, *9*(2), 179–194. https://doi.org/10.1006/nimg.1998.0395

DCAN-Labs. (2019). DCAN-Labs/abcd-hcp-pipeline. [WWW Document]. zenodo. https://doi.org/10.5281/zenodo.2587210

De Asis-Cruz, J., Bouyssi-Kobar, M., Evangelou, I., Vezina, G., & Limperopoulos, C. (2016). Functional properties of resting state networks in healthy full-term newborns. *Scientific Reports*, *5*(1), 17755. https://doi.org/10.1038/srep17755

De Martino, F., Valente, G., Staeren, N., Ashburner, J., Goebel, R., & Formisano, E. (2008). Combining multivariate voxel selection and support vector machines for mapping and classification of fMRI spatial patterns. *NeuroImage*, *43*(1), 44–58. https://doi.org/10.1016/j.neuroimage.2008.06.037

Demertzi, A., Soddu, A., & Laureys, S. (2013). Consciousness supporting networks. *Current Opinion in Neurobiology*, *23*(2), 239–244. https://doi.org/10.1016/j.conb.2012.12.003

Demeter, D. V., Engelhardt, L. E., Mallett, R., Gordon, E. M., Nugiel, T., Harden, K. P., …

Church, J. A. (2020). Functional Connectivity Fingerprints at Rest Are Similar across Youths and Adults and Vary with Genetic Similarity. *IScience*, *23*(1), 100801. https://doi.org/10.1016/j.isci.2019.100801

DeSerisy, M., Ramphal, B., Pagliaccio, D., Raffanello, E., Tau, G., Marsh, R., … Margolis, A. E. (2021). Frontoparietal and default mode network connectivity varies with age and intelligence. *Developmental Cognitive Neuroscience*, *48*, 100928. https://doi.org/10.1016/j.dcn.2021.100928

Dick, A. S., Lopez, D. A., Watts, A. L., Heeringa, S., Reuter, C., Bartsch, H., … Thompson, W. K. (2021). Meaningful Associations in the Adolescent Brain Cognitive Development Study. *NeuroImage*, 118262. https://doi.org/10.1016/j.neuroimage.2021.118262

Dipasquale, O., Sethi, A., Laganà, M. M., Baglio, F., Baselli, G., Kundu, P., … Cercignani, M. (2017). Comparing resting state fMRI de-noising approaches using multi- and single-echo acquisitions. *PLOS ONE*, *12*(3), e0173289. https://doi.org/10.1371/journal.pone.0173289

Dixon, M. L., De La Vega, A., Mills, C., Andrews-Hanna, J., Spreng, R. N., Cole, M. W., & Christoff, K. (2018). Heterogeneity within the frontoparietal control network and its relationship to the default and dorsal attention networks. *Proceedings of the National Academy of Sciences*, *115*(7), E1598–E1607. https://doi.org/10.1073/pnas.1715766115

Dosenbach, N. U. F., Fair, D. A., Cohen, A. L., Schlaggar, B. L., & Petersen, S. E. (2013). A dual-networks architecture of top-down control, *12*(3), 99–105. https://doi.org/10.1016/j.tics.2008.01.001.

Dosenbach, N. U. F., Nardos, B., Cohen, A. L., Fair, D. A., Power, J. D., Church, J. A., … Schlaggar, B. L. (2010). Prediction of Individual Brain Maturity Using fMRI. *Science*,

329(September). https://doi.org/10.1126/science.1194144

Dosenbach, N. U. F., Visscher, K. M., Palmer, E. D., Miezin, F. M., Wenger, K. K., Kang, H. C., … Petersen, S. E. (2006). A Core System for the Implementation of Task Sets. *Neuron*, *50*(5), 799–812. https://doi.org/10.1016/j.neuron.2006.04.031

Doucet, G., Naveau, M., Petit, L., Delcroix, N., Zago, L., Crivello, F., … Joliot, M. (2011). Brain activity at rest: a multiscale hierarchical functional organization. *Journal of Neurophysiology*, *105*(6), 2753–2763. https://doi.org/10.1152/jn.00895.2010

Duda, J. T., Cook, P. A., & Gee, J. C. (2014). Reproducibility of graph metrics of human brain structural networks. *Frontiers in Neuroinformatics*, *8*(MAY), 1–11. https://doi.org/10.3389/fninf.2014.00046

Dworetsky, A., Seitzman, B. A., Adeyemo, B., Neta, M., Coalson, R. S., Petersen, S. E., & Gratton, C. (2021). Probabilistic mapping of human functional brain networks identifies regions of high group consensus. *NeuroImage*, *237*(May), 118164. https://doi.org/10.1016/j.neuroimage.2021.118164

Dwyer, D. B., Harrison, B. J., Yucel, M., Whittle, S., Zalesky, A., Pantelis, C., … Fornito, A. (2014). Large-Scale Brain Network Dynamics Supporting Adolescent Cognitive Control. *Journal of Neuroscience*, *34*(42), 14096–14107. https://doi.org/10.1523/JNEUROSCI.1634-14.2014

Eggebrecht, A. T., Elison, J. T., Feczko, E., Todorov, A., Wolff, J. J., Kandala, S., … Pruett, J. R. (2017). Joint Attention and Brain Functional Connectivity in Infants and Toddlers. *Cerebral Cortex*, *27*(3), 1709–1720. https://doi.org/10.1093/cercor/bhw403

Engelhardt, L. E., Briley, D. A., Mann, F. D., Harden, K. P., & Tucker-Drob, E. M. (2015).

Genes Unite Executive Functions in Childhood. *Psychological Science*, *26*(8), 1151–1163. https://doi.org/10.1177/0956797615577209

Engelhardt, L. E., Harden, K. P., Tucker-Drob, E. M., & Church, J. A. (2019). The neural architecture of executive functions is established by middle childhood. *NeuroImage*, *185*(May 2018), 479–489. https://doi.org/10.1016/j.neuroimage.2018.10.024

Fair, D. A., Cohen, A. L., Power, J. D., Dosenbach, N. U. F., Church, J. A., Miezin, F. M., … Petersen, S. E. (2009). Functional brain networks develop from a "local to distributed" organization. *PLoS Computational Biology*, *5*(5), 14–23. https://doi.org/10.1371/journal.pcbi.1000381

Fair, D. A., Dosenbach, N. U. F., Church, J. A., Cohen, A. L., Brahmbhatt, S., Miezin, F. M., … Schlaggar, B. L. (2007). Development of distinct control networks through segregation and integration. *Proceedings of the National Academy of Sciences*, *104*(33), 13507–13512. https://doi.org/10.1073/pnas.0705843104

Fair, D. A., Posner, J., Nagel, B. J., Bathula, D., Costa Dias, T. G., Mills, K. L., … Nigg, J. T. (2010). Atypical Default Network Connectivity in Youth with ADHD. *Biological Psychiatry*, *68*(12), 1084–1091. https://doi.org/10.1016/j.biopsych.2010.07.003.Atypical

Farahani, F. V., Karwowski, W., & Lighthall, N. R. (2019). Application of Graph Theory for Identifying Connectivity Patterns in Human Brain Networks: A Systematic Review. *Frontiers in Neuroscience*, *13*(JUN), 1–27. https://doi.org/10.3389/fnins.2019.00585

Fedorenko, E., Duncan, J., & Kanwisher, N. (2013). Broad domain generality in focal regions of frontal and parietal cortex. *Proceedings of the National Academy of Sciences*, *110*(41), 16616–16621. https://doi.org/10.1073/pnas.1315235110

Ferguson, H. J., Brunsdon, V. E. A., & Bradford, E. E. F. (2021). The developmental trajectories of executive function from adolescence to old age. *Scientific Reports*, *11*(1), 1382. https://doi.org/10.1038/s41598-020-80866-1

Finn, E. S., Shen, X., Scheinost, D., Rosenberg, M. D., Huang, J., Chun, M. M., … Constable, R. T. (2015). Functional connectome fingerprinting: Identifying individuals using patterns of brain connectivity. *Nature Neuroscience*, *18*(11), 1664–1671. https://doi.org/10.1038/nn.4135

Fiske, A., & Holmboe, K. (2019). Neural substrates of early executive function development. *Developmental Review*, *52*(July), 42–62. https://doi.org/10.1016/j.dr.2019.100866

Fransson, P., Åden, U., Blennow, M., & Lagercrantz, H. (2011). The Functional Architecture of the Infant Brain as Revealed by Resting-State fMRI. *Cerebral Cortex*, *21*(1), 145–154. https://doi.org/10.1093/cercor/bhq071

Freund, J., Brandmaier, A. M., Lewejohann, L., Kirste, I., Kritzler, M., Krüger, A., … Kempermann, G. (2013). Emergence of individuality in genetically identical mice. *Science*, *340*(6133), 756–759. https://doi.org/10.1126/science.1235294

Fu, Y., Ma, Z., Hamilton, C., Liang, Z., Hou, X., Ma, X., … Zhang, N. (2015). Genetic influences on resting-state functional networks: A twin study. *Human Brain Mapping*, *36*(10), 3959–3972. https://doi.org/10.1002/hbm.22890

Gao, W., Gilmore, J. H., Giovanello, K. S., Smith, J. K., Shen, D., Zhu, H., & Lin, W. (2011). Temporal and Spatial Evolution of Brain Network Topology during the First Two Years of Life. *PLoS ONE*, *6*(9), e25278. https://doi.org/10.1371/journal.pone.0025278

Gao, W., Gilmore, J. H., Shen, D., Smith, J. K., Zhu, H., & Lin, W. (2013). The synchronization

within and interaction between the default and dorsal attention networks in early infancy. *Cerebral Cortex*, *23*(3), 594–603. https://doi.org/10.1093/cercor/bhs043

Gargouri, F., Kallel, F., Delphine, S., Ben Hamida, A., Lehéricy, S., & Valabregue, R. (2018). The Influence of Preprocessing Steps on Graph Theory Measures Derived from Resting State fMRI. *Frontiers in Computational Neuroscience*, *12*(February). https://doi.org/10.3389/fncom.2018.00008

Giedd, J. N., Blumenthal, J., Jeffries, N. O., Castellanos, F. X., Liu, H., Zijdenbos, A., … Rapoport, J. L. (1999). Brain development during childhood and adolescence: a longitudinal MRI study. *Nature Neuroscience*, *2*(10), 861–863. https://doi.org/10.1038/13158

Giedd, J. N., & Rapoport, J. L. (2010). Structural MRI of Pediatric Brain Development: What Have We Learned and Where Are We Going? *Neuron*, *67*(5), 728–734. https://doi.org/10.1016/j.neuron.2010.08.040

Glahn, D. C., Winkler, A. M., Kochunov, P., Almasy, L., Duggirala, R., Carless, M. A., … Blangero, J. (2010). Genetic control over the resting brain. *Proceedings of the National Academy of Sciences*, *107*(3), 1223–1228. https://doi.org/10.1073/pnas.0909969107

Glasser, M. F., Sotiropoulos, S. N., Wilson, J. A., Coalson, T. S., Fischl, B., Andersson, J. L., … Jenkinson, M. (2013). The minimal preprocessing pipelines for the Human Connectome Project. *NeuroImage*, *80*, 105–124. https://doi.org/10.1016/j.neuroimage.2013.04.127

Gordon, E. M., Laumann, T. O., Adeyemo, B., Huckins, J. F., Kelley, W. M., & Petersen, S. E. (2016). Generation and Evaluation of a Cortical Area Parcellation from Resting-State Correlations. *Cerebral Cortex*, *26*(1), 288–303. https://doi.org/10.1093/cercor/bhu239

Gordon, E. M., Laumann, T. O., Adeyemo, B., & Petersen, S. E. (2017a). Individual Variability

of the System-Level Organization of the Human Brain. *Cerebral Cortex*, *27*(1), 386–399. https://doi.org/10.1093/cercor/bhv239

Gordon, E. M., Laumann, T. O., Gilmore, A. W., Newbold, D. J., Greene, D. J., Berg, J. J., … Dosenbach, N. U. F. (2017b). Precision Functional Mapping of Individual Human Brains. *Neuron*, *95*(4), 791-807.e7. https://doi.org/10.1016/j.neuron.2017.07.011

Gordon, E. M., Lynch, C. J., Gratton, C., Laumann, T. O., Gilmore, A. W., Greene, D. J., … Nelson, S. M. (2018). Three Distinct Sets of Connector Hubs Integrate Human Brain Function. *Cell Reports*, *24*(7), 1687-1695.e4. https://doi.org/10.1016/j.celrep.2018.07.050

Gratton, C., Laumann, T. O., Nielsen, A. N., Greene, D. J., Gordon, E. M., Gilmore, A. W., … Petersen, S. E. (2018a). Functional Brain Networks Are Dominated by Stable Group and Individual Factors, Not Cognitive or Daily Variation. *Neuron*, *98*(2), 439-452.e5. https://doi.org/10.1016/j.neuron.2018.03.035

Gratton, C., Sun, H., & Petersen, S. E. (2018b). Control networks and hubs. *Psychophysiology*, *55*(3), e13032. https://doi.org/10.1111/psyp.13032

Grayson, D. S., & Fair, D. A. (2017). Development of large-scale functional networks from birth to adulthood: A guide to the neuroimaging literature. *NeuroImage*, *160*(January), 15–31. https://doi.org/10.1016/j.neuroimage.2017.01.079

Greene, D. J., Church, J. A., Dosenbach, N. U. F., Nielsen, A. N., Adeyemo, B., Nardos, B., … Schlaggar, B. L. (2016). Multivariate pattern classification of pediatric Tourette syndrome using functional connectivity MRI. *Developmental Science*, *19*(4), 581–598. https://doi.org/10.1111/desc.12407

Haak, K. V., Marquand, A. F., & Beckmann, C. F. (2018). Connectopic mapping with resting-

state fMRI. *NeuroImage*, *170*, 83–94. https://doi.org/10.1016/j.neuroimage.2017.06.075

Hagberg, A. A., Schult, D. A., & Swart, P. J. (2008). Exploring network structure, dynamics, and function using NetworkX. *Proceedings of the 7th Python in Science Conference (SciPy 2008)*, (SciPy), 11–15.

Hallquist, M. N., Hwang, K., & Luna, B. (2013). The nuisance of nuisance regression: Spectral misspecification in a common approach to resting-state fMRI preprocessing reintroduces noise and obscures functional connectivity. *NeuroImage*, *82*, 208–225. https://doi.org/10.1016/j.neuroimage.2013.05.116

Harden, K. P., Tucker-Drob, E. M., & Tackett, J. L. (2013). The Texas Twin Project. *Twin Research and Human Genetics*, *16*(01), 385–390. https://doi.org/10.1017/thg.2012.97

Hearne, L. J., Mattingley, J. B., & Cocchi, L. (2016). Functional brain networks related to individual differences in human intelligence at rest. *Scientific Reports*, *6*(August), 1–8. https://doi.org/10.1038/srep32328

Heine, L., Soddu, A., Gómez, F., Vanhaudenhuyse, A., Tshibanda, L., Thonnard, M., … Demertzi, A. (2012). Resting State Networks and Consciousness. *Frontiers in Psychology*, *3*(AUG), 1–12. https://doi.org/10.3389/fpsyg.2012.00295

Hilger, K., Ekman, M., Fiebach, C. J., & Basten, U. (2017a). Efficient hubs in the intelligent brain: Nodal efficiency of hub regions in the salience network is associated with general intelligence. *Intelligence*, *60*, 10–25. https://doi.org/10.1016/j.intell.2016.11.001

Hilger, K., Ekman, M., Fiebach, C. J., & Basten, U. (2017b). Intelligence is associated with the modular structure of intrinsic brain networks. *Scientific Reports*, *7*(1), 16088. https://doi.org/10.1038/s41598-017-15795-7

Hjelmervik, H., Hausmann, M., Osnes, B., Westerhausen, R., & Specht, K. (2014). Resting States Are Resting Traits – An fMRI Study of Sex Differences and Menstrual Cycle Effects in Resting State Cognitive Control Networks. *PLoS ONE*, *9*(7), e103492. https://doi.org/10.1371/journal.pone.0103492

Holanda Júnior, F. W. N., & Almondes, K. M. de. (2016). Sleep and executive functions in older adults: A systematic review. *Dementia & Neuropsychologia*, *10*(3), 185–197. https://doi.org/10.1590/S1980-5764-2016DN1003004

Horien, C., Shen, X., Scheinost, D., & Constable, R. T. (2019). The individual functional connectome is unique and stable over months to years. *NeuroImage*, *189*(203), 676–687. https://doi.org/10.1016/j.neuroimage.2019.02.002

Houston, S. M., Herting, M. M., & Sowell, E. R. (2014). The Neurobiology of Childhood Structural Brain Development: Conception Through Adulthood. In *Curr Top Behav Neurosci* (pp. 3–17). https://doi.org/10.1007/7854_2013_265

Jacob, R., & Parkinson, J. (2015). The Potential for School-Based Interventions That Target Executive Function to Improve Academic Achievement. *Review of Educational Research*, *85*(4), 512–552. https://doi.org/10.3102/0034654314561338

Jaeggi, S. M., Studer-Luethi, B., Buschkuehl, M., Su, Y.-F., Jonides, J., & Perrig, W. J. (2010). The relationship between n-back performance and matrix reasoning — implications for training and transfer. *Intelligence*, *38*(6), 625–635. https://doi.org/10.1016/j.intell.2010.09.001

Jung, R. E., & Haier, R. J. (2007). The Parieto-Frontal Integration Theory (P-FIT) of intelligence: Converging neuroimaging evidence. *Behavioral and Brain Sciences*, *30*(2),

135–154. https://doi.org/10.1017/S0140525X07001185

Kaufmann, T., Alnæs, D., Doan, N. T., Brandt, C. L., Andreassen, O. A., & Westlye, L. T. (2017). Delayed stabilization and individualization in connectome development are related to psychiatric disorders. *Nature Neuroscience*, *20*(4), 513–515. https://doi.org/10.1038/nn.4511

Kruschwitz, J. D., Waller, L., Daedelow, L. S., Walter, H., & Veer, I. M. (2018). General, crystallized and fluid intelligence are not associated with functional global network efficiency: A replication study with the human connectome project 1200 data set. *NeuroImage*, *171*(January), 323–331. https://doi.org/10.1016/j.neuroimage.2018.01.018

LaConte, S., Strother, S., Cherkassky, V., Anderson, J., & Hu, X. (2005). Support vector machines for temporal classification of block design fMRI data. *NeuroImage*, *26*(2), 317–329. https://doi.org/10.1016/j.neuroimage.2005.01.048

Lancichinetti, A., & Fortunato, S. (2012). Consensus clustering in complex networks. *Scientific Reports*, *2*(1), 336. https://doi.org/10.1038/srep00336

Langer, N., Pedroni, A., Gianotti, L. R. R., Hänggi, J., Knoch, D., & Jäncke, L. (2012). Functional brain network efficiency predicts intelligence. *Human Brain Mapping*, *33*(6), 1393–1406. https://doi.org/10.1002/hbm.21297

Last, B. S., Lawson, G. M., Breiner, K., Steinberg, L., & Farah, M. J. (2018). Childhood socioeconomic status and executive function in childhood and beyond. *PLOS ONE*, *13*(8), e0202964. https://doi.org/10.1371/journal.pone.0202964

Laumann, T. O., Gordon, E. M., Adeyemo, B., Snyder, A. Z., Joo, S. J., Chen, M.-Y., … Petersen, S. E. (2015). Functional System and Areal Organization of a Highly Sampled

Individual Human Brain. *Neuron*, *87*(3), 657–670. https://doi.org/10.1016/j.neuron.2015.06.037

Laumann, T. O., Snyder, A. Z., Mitra, A., Gordon, E. M., Gratton, C., Adeyemo, B., … Petersen, S. E. (2016). On the Stability of BOLD fMRI Correlations. *Cerebral Cortex*, *27*(10), 4719–4732. https://doi.org/10.1093/cercor/bhw265

Lawrence, N. S., Ross, T. J., Hoffmann, R., Garavan, H., & Stein, E. A. (2003). Multiple Neuronal Networks Mediate Sustained Attention. *Journal of Cognitive Neuroscience*, *15*(7), 1028–1038. https://doi.org/10.1162/089892903770007416

Lenroot, R. K., & Giedd, J. N. (2006). Brain development in children and adolescents: Insights from anatomical magnetic resonance imaging. *Neuroscience & Biobehavioral Reviews*, *30*(6), 718–729. https://doi.org/10.1016/j.neubiorev.2006.06.001

Liang, X., Wang, J., Yan, C., Shu, N., Xu, K., Gong, G., & He, Y. (2012). Effects of Different Correlation Metrics and Preprocessing Factors on Small-World Brain Functional Networks: A Resting-State Functional MRI Study. *PLoS ONE*, *7*(3), e32766. https://doi.org/10.1371/journal.pone.0032766

Lin, W., Zhu, Q., Gao, W., Chen, Y., Toh, C. H., Styner, M., … Gilmore, J. H. (2008). Functional connectivity MR imaging reveals cortical functional connectivity in the developing brain. *American Journal of Neuroradiology*, *29*(10), 1883–1889. https://doi.org/10.3174/ajnr.A1256

Lindquist, M. A., Geuter, S., Wager, T. D., & Caffo, B. S. (2019). Modular preprocessing pipelines can reintroduce artifacts into fMRI data. *Human Brain Mapping*, *40*(8), 2358–2376. https://doi.org/10.1002/hbm.24528

Liu, Y., Chen, Y., Liang, X., Li, D., Zheng, Y., Zhang, H., … Qiu, S. (2020). Altered Resting-State Functional Connectivity of Multiple Networks and Disrupted Correlation With Executive Function in Major Depressive Disorder. *Frontiers in Neurology*, *11*(April), 1–11. https://doi.org/10.3389/fneur.2020.00272

Loose, L. S., Wisniewski, D., Rusconi, M., Goschke, T., & Haynes, J.-D. (2017). Switch-Independent Task Representations in Frontal and Parietal Cortex. *The Journal of Neuroscience*, *37*(33), 8033–8042. https://doi.org/10.1523/JNEUROSCI.3656-16.2017

Lowe, M. J., Mock, B. J., & Sorenson, J. A. (1998). Functional Connectivity in Single and Multislice Echoplanar Imaging Using Resting-State Fluctuations. *NeuroImage*, *7*(2), 119–132. https://doi.org/10.1006/nimg.1997.0315

Luciana, M., Bjork, J. M., Nagel, B. J., Barch, D. M., Gonzalez, R., Nixon, S. J., & Banich, M. T. (2018). Adolescent neurocognitive development and impacts of substance use: Overview of the adolescent brain cognitive development (ABCD) baseline neurocognition battery. *Developmental Cognitive Neuroscience*, *32*(July 2017), 67–79. https://doi.org/10.1016/j.dcn.2018.02.006

Ma, X., Liu, J., Liu, T., Ma, L., Wang, W., Shi, S., … Wang, M. (2019). Altered Resting-State Functional Activity in Medication-Naive Patients With First-Episode Major Depression Disorder vs. Healthy Control: A Quantitative Meta-Analysis. *Frontiers in Behavioral Neuroscience*, *13*(May), 1–11. https://doi.org/10.3389/fnbeh.2019.00089

Marcus, D. S., Harwell, J., Olsen, T., Hodge, M., Glasser, M. F., Prior, F., … Van Essen, D. C. (2011). Informatics and Data Mining Tools and Strategies for the Human Connectome Project. *Frontiers in Neuroinformatics*, *5*(June), 1–12.

https://doi.org/10.3389/fninf.2011.00004

Marek, S., & Dosenbach, N. U. F. (2018). The frontoparietal network: function, electrophysiology, and importance of individual precision mapping. *Dialogues in Clinical Neuroscience*, *20*(2), 133–140.

Marek, S., Hwang, K., Foran, W., Hallquist, M. N., & Luna, B. (2015). The Contribution of Network Organization and Integration to the Development of Cognitive Control. *PLoS Biology*, *13*(12), 1–25. https://doi.org/10.1371/journal.pbio.1002328

Marek, S., Tervo-Clemmens, B., Calabro, F. J., Montez, D. F., Kay, B. P., Hatoum, A. S., … Dosenbach, N. (2020). Towards Reproducible Brain-Wide Association Studies. *BioRxiv*, *11*, 15–18. Retrieved from https://doi.org/10.1101/2020.08.21.257758

Mason, M. F., Norton, M. I., Van Horn, J. D., Wegner, D. M., Grafton, S. T., & Macrae, C. N. (2007). Wandering Minds: The Default Network and Stimulus-Independent Thought. *Science*, *315*(5810), 393–395. https://doi.org/10.1126/science.1131295

McKenna, R., Rushe, T., & Woodcock, K. A. (2017). Informing the Structure of Executive Function in Children: A Meta-Analysis of Functional Neuroimaging Data. *Frontiers in Human Neuroscience*, *11*(April), 1–17. https://doi.org/10.3389/fnhum.2017.00154

Mehnert, J., Akhrif, A., Telkemeyer, S., Rossi, S., Schmitz, C. H., Steinbrink, J., … Neufang, S. (2013). Developmental changes in brain activation and functional connectivity during response inhibition in the early childhood brain. *Brain and Development*, *35*(10), 894–904. https://doi.org/10.1016/j.braindev.2012.11.006

Micalizzi, L., Brick, L. A., Flom, M., Ganiban, J. M., & Saudino, K. J. (2019). Effects of socioeconomic status and executive function on school readiness across levels of household

chaos. *Early Childhood Research Quarterly*, *47*, 331–340. https://doi.org/10.1016/j.ecresq.2019.01.007

Mills, K. L., Goddings, A.-L., Herting, M. M., Meuwese, R., Blakemore, S.-J., Crone, E. A., … Tamnes, C. K. (2016). Structural brain development between childhood and adulthood: Convergence across four longitudinal samples. *NeuroImage*, *141*, 273–281. https://doi.org/10.1016/j.neuroimage.2016.07.044

Miranda-Dominguez, O., Feczko, E., Grayson, D. S., Walum, H., Nigg, J. T., & Fair, D. A. (2018). Heritability of the human connectome: A connectotyping study. *Network Neuroscience*, *2*(2), 175–199. https://doi.org/10.1162/netn_a_00029

Miranda-Dominguez, O., Mills, B. D., Carpenter, S. D., Grant, K. A., Kroenke, C. D., Nigg, J. T., & Fair, D. A. (2014). Connectotyping: Model based fingerprinting of the functional connectome. *PLoS ONE*, *9*(11). https://doi.org/10.1371/journal.pone.0111048

Mišić, B., & Sporns, O. (2016). From regions to connections and networks: new bridges between brain and behavior. *Current Opinion in Neurobiology*, *40*, 1–7. https://doi.org/10.1016/j.conb.2016.05.003

Mitra, A., Snyder, A. Z., Tagliazucchi, E., Laufs, H., Elison, J., Emerson, R. W., … Raichle, M. (2017). Resting-state fMRI in sleeping infants more closely resembles adult sleep than adult wakefulness. *PLoS ONE*, *12*(11), 1–19. https://doi.org/10.1371/journal.pone.0188122

Murphy, K., Bodurka, J., & Bandettini, P. A. (2007). How long to scan? The relationship between fMRI temporal signal to noise ratio and necessary scan duration. *NeuroImage*, *34*(2), 565–574. https://doi.org/10.1016/j.neuroimage.2006.09.032

Noble, S., Scheinost, D., Finn, E. S., Shen, X., Papademetris, X., McEwen, S. C., … Constable,

R. T. (2017). Multisite reliability of MR-based functional connectivity. *NeuroImage*, *146*(1), 959–970. https://doi.org/10.1016/j.neuroimage.2016.10.020

Nowrangi, M. A., Lyketsos, C., Rao, V., & Munro, C. A. (2014). Systematic Review of Neuroimaging Correlates of Executive Functioning: Converging Evidence From Different Clinical Populations. *The Journal of Neuropsychiatry and Clinical Neurosciences*, *26*(2), 114–125. https://doi.org/10.1176/appi.neuropsych.12070176

Nugiel, T., Roe, M. A., Engelhardt, L. E., Mitchell, M. E., Zheng, A., & Church, J. A. (2020). Pediatric ADHD symptom burden relates to distinct neural activity across executive function domains. *NeuroImage: Clinical*, *28*(July), 102394. https://doi.org/10.1016/j.nicl.2020.102394

Paldino, M. J., Golriz, F., Zhang, W., & Chu, Z. D. (2019). Normalization enhances brain network features that predict individual intelligence in children with epilepsy. *PLOS ONE*, *14*(3), e0212901. https://doi.org/10.1371/journal.pone.0212901

Pedregosa, F., Varoquaux, G., Gramfort, A., Michel, V., Thirion, B., Grisel, O., … Duchesnay, É. (2011). Scikit-learn: Machine Learning in Python Gaël Varoquaux Bertrand Thirion Vincent Dubourg Alexandre Passos PEDREGOSA, VAROQUAUX, GRAMFORT ET AL. Matthieu Perrot. *Journal of Machine Learning Research*, *12*, 2825–2830. https://doi.org/10.1007/s13398-014-0173-7.2

Peirce, J. W. (2007). PsychoPy—Psychophysics software in Python. *Journal of Neuroscience Methods*, *162*(1–2), 8–13. https://doi.org/10.1016/j.jneumeth.2006.11.017

Pessoa, L. (2014). Understanding brain networks and brain organization. *Physics of Life Reviews*, *11*(3), 400–435. https://doi.org/10.1016/j.plrev.2014.03.005

Petersen, S. E., & Posner, M. I. (2012). The Attention System of the Human Brain: 20 Years After. *Annual Review of Neuroscience*, *35*(1), 73–89. https://doi.org/10.1146/annurev-neuro-062111-150525

Petersen, S. E., & Sporns, O. (2015). Brain Networks and Cognitive Architectures. *Neuron*, *88*(1), 207–219. https://doi.org/10.1016/j.neuron.2015.09.027

Poldrack, R. A., Laumann, T. O., Koyejo, O., Gregory, B., Hover, A., Chen, M.-Y., … Mumford, J. A. (2015). Long-term neural and physiological phenotyping of a single human. *Nature Communications*, *6*(1), 8885. https://doi.org/10.1038/ncomms9885

Power, J. D., Barnes, K. A., Snyder, A. Z., Schlaggar, B. L., & Petersen, S. E. (2012). Spurious but systematic correlations in functional connectivity MRI networks arise from subject motion. *NeuroImage*, *59*(3), 2142–2154. https://doi.org/10.1016/j.neuroimage.2011.10.018

Power, J. D., Cohen, A. L., Nelson, S. M., Wig, G. S., Barnes, K. A., Church, J. A., … Petersen, S. E. (2011). Functional Network Organization of the Human Brain. *Neuron*, *72*(4), 665–678. https://doi.org/10.1016/j.neuron.2011.09.006

Power, J. D., Fair, D. A., Schlaggar, B. L., & Petersen, S. E. (2010). The Development of Human Functional Brain Networks. *Neuron*, *67*(5), 735–748. https://doi.org/10.1016/j.neuron.2010.08.017

Power, J. D., Mitra, A., Laumann, T. O., Snyder, A. Z., Schlaggar, B. L., & Petersen, S. E. (2014). Methods to detect, characterize, and remove motion artifact in resting state fMRI. *NeuroImage*, *84*, 320–341. https://doi.org/10.1016/j.neuroimage.2013.08.048

Power, J. D., & Petersen, S. E. (2013). Control-related systems in the human brain. *Current Opinion in Neurobiology*, *23*(2), 223–228. https://doi.org/10.1016/j.conb.2012.12.009

Power, J. D., Schlaggar, B. L., Lessov-Schlaggar, C. N., & Petersen, S. E. (2013). Evidence for Hubs in Human Functional Brain Networks. *Neuron*, *79*(4), 798–813. https://doi.org/10.1016/j.neuron.2013.07.035

Price, G. R., Yeo, D. J., Wilkey, E. D., & Cutting, L. E. (2018). Prospective relations between resting-state connectivity of parietal subdivisions and arithmetic competence. *Developmental Cognitive Neuroscience*, *30*, 280–290. https://doi.org/10.1016/j.dcn.2017.02.006

Raichle, M. E. (2015). The Brain's Default Mode Network. *Annual Review of Neuroscience*, *38*(1), 433–447. https://doi.org/10.1146/annurev-neuro-071013-014030

Raven, J. C. (1941). Standardization of Progressive Matrices, 1938. *British Journal of Medical Psychology*, *19*(1), 137–150. https://doi.org/10.1111/j.2044-8341.1941.tb00316.x

Reineberg, A. E., Gustavson, D. E., Benca, C., Banich, M. T., & Friedman, N. P. (2018). The Relationship Between Resting State Network Connectivity and Individual Differences in Executive Functions. *Frontiers in Psychology*, *9*(SEP), 1–14. https://doi.org/10.3389/fpsyg.2018.01600

Rosvall, M., & Bergstrom, C. T. (2008). Maps of random walks on complex networks reveal community structure. *Proceedings of the National Academy of Sciences*, *105*(4), 1118–1123. https://doi.org/10.1073/pnas.0706851105

Rubia, K. (2013). Functional brain imaging across development. *European Child & Adolescent Psychiatry*, *22*(12), 719–731. https://doi.org/10.1007/s00787-012-0291-8

Rubinov, M., & Sporns, O. (2010). Complex network measures of brain connectivity: Uses and interpretations. *NeuroImage*, *52*(3), 1059–1069.

https://doi.org/10.1016/j.neuroimage.2009.10.003

Rubinov, M., & Sporns, O. (2011). Weight-conserving characterization of complex functional brain networks. *NeuroImage*, *56*(4), 2068–2079. https://doi.org/10.1016/j.neuroimage.2011.03.069

Salas-Gomez, D., Fernandez-Gorgojo, M., Pozueta, A., Diaz-Ceballos, I., Lamarain, M., Perez, C., … Sanchez-Juan, P. (2020). Physical Activity Is Associated With Better Executive Function in University Students. *Frontiers in Human Neuroscience*, *14*(February), 1–8. https://doi.org/10.3389/fnhum.2020.00011

Satterthwaite, T. D., Wolf, D. H., Loughead, J., Ruparel, K., Elliott, M. A., Hakonarson, H., … Gur, R. E. (2012). Impact of in-scanner head motion on multiple measures of functional connectivity: Relevance for studies of neurodevelopment in youth. *NeuroImage*, *60*(1), 623–632. https://doi.org/10.1016/j.neuroimage.2011.12.063

Satterthwaite, T. D., Wolf, D. H., Roalf, D. R., Ruparel, K., Erus, G., Vandekar, S., … Gur, R. C. (2015). Linked Sex Differences in Cognition and Functional Connectivity in Youth. *Cerebral Cortex*, *25*(9), 2383–2394. https://doi.org/10.1093/cercor/bhu036

Satterthwaite, T. D., Wolf, D. H., Ruparel, K., Erus, G., Elliott, M. A., Eickhoff, S. B., … Gur, R. C. (2013). Heterogeneous impact of motion on fundamental patterns of developmental changes in functional connectivity during youth. *NeuroImage*, *83*(11), 45–57. https://doi.org/10.1016/j.neuroimage.2013.06.045

Sherman, L. E., Rudie, J. D., Pfeifer, J. H., Masten, C. L., McNealy, K., & Dapretto, M. (2014). Development of the Default Mode and Central Executive Networks across early adolescence: A longitudinal study. *Developmental Cognitive Neuroscience*, *10*, 148–159.

https://doi.org/10.1016/j.dcn.2014.08.002

Sinclair, B., Hansell, N. K., Blokland, G. A. M., Martin, N. G., Thompson, P. M., Breakspear, M., … McMahon, K. L. (2015). Heritability of the network architecture of intrinsic brain functional connectivity. *NeuroImage*, *121*, 243–252. https://doi.org/10.1016/j.neuroimage.2015.07.048

Smith, S. M., Jenkinson, M., Woolrich, M. W., Beckmann, C. F., Behrens, T. E. J., Johansen-Berg, H., … Matthews, P. M. (2004). Advances in functional and structural MR image analysis and implementation as FSL. *NeuroImage*, *23*, S208–S219. https://doi.org/10.1016/j.neuroimage.2004.07.051

Sporns, O. (2018). Graph theory methods: applications in brain networks. *Dialogues in Clinical Neuroscience*, *20*(2), 111–120. https://doi.org/10.31887/DCNS.2018.20.2/osporns

Stanley, M. L., Simpson, S. L., Dagenbach, D., Lyday, R. G., Burdette, J. H., & Laurienti, P. J. (2015). Changes in brain network efficiency and working memory performance in aging. *PLoS ONE*, *10*(4), 1–17. https://doi.org/10.1371/journal.pone.0123950

Stiles, J., & Jernigan, T. L. (2010). The Basics of Brain Development. *Neuropsychology Review*, *20*(4), 327–348. https://doi.org/10.1007/s11065-010-9148-4

Szucs, D., & Ioannidis, J. P. (2020). Sample size evolution in neuroimaging research: An evaluation of highly-cited studies (1990–2012) and of latest practices (2017–2018) in high-impact journals. *NeuroImage*, *221*(July), 117164. https://doi.org/10.1016/j.neuroimage.2020.117164

Thomas Yeo, B. T., Krienen, F. M., Sepulcre, J., Sabuncu, M. R., Lashkari, D., Hollinshead, M., … Buckner, R. L. (2011). The organization of the human cerebral cortex estimated by

intrinsic functional connectivity. *Journal of Neurophysiology*, *106*(3), 1125–1165. https://doi.org/10.1152/jn.00338.2011

Thornburgh, C. L., Narayana, S., Rezaie, R., Bydlinski, B. N., Tylavsky, F. A., Papanicolaou, A. C., … Völgyi, E. (2017). Concordance of the Resting State Networks in Typically Developing, 6-to 7-Year-Old Children and Healthy Adults. *Frontiers in Human Neuroscience*, *11*(April). https://doi.org/10.3389/fnhum.2017.00199

Ullman, H., Almeida, R., & Klingberg, T. (2014). Structural Maturation and Brain Activity Predict Future Working Memory Capacity during Childhood Development. *Journal of Neuroscience*, *34*(5), 1592–1598. https://doi.org/10.1523/JNEUROSCI.0842-13.2014

van den Heuvel, M. P., & Sporns, O. (2013). Network hubs in the human brain. *Trends in Cognitive Sciences*, *17*(12), 683–696. https://doi.org/10.1016/j.tics.2013.09.012

van den Heuvel, M. P., Stam, C. J., Kahn, R. S., & Hulshoff Pol, H. E. (2009). Efficiency of Functional Brain Networks and Intellectual Performance. *Journal of Neuroscience*, *29*(23), 7619–7624. https://doi.org/10.1523/JNEUROSCI.1443-09.2009

Van Dijk, K. R. A., Sabuncu, M. R., & Buckner, R. L. (2012). The influence of head motion on intrinsic functional connectivity MRI. *NeuroImage*, *59*(1), 431–438. https://doi.org/10.1016/j.neuroimage.2011.07.044

Van Essen, D. C., Smith, S. M., Barch, D. M., Behrens, T. E. J., Yacoub, E., & Ugurbil, K. (2013). The WU-Minn Human Connectome Project: An overview. *NeuroImage*, *80*, 62–79. https://doi.org/10.1016/j.neuroimage.2013.05.041

van Wijk, B. C. M., Stam, C. J., & Daffertshofer, A. (2010). Comparing Brain Networks of Different Size and Connectivity Density Using Graph Theory. *PLoS ONE*, *5*(10), e13701.

https://doi.org/10.1371/journal.pone.0013701

Volkow, N. D., Koob, G. F., Croyle, R. T., Bianchi, D. W., Gordon, J. A., Koroshetz, W. J., … Weiss, S. R. B. (2018). The conception of the ABCD study: From substance use to a broad NIH collaboration. *Developmental Cognitive Neuroscience*, *32*(April 2017), 4–7. https://doi.org/10.1016/j.dcn.2017.10.002

Wang, J. (2010). Graph-based network analysis of resting-state functional MRI. *Frontiers in Systems Neuroscience*, *4*(June), 1–14. https://doi.org/10.3389/fnsys.2010.00016

Whitfield-Gabrieli, S., Moran, J. M., Nieto-Castañón, A., Triantafyllou, C., Saxe, R., & Gabrieli, J. D. E. (2011). Associations and dissociations between default and self-reference networks in the human brain. *NeuroImage*, *55*(1), 225–232. https://doi.org/10.1016/j.neuroimage.2010.11.048

Whitlow, C. T., Casanova, R., & Maldjian, J. A. (2011). Effect of Resting-State Functional MR Imaging Duration on Stability of Graph Theory Metrics of Brain Network Connectivity. *Radiology*, *259*(2), 516–524. https://doi.org/10.1148/radiol.11101708

Wig, G. S. (2017). Segregated Systems of Human Brain Networks. *Trends in Cognitive Sciences*, *21*(12), 981–996. https://doi.org/10.1016/j.tics.2017.09.006

Wu, K., Taki, Y., Sato, K., Hashizume, H., Sassa, Y., Takeuchi, H., … Fukuda, H. (2013). Topological Organization of Functional Brain Networks in Healthy Children: Differences in Relation to Age, Sex, and Intelligence. *PLoS ONE*, *8*(2), e55347. https://doi.org/10.1371/journal.pone.0055347

Xu, J., Yin, X., Ge, H., Han, Y., Pang, Z., Liu, B., … Friston, K. (2017). Heritability of the Effective Connectivity in the Resting-State Default Mode Network. *Cerebral Cortex*,

27(12), 5626–5634. https://doi.org/10.1093/cercor/bhw332

Xu, T., Opitz, A., Craddock, R. C., Wright, M. J., Zuo, X. N., & Milham, M. P. (2016). Assessing Variations in Areal Organization for the Intrinsic Brain: From Fingerprints to Reliability. *Cerebral Cortex*, *26*(11), 4192–4211. https://doi.org/10.1093/cercor/bhw241

Zanto, T. P., & Gazzaley, A. (2013). Fronto-parietal network: flexible hub of cognitive control. *Trends in Cognitive Sciences*, *17*(12), 602–603. https://doi.org/10.1016/j.tics.2013.10.001

Zelazo, P. D. (2006). The Dimensional Change Card Sort (DCCS): a method of assessing executive function in children. *Nature Protocols*, *1*(1), 297–301. https://doi.org/10.1038/nprot.2006.46

Zelazo, P. D., Anderson, J. E., Richler, J., Wallner-Allen, K., Beaumont, J. L., & Weintraub, S. (2013). II. NIH TOOLBOX COGNITION BATTERY (CB): MEASURING EXECUTIVE FUNCTION AND ATTENTION. *Monographs of the Society for Research in Child Development*, *78*(4), 16–33. https://doi.org/10.1111/mono.12032

Zhao, N., Yuan, L.-X., Jia, X.-Z., Zhou, X.-F., Deng, X.-P., He, H.-J., … Zang, Y.-F. (2018). Intra- and Inter-Scanner Reliability of Voxel-Wise Whole-Brain Analytic Metrics for Resting State fMRI. *Frontiers in Neuroinformatics*, *12*(August), 1–9. https://doi.org/10.3389/fninf.2018.00054